LOUDSPEAKER BEHAVIOUR UNDER INCIDENT SOUND FIELDS

THÈSE N^{O} 2583 (2002)

PRÉSENTÉE À LA FACULTÉ SCIENCES ET TECHNIQUES DE L'INGÉNIEUR

ÉCOLE POLYTECHNIQUE FÉDÉRALE DE LAUSANNE

POUR L'OBTENTION DU GRADE DE DOCTEUR ÈS SCIENCES TECHNIQUES

DANS LE DOMAINE DE L'ÉLECTRICITÉ

PAR

Véronique ADAM

ingénieure en microtechnique diplômée EPF
de nationalité suisse et originaire de Montana (VS)

acceptée sur proposition du jury:

Prof. M. Rossi, directeur de thèse
Prof. M. Jufer, rapporteur
M. H. Massin, rapporteur
Dr R. Small, rapporteur

Lausanne, EPFL
2002

LOUDSPEAKER BEHAVIOUR UNDER INCIDENT SOUND FIELDS

Ph.D. Student: Véronique ADAM

Thesis Advisor: Prof. Mario ROSSI

18th June 2002

Swiss Federal Institute of Technology of Lausanne
Laboratory of Electromagnetics and Acoustics

To my parents and my brother,

"Toute la suite des hommes pendant le cours de tant de siècles doit être considérée comme un même homme qui subsiste toujours et qui apprend continuellement."

Blaise Pascal

Abstract

Within the framework of an outdoor active noise control project, a need arose, namely to establish whether electrodynamic loudspeakers are likely to be affected by the primary noise or by the interactions between them. The aim of this thesis is therefore to provide computation and measurement methods allowing to predict whether the effects of an incident sound field on a loudspeaker have to be taken into account.

The study comprises two main parts involving modelling, theory and calculations for the first part, and experimental validations in an anechoic chamber for the second one.

The equivalent circuit modelling of an electrodynamic loudspeaker shows that its behaviour can be completely determined from its input impedance. The thesis starts with the reflection that the modifications in loudspeaker behaviour due to the presence of an incident sound pressure applied on its radiating membrane could then also be analysed in the same way. The chosen process then consists in analysing the loudspeaker modifications in behaviour, no longer as variations of its radiation impedance, but as variations of its volume velocity and input impedance. The latter, which is located at the electrical loudspeaker terminals, offers the advantage of being easily measurable.

Within the scope of this thesis, the loudspeakers are assumed to behave like flat rigid pistons. Based on Thiele and Small parameters and using Rayleigh's surface integral and the unified and geometrical theories of diffraction, the calculations enable input impedance, volume velocity, near and far field sound pressure, as well as medium reaction force and radiation impedance to be obtained for each loudspeaker. Taking into account interaction effects, they also enable the modifications of all these quantities in modulus and phase to be predicted. A discrete approach is chosen in order to minimize the computation time. The calculations were however fine tuned in such a way as to ensure sufficient accuracy in relation to measurement uncertainties.

In order to evaluate the orders of magnitude of the modifications in loudspeaker behaviour, some preliminary calculations are first carried out in the simple case of two closed-box loudspeakers mounted in the same infinite baffle. This part also leads to understand how input impedance and volume velocity modifications vary according to excitation ratio, excitation difference of phase and distance between piston centres. Then and in order to get closer to realistic configurations, the calculations are carried out in the cases of two adjacent and distant closed-box loudspeakers.

A test bench enables then the effects of an incident sound field on a closed-box loudspeaker to be measured. The configuration is chosen in order to eliminate any diffraction and significant mutual effects

likely to distort the results. The aim of this first experiment is to highlight every potential measurement difficulty in order to determine the measurement setup, as well as to validate the choice of the measured quantities (input impedance and volume velocity).

Once the orders of magnitude of the modifications in loudspeaker behaviour are evaluated, the study focuses on three different loudspeaker configurations beginning with the most simple case of two closed-box systems mounted in a baffle, and ending with most realistic ones, corresponding to the configurations of loudspeakers mounted in an array (two adjacent and distant closed-box systems).

It is worth noting here that the measurement accuracy of the Thiele and Small's parameters plays an essential role in this study.

The results of the measurements carried out in each configuration are finally compared to the theoretical predictions, enabling calculation methods to be validated.

Version abrégée

Dans le cadre d'un projet de contrôle actif du bruit en extérieur, il s'est avéré nécessaire de savoir de quelle façon le comportement d'une source secondaire (haut-parleur électrodynamique monté dans un réseau) pouvait être modifié par l'effet du champ primaire incident ou par celui du champ provenant des autres haut-parleurs du réseau. Comme ces modifications de comportement n'ayant à notre connaissance jamais été considérées lors de la conception de systèmes haut-parleurs, cette thèse propose des méthodes de calcul et de mesure permettant de prédire s'il y a lieu d'en tenir compte.

L'étude se divise en deux parties. La première est consacrée aux modélisations, aux aspects théoriques et aux calculs, alors que la deuxième présente les validations expérimentales en chambre anéchoïque.

La modélisation d'un haut-parleur électrodynamique par des schémas équivalents démontre que son comportement peut être entièrement déterminé à partir de son impédance électrique d'entrée. L'idée de départ est de postuler que les modifications de comportement dues à la présence d'un champ incident devraient pouvoir être analysées à partir de cette impédance. La méthode choisie consiste ainsi à analyser ces modifications non plus sous la forme d'une impédance de rayonnement, mais en termes de débit et d'impédance électrique d'entrée. Etant définie aux bornes du haut-parleur, cette dernière grandeur présente l'avantage non négligeable d'être très facilement mesurable.

Dans le cadre de cette thèse, les haut-parleurs sont supposés se comporter en pistons plats rigides. Les calculs sont basés sur les paramètres de Thiele et Small, sur l'intégrale de Rayleigh et sur les théories géométrique et unifiée de la diffraction. Ils permettent d'obtenir, pour chaque haut-parleur, aussi bien son impédance d'entrée, son débit, sa pression acoustique rayonnée en champ proche ou lointain, que sa force d'action ou son impédance de rayonnement. Tenant compte des effets d'interaction, ils permettent également de prédire les modifications de toutes ces grandeurs aussi bien en amplitude qu'en phase. Une approche numérique a été choisie afin de minimiser les temps de calcul. Les différentes discrétisations sont fixées de manière à assurer une précision suffisante eu égard aux incertitudes des mesures de validation.

Afin de procéder à l'évaluation des ordres de grandeur des modifications, des calculs ont tout d'abord été effectués dans le cas simple de deux haut-parleurs montés sur enceintes closes en écran infini. Ces calculs ont également permis de mettre en évidence les variations des modifications d'impédance d'entrée et de débit en fonction des excitations (rapport et déphasage) et de la distance séparant les centres des pistons. L'étude s'est ensuite tournée vers des configurations plus réalistes, mettant en jeu deux haut-parleurs montés sur enceintes closes, adjacents, puis distants.

Un banc de mesure destiné à l'évaluation des effets d'un champ incident sur le comportement d'un haut-parleur monté en enceinte close a été réalisé. Afin de mettre en évidence toutes les difficultés potentielles de cette mesure, la configuration choisie élimine tout effet de diffraction ou d'interaction pouvant altérer les résultats. Elle permet également de valider le choix des deux grandeurs à mesurer (impédance d'entrée et débit).

Une fois les ordres de grandeur des modifications de l'impédance d'entrée et du débit évalués, l'étude se consacre aux mesures proprement dites. Cette dernière partie débute par une configuration simple de deux haut-parleurs montés en enceintes closes sur un écran, pour aboutir à des cas plus réalistes correspondant par exemple à ceux de haut-parleurs montés en réseau (deux haut-parleurs montés en enceintes closes, adjacents et distants).

Il est intéressant de noter l'importance de la précision des paramètres de Thiele et Small dans ce travail. Il a été nécessaire de vouer un soin extrême à leur détermination et à l'étude des effets de leur incertitude.

Les résultats des mesures effectuées dans chaque configuration sont finalement confrontés aux prévisions théoriques, permettant ainsi de valider les méthodes de calcul proposées.

Acknowledgements

While a thesis is generally considered as being an individual work, I would like to thank all the people who have been involved in its realisation.

First of all, I would like to express my most sincere gratitude to Prof. Mario Rossi who offered me the possibility to join the LEMA. Before accepting to supervise this thesis, he gave me the opportunity to work for three years as a research assistant within the framework of different European and industrial projects. Many thanks to him for having put his trust in me.

I would also like to express my gratitude to the members of the jury, Dr R.H.Small, M. H.Massin, Prof. M.Jufer and Prof. Ph.Robert, for accepting the task of examining my work and helping me to improve the quality of the manuscript with their suggestions. Many thanks also to Dr Ph.Herzog for the constructive endless "discussions" about loudspeakers. I hope to have taken in at least twenty percent of the huge amount of information he has been able to share.

I would like to address a special thanks to my favourite singer Patrick R.W. Roe, who helped me to improve the english of this thesis. I thank him also warmly for his English sense of humour and generosity of spirit.

Also sincere thanks to Prof. Juan Mosig, head of the LEMA, for sharing his joy of living and his passion for music. My warmest thanks go also to the LEMA staff from the present and past, Alix Wend and Roland Dupuis to begin with, who have contributed to render my stay in this laboratory pleasant and funny. Special thanks to Delphine Bard and Olivier Meylan, my co-sharing office colleagues, for having put up with my moody behaviour during the last months of this thesis.

Last but by no means least, I would like to thank warmly my parents, my brother Benoît and his wife Teresa for they support in all events. I would also like to thank them for their understanding and patience during all the time of my studies. All my love...

A last word to say that this work was partly supported by the Swiss Federal Office for Education and Science (OFES), within the framework of the European outdoor active noise control project entitled *Silence Light*.

Contents

Introduction

Framework

Within the framework of an outdoor active noise control project, an unusual and specific need arose, namely to establish whether anti-noise sources (loudspeakers mounted in an array) are likely to be affected by the primary noise or by the interactions between them. These kinds of modifications in behaviour are almost never considered during the design of conventional loudspeaker systems.

The focus of this thesis will be solely on electrodynamic loudspeakers, invented in 1925 by C.W. Rice and E.W. Kellogg. The reason is that from that time on, they established themselves as the leading kind of driver in the great majority of applications.

It is also worth noting here that, within the scope of this thesis, the loudspeakers will be mounted only on closed boxes. This choice was made according to the sources specifications of the active noise control project, which contained an essential requirement related to the quality of the phase response, that is, a group delay as small as possible. Some analyses and syntheses carried out within the framework of the project showed that at comparable performance the group delay is in general higher with vented systems as opposed to closed-box systems (see the paper entitled "Amplitude and phase synthesis of loudspeaker systems").

Objectives

The aim of this thesis is therefore to provide computation and measurement methods allowing to predict whether the effects of an incident sound field on a loudspeaker have to be taken into account during the design phase.

The purpose of this thesis is to judge if these effects can be effectively studied as modifications of input impedance and volume velocity, instead of the usual radiation impedance. On the one hand, the electrical quantities (current and voltage), that are located at the driver terminals, offer the advantage of being easily measurable when the radiation impedance and sound pressure are non uniform. On the other hand, the volume velocity modifications offer the advantage of being more or less of the same order of magnitude as those of radiated sound pressure.

Thesis structure

This thesis comprises a theoretical part involving modelling, theory and computations using tools such as *Matlab* or *Mathematica*, and an experimental part carried out in an anechoic chamber, the aim of which is to validate the calculations.

- The first chapter treats lumped-constant models which are the basis of any loudspeaker analyses and syntheses in the low-frequency range. Once reduced to equivalent electrical, mechanical or acoustical circuits, they enable electrical input impedance and volume velocity in amplitude and phase to be calculated. The chapter ends with an elementary theoretical development enabling the whole thesis content to be easily understood.
- The second chapter states the theories necessary for the interaction calculations between two closed-box loudspeakers mounted firstly in an infinite baffle, secondly in a limited baffle and finally without any baffle. This chapter goes through a numerical approach of the Rayleigh's surface integral as well as geometrical and unified theories of diffraction.
- The third chapter applies the theories of the second chapter to the concrete case of a loudspeaker model determined by the parameters stemming from the first chapter. The calculations, carried out in the case of two closed-box loudspeakers mounted in an infinite baffle, enable the input impedance, volume velocity, near and far field sound pressure, as well as medium reaction force and radiation impedance to be obtained for each loudspeaker. Taking into account interaction effects, they also enable the modifications of all these quantities in modulus and phase to be predicted. These modifications are also studied according to the excitations ratio, excitations difference of phase and distance between piston centres. Then, the calculations are recalculated in the case of two adjacent and distant closed-box loudspeakers, taking into account the diffraction at the enclosure edges.
- The fourth chapter proposed a preliminary experiment, which is devised in order to highlight every potential measurement difficulty enabling the measurement set-ups to be determined as well as the choice of the measured quantities (input impedance and volume velocity) to be validated. Then, after a discussion about the variations of measured TS parameters, the chapter focuses on three experimental configurations leading to theoretical prediction validations.

Finally, the experimental configuration of two closed-box loudspeakers mounted face-to-face is proposed in appendix. Whilst this case does not meet any technological need, it is nevertheless interesting because it shows two loudspeakers highly coupled.

Terminology

In this thesis, the terms driver and loudspeaker are used indifferently in order to describe the component assembly shown in figure 1.1. The symbols, acronyms and abbreviations are listed after the appendices.

Chapter 1

Loudspeaker system models

Sections 1.1 to 1.5 constitute above all a digest of well-known work that is necessary to understand this thesis. Readers familiar with this material can go straight to Section 1.6.

1.1 Description of an electrodynamic loudspeaker

The purpose of loudspeakers is to radiate sound, converting electrical power into acoustic waves practically always via an electro-mechanical transduction. Electrodynamic loudspeakers carry out this process using a diaphragm (generally cone shaped) which is set in motion by an electrodynamic motor. Figure 1.1 shows the cutaway view of a typical mid-range driver, such as those used in this work.

As shown in this figure, an electrodynamic driver comprises four parts according to their functions:

1. Made up of a cone and a dust cap, the **diaphragm** is the radiating component. The dust cap, in the shape of a dome or inverted dome, is used to avoid any dust or foreign particles getting into the motor.

2. The **suspensions** are the spider (inner part) and the surround or hinge (outer part). They play a key role in the smooth functioning of the whole system. Their main purpose consists in holding the diaphragm while guiding it axially, as well as exerting a restoring force on the voice coil to keep it in the air gap.

3. The electrodynamic **motor** is made up of a voice coil and a magnetic circuit (pole piece, back and front plates and magnet). The voice coil is located in the air gap between pole piece and front plate.

4. The **frame**, often called basket or chassis, has to ensure the accurate alignment of all the driver components. It can also contribute, in some cases, to the motor heat dissipation. An optional gasket may be added to the cone perimeter to avoid supplementary leakages and facilitate the driver mounting on a baffle or box.

The **moving system** is made up of the diaphragm, the suspensions and the voice coil. It represents a mechanical resonator.

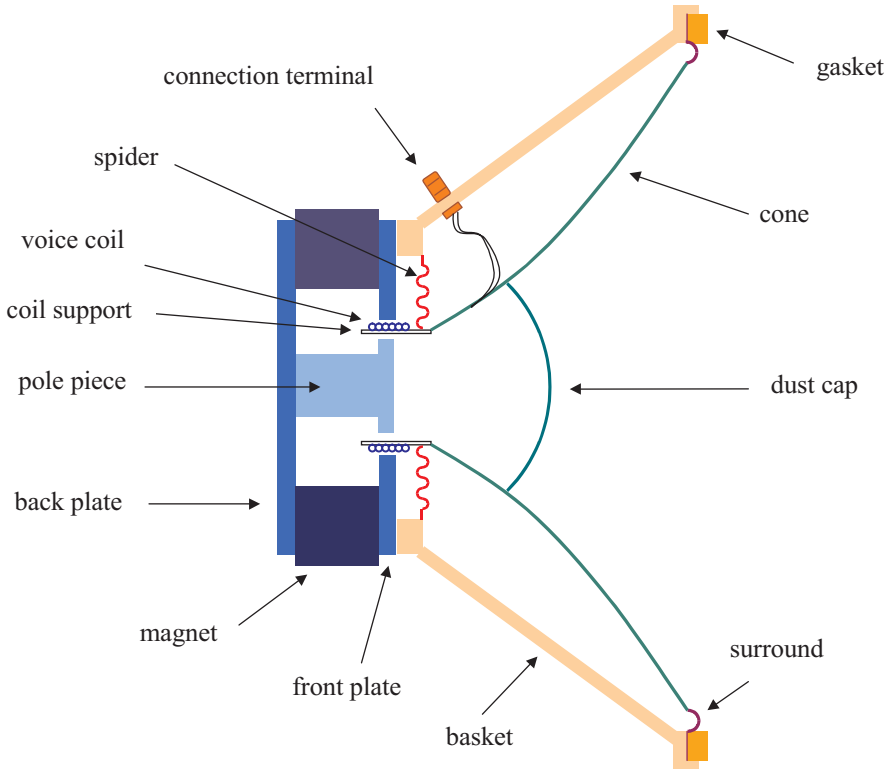

Figure 1.1 - *Drawing of an electrodynamic loudspeaker (mid-range woofer)*

1.2 Low frequency model

When the loudspeaker size is considered to be small compared to the wavelength in air, its diaphragm is assumed to behave like a flat rigid piston of radius a ($ka < \sqrt{2}$). Mounted in an infinite baffle or in a box in order to separate backward and forward radiations, the loudspeaker can then be described by a lumped-constant circuit comprising electrical, mechanical and acoustic elements [12] (fig. 1.2).

The use of a gyrator for the electromechanical coupling has been preferred in order to be in an impedance-type analogy. In order to remain in the direct analogy, the mechanoacoustical coupling is represented by a transformer, in order to have the volume velocity as a through quantity.

Let us describe the electrical, mechanical and acoustic parts, according to the elements in figure 1.2.

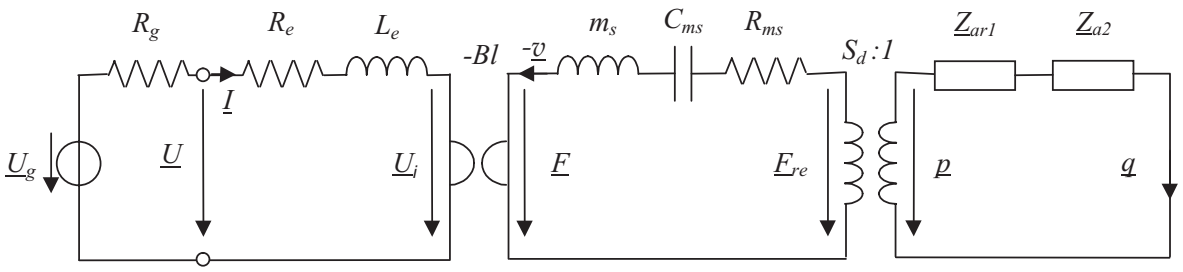

Figure 1.2 - *Lumped-constant model of an electrodynamic loudspeaker mounted in an infinite baffle or in a box*

The two coupling coefficients are the electrodynamic one Bl, in which B is the radial induction in the gap and l the length of the conductor (voice-coil), and the effective projected surface area of the loudspeaker diaphragm $S_d = \pi a^2$.

The electrical part includes the amplifier, the connecting wires and the voice-coil. The former is represented by the no-load voltage $\underline{U}_g$ of a real voltage source and its internal resistance R_g. The latter is represented by the self-inductance L_e and the resistance R_e equivalent to the electrical and magnetic losses in the motor. The quantities are:

- the voltage at the loudspeaker terminals $\underline{U}$,
- the current across the loudspeaker $\underline{I}$,
- the induced voltage $\underline{E} = -\underline{U}_i = -(Bl)\,\underline{v}$.

The input impedance $\underline{Z}$ is the ratio: $\underline{U}/\underline{I}$.

The moving system constitutes the mechanical part. It is made up of a moving mass m_s, a mechanical compliance C_{ms} corresponding to the suspensions and a mechanical loss resistance R_{ms} due to suspensions internal frictions. The quantities are:

- the magnetic force $\underline{F} = (Bl)\,\underline{I}$,
- the reaction force of the medium $\underline{F}_{re}$, representing the sound pressure at the diaphragm surface,
- the moving system velocity $\underline{v}$.

The acoustic part is made up of two acoustic impedances: the forward radiation one $\underline{Z}_{ar1}$ and the backward one $\underline{Z}_{a2}$. The latter corresponds to the radiation impedance $\underline{Z}_{ar2}$ in the case of a loudspeaker mounted in a baffle, and to the box impedance $\underline{Z}_{ab}$ in the case of loudspeaker mounted in a box. The quantities are:

- the sound pressure $\underline{p} = \underline{F}_{re}/S_d$,
- the volume velocity $\underline{q}$.

1.3 Equivalent circuits

In order to simplify loudspeaker analysis and synthesis in the low-frequency range, it is possible and usual to represent the circuit of figure 1.2 by its equivalent acoustical, electrical or mechanical circuits, depending on the needs [14, 15]. As a rule and in order to identify easily the nature of components, the mechanical components are identified by "m" and the acoustic ones by "a".

In the low-frequency range and as a first approximation, the voice coil inductance L_e and its equivalents may be neglected, as we shall see later (R_e^2 large compared with $\omega^2 L_e^2$). They are thus removed from the equivalent circuits.

Let us first discuss the case of a loudspeaker mounted in an infinite baffle. Reduced to three elements in series, the equivalent acoustical circuit drawn in figure 1.3, appears to be the most interesting out of the three because it enables the volume velocity to be calculated as a function of the electrical excitation through its acoustical equivalent:

$$\underline{p}_g = \frac{\underline{U}_g Bl}{S_d(R_g + R_e)} \tag{1.1}$$

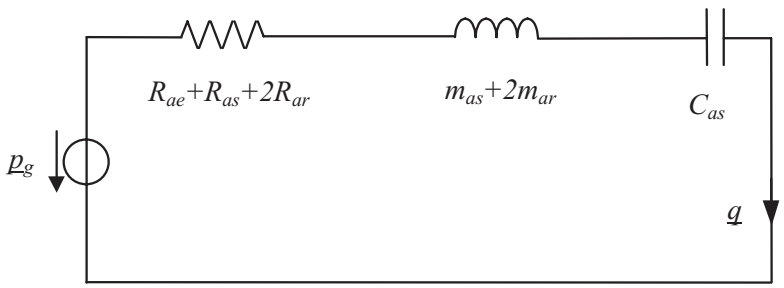

Figure 1.3 - *Equivalent acoustical circuit of an electrodynamic loudspeaker mounted in an infinite baffle*

The acoustic backward and forward radiation impedances are identical. They are represented by the acoustic radiation mass m_{ar} and acoustic resistance R_{ar}. The elements R_{ae}, R_{as}, m_{as} and C_{as} are the acoustic equivalents of the electrical and mechanical components $R_g + R_e$, R_{ms}, m_s and C_{ms}:

$$R_{ae} = \frac{(Bl)^2}{S_d^2(R_g + R_e)} \tag{1.2}$$

$$R_{as} = \frac{R_{ms}}{S_d^2} \tag{1.3}$$

$$m_{as} = \frac{m_s}{S_d^2} \tag{1.4}$$

$$C_{as} = S_d^2 C_{ms} \tag{1.5}$$

Let us now draw the corresponding equivalent electrical circuit, enabling the input impedance $\underline{Z}$ to be easily calculated (fig. 1.4).

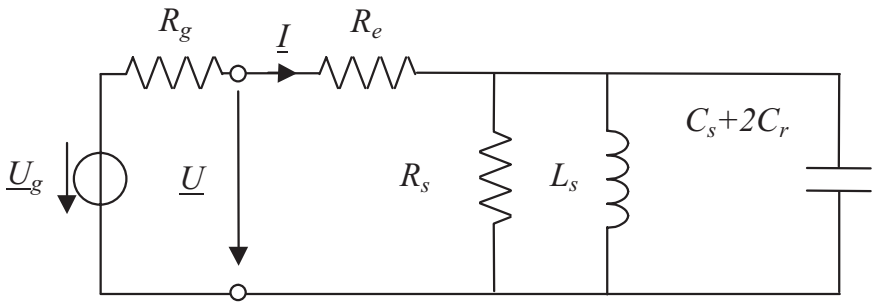

Figure 1.4 - *Equivalent electrical circuit of an electrodynamic loudspeaker mounted in an infinite baffle*

The elements R_s, L_s, C_s and C_r are respectively equivalent to the mechanical and acoustic elements R_{ms} and R_{ar}, C_{ms}, m_s and m_{ar}, with:

$$R_s = \frac{(Bl)^2}{R_{ms} + 2\ S_d^2 R_{ar}} \tag{1.6}$$

$$L_s = C_{ms}(Bl)^2 \tag{1.7}$$

$$C_s = \frac{m_s}{(Bl)^2} \tag{1.8}$$

$$C_r = \frac{m_{ar} S_d^2}{(Bl)^2} \tag{1.9}$$

When the driver is mounted in a closed box of internal net volume V_b, the acoustic backward radiation impedance is identified as an acoustic compliance:

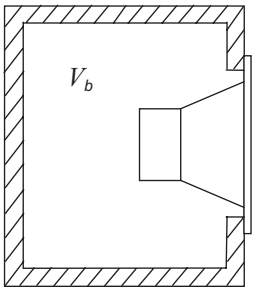

Figure 1.5 - *Cutaway view of a closed-box loudspeaker*

$$C_{ab} = \frac{\beta V_b}{\rho c^2} \qquad (1.10)$$

where ρ is the mass density, c the speed of sound and β a compliance factor equal to 1 for an empty box

In order to improve the model accuracy, an acoustic resistance R_{ab} (losses in the box) and an acoustic mass m_{ab} (kinetic energy) are associated to this compliance. The acoustic forward radiation impedance is again represented by an acoustic radiation mass (m_{ar}) and an acoustic radiation resistance (R_{ar}).

As previously, the equivalent acoustical circuit may be simplified to three elements in series (fig. 1.6): the acoustic resistance R_{ac}, the acoustic mass m_{ac} and the acoustic compliance C_{ac}.

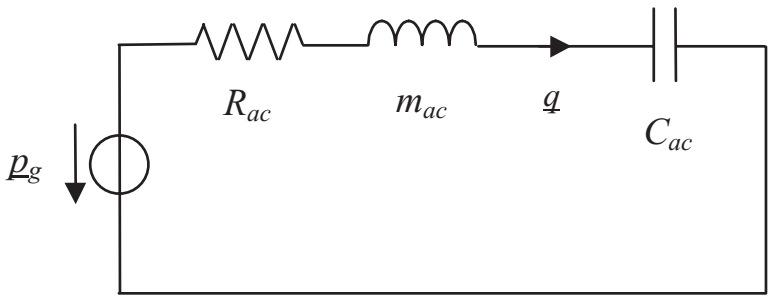

Figure 1.6 - *Equivalent acoustical circuit of an electrodynamic loudspeaker mounted in a closed box*

$$R_{ac} = R_{ae} + R_{as} + R_{ar} + R_{ab} \qquad (1.11)$$

$$m_{ac} = m_{as} + m_{ar} + m_{ab} \qquad (1.12)$$

$$C_{ac}^{-1} = C_{as}^{-1} + C_{ab}^{-1} \tag{1.13}$$

This acoustical equivalent circuit enables the membrane volume velocity to be readily calculated as a function of frequency:

$$\underline{q} = \frac{\underline{p}_g}{R_{ac} + j\omega m_{ac} + \frac{1}{j\omega C_{ac}}} \tag{1.14}$$

The equivalent electrical circuit may be reduced to the simplified one, drawn in figure 1.7.

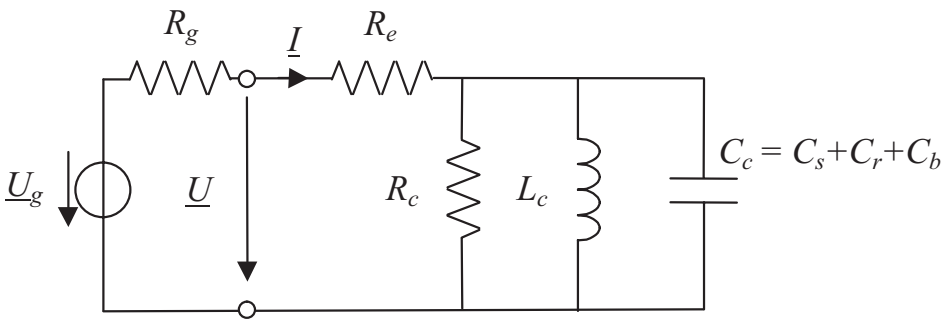

Figure 1.7 - *Equivalent electrical circuit of an electrodynamic loudspeaker mounted in a closed box*

The elements R_c, L_c and C_c are respectively equivalent to the mechanical or acoustic elements:

$$R_c = \frac{(Bl)^2}{R_{ms} + S_d^2\,(R_{ar} + R_{ab})} \tag{1.15}$$

$$L_c^{-1} = L_s^{-1} + L_b^{-1} \quad with \quad L_b = \frac{C_{ab}\,(Bl)^2}{S_d^2} \tag{1.16}$$

$$C_c = \frac{m_s}{(Bl)^2} + \frac{(m_{ar} + m_{ab})\,S_d^2}{(Bl)^2} \tag{1.17}$$

This electrical equivalent circuit enables the input impedance to be readily calculated as a function of frequency:

$$\underline{Z} = \frac{\underline{U}}{\underline{I}} = R_e + \frac{1}{\frac{1}{R_c} + j\omega C_c + \frac{1}{j\omega L_c}} = R_e + \frac{Bl^2/S_d^2}{R_{as} + R_{ar} + R_{ab} + j\omega m_{ac} + \frac{1}{j\omega C_{ac}}} \tag{1.18}$$

1.4 Thiele and Small parameters

The behaviour of a loudspeaker mounted in different assemblies is better described using the small-signal parameters, called the Thiele and Small's parameters. In the following, these parameters will be named TS parameters [14–16, 20, 21].

In the case of a loudspeaker mounted in an infinite baffle, they are:

- the resonance frequency

$$f_s = \frac{1}{2\pi\sqrt{(m_{as} + 2m_{ar})C_{as}}} = \frac{1}{2\pi\sqrt{(C_s + 2C_r)L_s}} \tag{1.19}$$

- the electrical quality factor at f_s

$$Q_e = 2\pi f_s (C_s + 2C_r)(R_g + R_e) \tag{1.20}$$

  which becomes Q_{es} when R_g is zero.

- the mechanical quality factor at f_s

$$Q_{ms} = 2\pi f_s (C_s + 2C_r) R_s \tag{1.21}$$

- the total quality factor at f_s

$$Q_t = \frac{Q_e Q_{ms}}{Q_e + Q_{ms}} \tag{1.22}$$

  which becomes Q_{ts} when R_g is zero.

- the equivalent volume of air V_{as}

$$V_{as} = \rho\, c^2\, S_d^2\, C_{ms} \tag{1.23}$$

In addition to these parameters there are three other ones:

- the output resistance of source R_g,
- the voice coil DC resistance R_e, and
- the effective projected area S_d of loudspeaker diaphragm, the diameter of which $2a$ is generally measured from the middle of the flexible edge suspensions.

In the same way, the TS parameters related to a loudspeaker mounted in a closed box are:

- the resonance frequency

$$f_c = \frac{1}{2\pi\sqrt{m_{ac}C_{ac}}} = \frac{1}{2\pi\sqrt{C_c L_c}} \tag{1.24}$$

- the electrical quality factor at f_c

$$Q_{ec} = 2\pi f_c C_c (R_g + R_e) \tag{1.25}$$

  which becomes Q_{eco} when R_g is zero.

- the mechanical quality factor at f_c

$$Q_{mc} = 2\pi f_c C_c R_c \tag{1.26}$$

- the total quality factor at f_c

$$Q_{tc} = \frac{Q_{ec}Q_{mc}}{Q_{ec} + Q_{mc}} \tag{1.27}$$

  which becomes Q_{tco} when R_g is zero.

Finally, the parameters related to the box of internal volume V_b are: the compliance factor β, the acoustic resistance R_{ab} and mass m_{ab}, and the compliance ratio

$$\alpha = \frac{C_{as}}{C_{ab}} = \frac{V_{as}}{\beta V_b} \tag{1.28}$$

The TS parameters are generally given by loudspeaker manufacturers. Due to production tolerances, these parameters differ from each individual loudspeaker of the same type. As it will be seen

in Subsection 4.2.3, this parameter dispersion is deemed to be unacceptable in the framework of this thesis. Furthermore, these parameters vary notably on the one hand with the voice-coil heating (non-invariant), and on the other hand with the excitation (non-linearity of suspension, ...). They have thus to be carefully measured for each loudspeaker working conditions, related to the excitation amplitude and preheating state, as far as possible. The chosen measurement method of these parameters is developed in Appendix B.

1.5 Basic relations

Many computations in this thesis are based on the following set of basic relations [12], deduced from the TS parameters as follows, with C_{ab} and α according respectively to equations 1.10 and 1.28:

$$Bl = \sqrt{\frac{R_e \rho c^2 S_d^2}{2\pi f_s Q_{es} V_{as}}} \tag{1.29}$$

$$C_{as} = \frac{V_{as}}{\rho c^2} \tag{1.30}$$

$$R_{ae} = \frac{Bl^2}{S_d^2 (R_g + R_e)} \tag{1.31}$$

$$R_{as} = \frac{1}{Q_{ms} 2\pi f_s C_{as}} \tag{1.32}$$

$$f_c = f_s \sqrt{1 + \alpha} \tag{1.33}$$

$$Q_{mc} = Q_{ms} \frac{f_c}{f_s} \tag{1.34}$$

$$Q_{tc} = Q_{ts} \frac{R_g + R_e}{R_e} \frac{f_c}{f_s} \tag{1.35}$$

$$Q_{ec} = Q_{es} \frac{R_g + R_e}{R_e} \frac{f_c}{f_s} \tag{1.36}$$

$$C_{ac} = \frac{C_{as} C_{ab}}{C_{as} + C_{ab}} \tag{1.37}$$

$$m_{ac} = \frac{C_{ac}}{(2\pi f_c)^2} \tag{1.38}$$

Once all these quantities are known, the volume velocity $\underline{q}$ and input impedance $\underline{Z}$ calculations may be carried out.

In synthesis, the parameters are determined according to the required target performance of the system. The difficulty lies here in the fulfilment of several constraints which could lead to a supernumerary data synthesis problem, due to system specifications and technical feasibility. Let us note in passing that an illustration of the difficulties met in supernumerary data syntheses is given in the AES preprint "Amplitude and phase synthesis of loudspeaker systems" (see Author's publications). Synthesis will not be investigated in this thesis.

1.6 One closed-box loudspeaker subjected to an external force

A closed-box loudspeaker can also be modelled from its equivalent mechanical circuit, where $\underline{F}_{re}$ is the reaction force of the medium, $\underline{Z}_{mr}$ the radiation impedance and $\underline{v}$ the uniform membrane velocity (rigid piston hypothesis of Section 1.2).

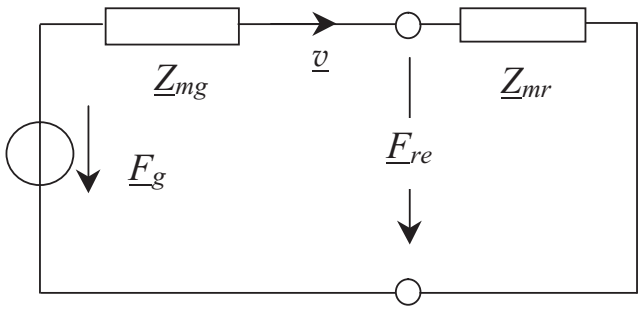

Figure 1.8 - *Equivalent mechanical circuit of a closed-box loudspeaker*

With the force source written as:

$$\underline{F}_g = \underline{U}_g \frac{Bl}{R_g + R_e} \tag{1.39}$$

and the source impedance as:

$$\underline{Z}_{mg} = \frac{(Bl)^2}{(R_g + R_e)} + (R_{ms} + S_d^2 R_{ab}) + j\omega(m_s + S_d^2 m_{ab}) + \frac{S_d^2}{j\omega C_{ac}} \tag{1.40}$$

Let us now suppose that the excitation voltage $\underline{U}_g$ is zero, therefore $\underline{F}_g$ is also zero, and that an external force is applied on the driver, for example the one of an incident sound field. Because an

electrodynamic loudspeaker is reversible, it behaves as a sound sensor. Thus, if the resistance R_g, consequently $\underline{Z}_{mg}$, remain unchanged, the equivalent mechanical circuit becomes that of figure 1.9.

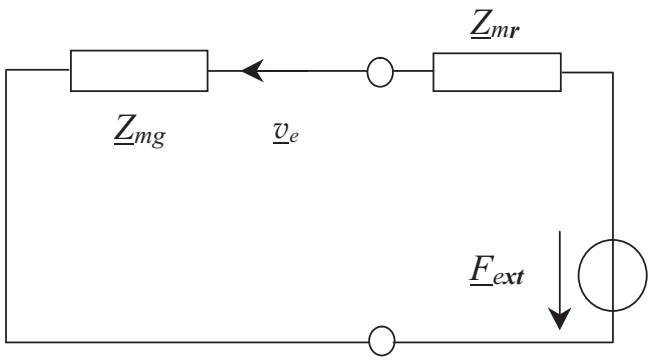

Figure 1.9 - *Equivalent mechanical circuit of a closed-box loudspeaker behaving as a sound sensor*

The principle of superposition enables the loudspeaker behaviour subjected simultaneously to an electrical excitation $\underline{U}_g$ represented by $\underline{F}_g$, and to an acoustical one, represented by $\underline{F}_{ext}$, to be found. As shown in figure 1.10, the acoustical prompting effect leads to a modification of the velocity $\underline{v}$ in $\underline{v}' = \underline{v} + \underline{v}_e$. The volume velocity $\underline{q}$ will be thus modified in $\underline{q}'$ in the same way.

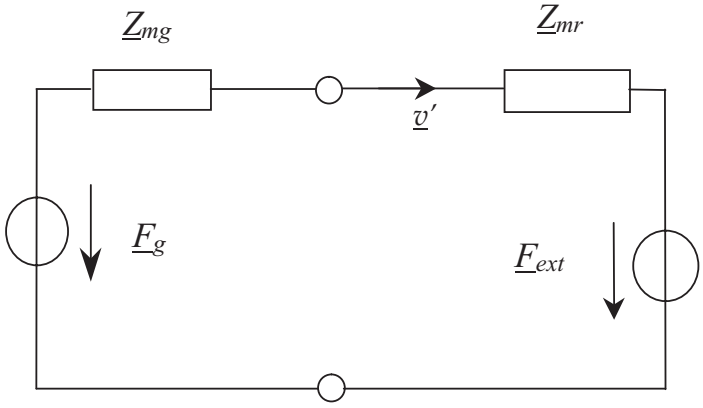

Figure 1.10 - *Equivalent mechanical circuit of a closed-box loudspeaker subjected to electrical and acoustical promptings*

1.7 Interactions between two closed-box loudspeakers: elementary theory

The problem of interaction between two loudspeakers can be simply defined by the following elementary development.

Let us assume that LSP_0 and LSP_1 are two loudspeakers. Each of them are assumed to be driven by an independent source, being able to be controlled separately. Thus, it is possible to consider three successive cases, where only LSP_0 is fed, then where only LSP_1 is fed, and finally where the both are driven simultaneously. In the two first cases, the reflections made in Section 1.6 may be applied, enabling the equivalent piston velocities to be found for each piston, and consequently every interesting quantities, according to the equations:

$$\underline{F}_{g_0} - (\underline{Z}_{mg_0} + \underline{Z}_{mr_0})\,\underline{v}_0 = 0 \tag{1.41}$$

$$\underline{F}_{g_1} - (\underline{Z}_{mg_1} + \underline{Z}_{mr_1})\,\underline{v}_1 = 0 \tag{1.42}$$

In the third case, each loudspeaker is assumed to be subjected to an external force $\underline{F}_{ext}$ due to the sound pressure radiated by the other one. The force of LSP_0 on LSP_1 is called $\underline{F}_{10}$ and conversely, the force of LSP_1 on LSP_0 is called $\underline{F}_{01}$. Thus, two new equations can be written from the circuit of figure 1.10:

$$\underline{F}_{g_0} - (\underline{Z}_{mg_0} + \underline{Z}_{mr_0})\,\underline{v}'_0 - \underline{F}_{01} = 0 \tag{1.43}$$

$$\underline{F}_{g_1} - (\underline{Z}_{mg_1} + \underline{Z}_{mr_1})\,\underline{v}'_1 - \underline{F}_{10} = 0 \tag{1.44}$$

These equations enable the new velocities $\underline{v}'_0$ and $\underline{v}'_1$ to be found. It is of course obvious that the problem here is to calculate the external forces $\underline{F}_{01}$ and $\underline{F}_{10}$.

Let us tackle this calculation on the basis of two simplifying hypotheses:

1. The loudspeakers radiate as monopoles. The sound pressures at a distance d can be thus written as [12]:

$$\underline{p}_0 = j\ Z_c\ k\ \underline{q}'_0\ \frac{e^{-jkd_0}}{4\pi d_0} \tag{1.45}$$

$$\underline{p}_1 = j\ Z_c\ k\ \underline{q}'_1\ \frac{e^{-jkd_1}}{4\pi d_1} \tag{1.46}$$

with the volume velocities $q'_{0,1}$ being the product $S_{d_{0,1}}\ \underline{v}'_{0,1}$, where $S_{d_{0,1}}$ are the equivalent pistons surfaces of LSP_0 and LSP_1.

2. The sound pressure radiated by LSP_0 is uniformly distributed on LSP_1 surface, and conversely. The external forces may be thus simply written as:

$$\underline{F}_{01} = S_{d_0}\ \underline{p}_{01} = S_{d_0}\ j\ Z_c\ k\ \underline{v}'_1\ S_{d_1}\ \frac{e^{-jkr}}{2\pi r} \tag{1.47}$$

$$\underline{F}_{10} = S_{d_1}\ \underline{p}_{10} = S_{d_1}\ j\ Z_c\ k\ \underline{v}'_0\ S_{d_0}\ \frac{e^{-jkr}}{2\pi r} \tag{1.48}$$

where r is the distance between piston centres, as shown in figure 1.11.

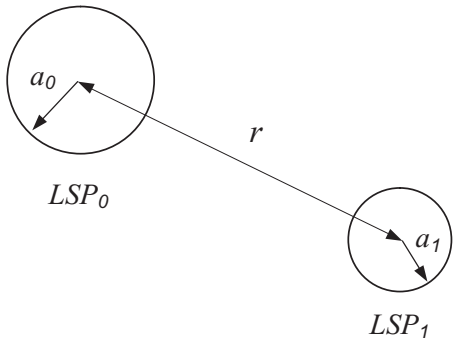

Figure 1.11 - *Depiction of two pistons separated by a distance r*

The introductions of relations 1.47 in 1.43, respectively the 1.48 in 1.44, give the below set of two equations with two unknowns $\underline{v}'_0$ and $\underline{v}'_1$:

$$\underline{F}_{g_0} - (\underline{Z}_{mg_0} + \underline{Z}_{mr_0})\ \underline{v}'_0 - S_{d_0}\ j\ Z_c\ k\ \underline{v}'_1\ S_{d_1}\ \frac{e^{-jkr}}{4\pi r} = 0 \tag{1.49}$$

$$\underline{F}_{g_1} - (\underline{Z}_{mg_1} + \underline{Z}_{mr_1})\ \underline{v}'_1 - S_{d_1}\ j\ Z_c\ k\ \underline{v}'_0\ S_{d_0}\ \frac{e^{-jkr}}{4\pi r} = 0 \tag{1.50}$$

These two equations lead thus to the values of $\underline{v}'_0$ and $\underline{v}'_1$, that now still have to be compared to the velocity values $\underline{v}_0$ and $\underline{v}_1$ without any interactions (equ. 1.41 and 1.42)

In reality, the two hypotheses 1 and 2 are too simplistic, because the interactions are expected to be significant above all for small distances between loudspeaker centres (according of course to their dimensions). Thus, it should be necessary, a priori, to develop analytical expressions giving loudspeaker near field sound pressure.

In this thesis, a more direct approach is preferred: instead of using complicated analytical expressions, it is proposed to carry out numerical calculations, reiterated as often as necessary so as to fulfil all required criteria. The computed values will then be compared to experimental results in view of validations.

The starting point is to sum, at the equivalent piston surface of LSP_0, the sound pressures due to a given distribution of elementary sources located on the equivalent piston surface of LSP_1, and vice versa. Once the external forces acting on the two pistons are obtained, the new volume velocities are then calculated in order to reiterate the process. The next chapters will show that two or three iterations will usually be sufficient.

To conclude this chapter, it is important to note that while this thesis work focuses on two identical closed-box loudspeakers, the numerical approach developed in Chapter 2 and applied in Chapter 3 can be generalized without any theoretical problems to configurations comprising several loudspeakers, identical or not. In this case, it is worth noting that the loudspeaker number could be limited by the computer memory capacity.

Chapter 2

Radiation and diffraction theories

2.1 Introduction

The aim of this chapter is to choose the most suitable theoretical methods, according to different loudspeaker configurations, that enable the sound pressure to be calculated anywhere in space.

The sound pressure computation, given as a function of the loudspeaker volume velocity, is carried out without going through the radiated acoustic power. This offers the distinctive advantage of obtaining the phase response of the system. The medium reaction force and the radiation impedance are then calculated according to the sound pressure at the loudspeaker membrane.

First of all, this chapter deals with the theory related to one piston mounted in an infinite baffle (see Section 2.2) in order to establish the necessary basis for calculating the interactions between two pistons mounted in the same infinite baffle (see Section 2.3). Section 2.4 then treats two diffraction theories necessary for the calculations of the sound pressure radiated by a closed-box piston. Finally, these theories are applied to the interaction calculations of two adjacent and separated closed-box pistons (see Section 2.5).

2.2 One loudspeaker in an infinite baffle

At low frequencies, the theory related to one loudspeaker mounted in an infinite baffle is reduced to that of a flat circular piston (radius a) of uniform velocity $\underline{v}$ mounted in an infinite rigid baffle. The latter allows to do away with some phenomena such as interactions between front and rear, reflections or diffractions at the boundaries.

Due to the fact that the Green's function is known, the Huygens-Rayleigh surface integral offers the advantage of being an exact solution of the standard boundary integral equation method [13]. This formula is valid in the near field as well as in the far field.

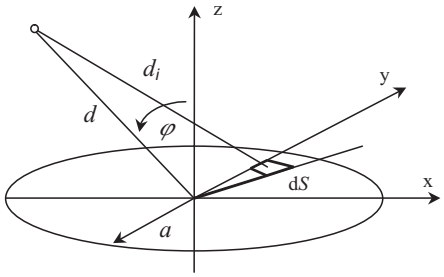

Figure 2.1 - *Piston geometry and observation point*

$$\underline{p} = \frac{jZ_c k\,\underline{v}}{2\pi} \int_{S_d} \frac{e^{-jkd_i}}{d_i}\,\mathrm{d}S \tag{2.1}$$

In the far field, this formula is generally simplified as [12]:

$$\underline{p}(d,\varphi) = jZ_c k S_d\,\underline{v}\,\frac{e^{-jkd}}{2\pi d}\,\frac{2J_1(k\sin\varphi)}{k\sin\varphi} \tag{2.2}$$

The calculation of the reaction force $\underline{F}_{re}$ on the whole piston requires the knowledge of the sound pressure in the immediate vicinity of the piston surface [12]. Thus and according to figure 2.2, the force of a piston on itself is given by:

$$\underline{F}_{re} = \frac{jZ_c k\underline{v}}{2\pi} \int_0^a \rho\,\mathrm{d}\rho \int_0^{2\pi} \mathrm{d}\psi \int_0^a \rho'\,\mathrm{d}\rho' \int_0^{2\pi} \frac{e^{-jkr_s}}{r_s}\,\mathrm{d}\psi' \tag{2.3}$$

ρ and ψ: polar coordinates of dS = ρ dψ dρ

r_s: distance between surface elements

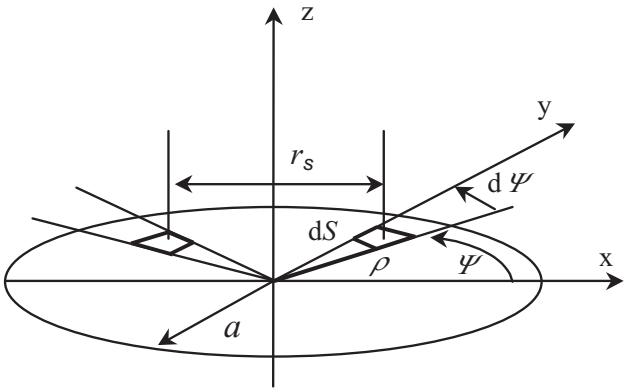

Figure 2.2 - *Piston geometry in cartesian and polar coordinates*

The double surface integral (equ. 2.3) has been solved by Lord Rayleigh in terms of Bessel and Struve functions of first order:

$$\underline{F}_{re} = \underline{q}\rho c\left[1 - \frac{J_1(2ka)}{ka}\right] + j\left[\frac{S_1(2ka)}{ka}\right] \tag{2.4}$$

with

$$\underline{q} = S_d\,\underline{v} \tag{2.5}$$

The radiation impedance (acoustic resistance and reactance) is easily calculated from this force as follows:

$$\underline{Z}_{ar} = \frac{\underline{F}_{re}}{S_d\underline{q}} \tag{2.6}$$

$$R_{ar} = \frac{\rho c}{S_d}\left[1 - \frac{J_1(2ka)}{ka}\right] \qquad and \qquad X_{ar} = \frac{\rho c}{S_d}\left[\frac{S_1(2ka)}{ka}\right] \tag{2.7}$$

A numerical approach may replace the continuous one. To do that, a double surface division is necessary in order to obtain the force and the radiation impedance. Whilst the discrete approach does not improve calculations in terms of time saving due to the simplicity of the analytical solution, it will nevertheless be necessary to study this method in anticipation of interaction computations between two drivers. In the case where the force and radiation impedance have no simple analytical solutions, the discrete approach may even replace the continuous one in order to save computation time (see Section 2.3). Thus, the discrete calculations carried out for a loudspeaker mounted in an infinite baffle, will be useful to determine the numbers of surface elements necessary for accurate calculations of the force.

These two chosen numbers of surface elements are determined by comparing the discrete results with the analytical ones, in such a way as to keep the differences below acceptable quantities (see Subsections 3.3.4 and 3.3.6). These numbers will be used as default values in the next section treating interaction problems between two loudspeakers.

Although detailed studies on the optimal piston surface divisions show that irregular partitions give very good results [2], the method proposed below is nevertheless based on regular surface divisions, which is accurate enough with regard to the computations carried out in this thesis (see Subsections 3.3.4 and 3.3.6).

In a first step, the surface S_d is divided into a discrete number n of small radiating surfaces of same area. The piston is divided in concentric rings of same length, each of them containing $2i$ elements more

than the previous one, i being the elements number of the central circular surface, which is 4 in our case (fig. 2.3).

The near field sound pressure can be thus calculated as [18].

$$\underline{p}_i = \underline{q}_i \frac{jZ_c k}{2\pi d_i} e^{-jkd_i} \tag{2.8}$$

$$\underline{p}\,(x, y, z) = \sum_{i=1}^{n} \underline{p}_i \tag{2.9}$$

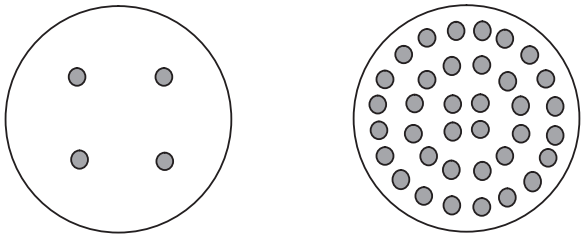

Figure 2.3 - *Examples of piston membrane surface divisions - 4 and 36 radiating elements of same surface area*

A second sampling, in m elements, enables the force and therefore the radiation impedance to be calculated. Any superposition of the element centres is avoided.

$$\underline{F}_{re} = \frac{S_d}{m} \sum_{j=1}^{m} \underline{p}\,(x_j, y_j, 0) \tag{2.10}$$

The values of m_{ar} and R_{ar} can be now deduced from equation 2.10, according to equation 2.6.

This calculated one-side radiation impedance has now to be inserted into the input impedance and volume velocity computations in order to converge to the accurate system responses. Thus, m_{ar} is going to replace the acoustic radiation mass coming from the basic small-signal parameters, while R_{ar} is going to be quite simply added to the system modelling.

2.3 Two loudspeakers in an infinite baffle

Without taking into account the interactions between the loudspeakers LSP_0 and LSP_1, the total sound pressure is calculated via the principle of superposition, by adding pressures relating to the different element volume velocities belonging to each driver.

However, in the case where the interactions can not be neglected, the LSP_0 behaviour is modified according to the activity of LSP_1, and vice-versa. These variations of behaviour are calculated as modifications of force, which lead to modifications of radiation impedance and therefore of volume velocity and input impedance. In the following, LSP_1 will represent the disturbing source and LSP_0 the modified one, with r being the distance between them (fig. 2.4).

Contrary to the preliminary theory given in Section 1.6, this configuration can not be solved analytically, given that the sound pressure distributions on surface may not be considered as uniform (small r).

In most cases, the action of a loudspeaker on another one is described in terms of radiation impedance modifications. The LSP_0 radiation impedance becomes:

$$\underline{Z}'_{ar_0} = \underline{Z}_{ar_0} + \underline{Z}_{ar_{01}} = R'_{ar_0} + j\ X'_{ar_0} = (R_{ar_0} + R_{ar_{01}}) + j(X_{ar_0} + X_{ar_{01}}) \tag{2.11}$$

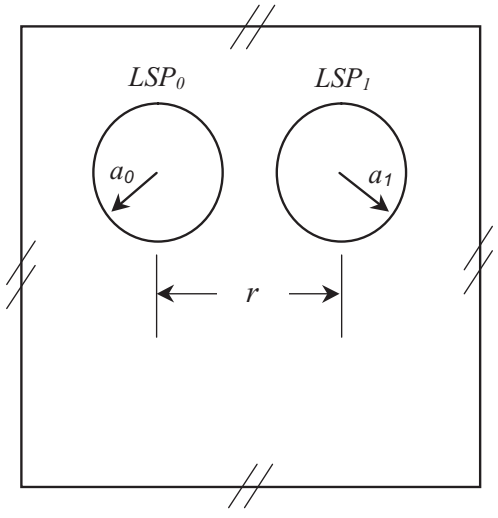

Figure 2.4 - *Depiction of two pistons mounted in an infinite baffle*

Two evaluations of radiation impedance modifications have been given by Pritchard [11] and then by Jacobsen [5] for $r \gg a_{0,1}$ and $ka_{0,1} \ll 1$:

$$R_{ar_{01}} = R_{ar_0}\left[\frac{q_1}{q_0}\,\frac{\sin(kr+\phi)}{kr}\right] \quad m_{ar_{01}} = m_{ar_0}\left[\frac{3\pi}{16}\,\frac{q_1\,a_0}{q_0 r}\,\cos(kr+\phi)\right] \tag{2.12}$$

ϕ : difference of phase between $\underline{q}_1$ *and* $\underline{q}_0$

These results do not take into account the finite size of the disturbing source. It is worth noting that the coupling term tends towards zero if $kr > 1$ (non interacting pistons).

These formulas give a first evaluation of interactions as long as the distance between pistons remains much greater than piston size. This poor resulting accuracy does not fulfil all requirements of this thesis.

Within the framework of the thesis, the modifications are analysed in terms of forces, which lead to volume velocity and input impedance variations. The force exerted by LSP_1 on LSP_0 may be written under the following analytical form, according to [9]:

$$\underline{F}_{01} = \frac{jZ_c k\,\underline{v}_1}{2\pi}\int_0^{a_0}\int_0^{2\pi}\int_{-\sin^{-1}(a_1/r_0)}^{\sin^{-1}(a_1/r_0)}\int_{r_0\cos\alpha-\sqrt{a_1^2-r_0^2\sin^2\alpha}}^{r_0\cos\alpha+\sqrt{a_1^2-r_0^2\sin^2\alpha}} \rho\, e^{-jkr_s}\,\mathrm{d}\rho\,\mathrm{d}\psi\,\mathrm{d}r_s\,\mathrm{d}\alpha \tag{2.13}$$

Figure 2.5 shows the geometry necessary to the understanding of the force analytical equation 2.13 [9].

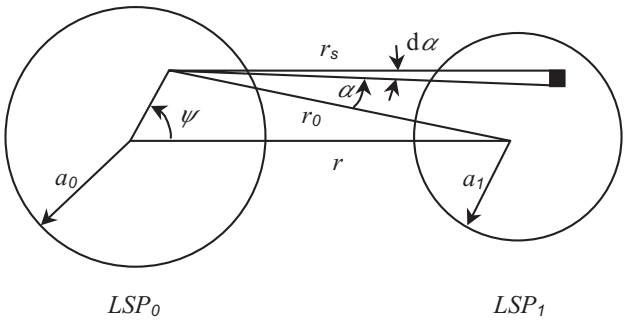

Figure 2.5 - *Geometry necessary to the calculation of the analytical force (equ. 2.13)*

As this integral has no main analytical solution, excepted in particular cases [9], the purpose in this thesis is nevertheless to be able to compute it. That is why a discrete approach is proposed, as mentioned in Subsection 1.7. Let us thus subdivide the surface S_{d_1} into n_1 elements and S_{d_0} into m_0 elements:

$$\underline{p}_{1_i} = \underline{q}_{1_i}\frac{jZ_c k}{2\pi d_{1_i}}e^{-jkd_{1_i}} \quad \rightarrow \quad \underline{p}_1(x,y,z) = \sum_{i=1}^{n_1}\underline{p}_{1_i} \tag{2.14}$$

$$\underline{F}_{01} = \frac{S_{d_0}}{m_0} \sum_{i=1}^{m_0} \underline{p}_1(x_{0_i}, y_{0_i}, 0) \quad \Rightarrow \quad \underline{Z}_{ar_{01}} = \frac{\underline{F}_{01}}{S_{d_0}\underline{q}_0} \quad \Rightarrow \quad R_{ar_{01}} \quad and \quad m_{ar_{01}} \tag{2.15}$$

2.4 One closed-box loudspeaker

The study of a piston mounted in an infinite baffle developed in Section 2.2 is peculiar in that its radiation may be calculated according to analytical approaches. Whilst this assembly is commonly considered to be the ideal theoretical one due to the absence of any corrupting phenomena, it is of small interest in practice, except for dedicated applications where drivers are mounted on bare walls, being considered as infinite baffles with regard to piston size. Normally, loudspeakers are mounted in closed or vented boxes which are designed on the basis of driver types and application requirements.

The enclosure does away with direct interferences resulting from front and rear driver radiations. However, the diffraction at the enclosure edges has now to be taken into account. The diffracted field may be calculated in the form of infinite series only for elementary cases where the wave equation is resolved by variable separation. However, in most cases we can have recourse to approximate solutions.

Since these series converge very slowly at high frequencies, the diffraction field may be calculated using asymptotic methods (Kirchhoff formulation). The scope of the application related to this approximate theory is restricted to wavelengths much smaller than source and distance, due also to the fact that propagation is studied here as a local phenomenon. As it will be seen later, Vanderkooy showed however that the frequency range may be widely extended downwards [22].

According to the Keller's Geometrical Theory of Diffraction (GTD) and to the fact that the driver is mounted in an enclosure, the total sound pressure may be directly calculated by adding direct and diffracted waves [1, 3, 23]. Figure 2.6 shows this principle.

$$\underline{p} = \underline{p}_{direct} + \underline{p}_{diffr} \tag{2.16}$$

The direct contribution corresponds to the radiation of a flat piston assumed to be mounted on an infinite baffle:

$$\underline{p}_{direct}(x, y, z) = \frac{jZ_c k}{2\pi} \sum_{i=1}^{n} \frac{\underline{q}_i}{d_i} e^{-jkd_i} \tag{2.17}$$

The diffracted field $\underline{p}_{diffr}$ is calculated from incident waves interacting with the enclosure edges divided into "l" scattered elements. At each one of these points of diffraction, the sound pressure may be calculated as:

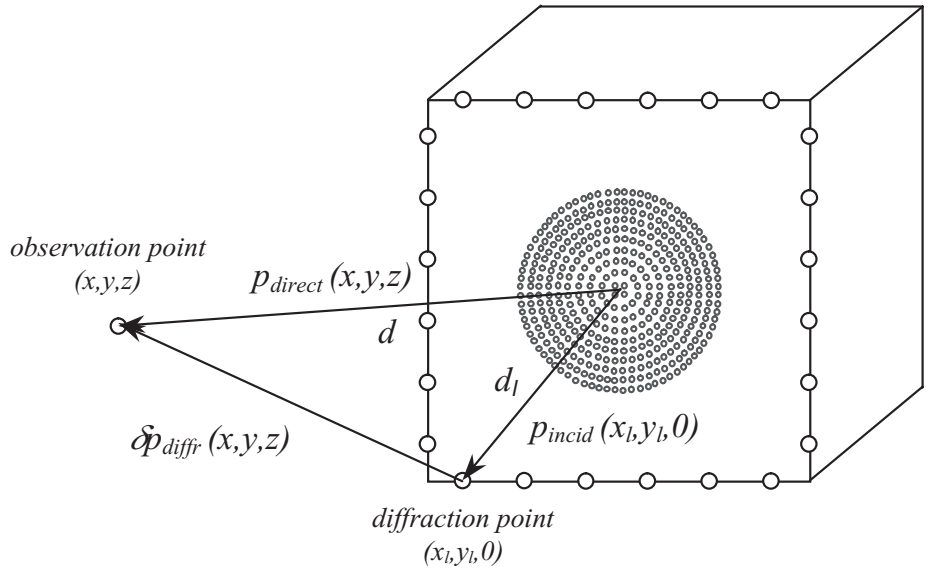

Figure 2.6 - *Concept of geometrical theory of diffraction applied to a flat piston mounted in a closed box*

$$\underline{p}_{incid}(x_l, y_l, 0) = \frac{j Z_c k}{4\pi} \sum_{i=1}^{n} \frac{\underline{q}_i}{d_{l_i}} e^{-jkd_{l_i}} \tag{2.18}$$

The diffracted field is thus computed from "*l*" virtual secondary sources of $\underline{p}_{incid}$ excitation value and placed at the points of diffraction.

Vanderkooy showed and explained that the diffraction contributions depend on the observation angle $\theta_l = \arctan(z/\sqrt{(x-x_l)^2+(y-y_l)^2})$ and that a phase reversal phenomenon in the illuminated zone has to be taken into account [22].

Thus, the sound pressure diffracted by each boundary element of wedge angle 2Ω is given by:

$$\delta\underline{p}_{diffr}(x, y, z) = \underline{p}_{incid}(x_l, y_l, 0) \frac{e^{-jk\sqrt{(x-x_l)^2+(y-y_l)^2+z^2}}}{4\pi l \sqrt{(x-x_l)^2+(y-y_l)^2+z^2}} F_{gtd}(x_l, y_l, \Omega) \tag{2.19}$$

with

$$F_{gtd}(x_l, y_l, \Omega) = \frac{1}{\nu} \sin\frac{\pi}{\nu} \left[\frac{1}{\cos\frac{\pi}{\nu} - \cos\frac{\theta_l}{\nu}} + \frac{1}{\cos\frac{\pi}{\nu} + \cos\frac{2\pi-\theta_l-2\Omega}{\nu}} \right] \tag{2.20}$$

and $\nu = (2\pi - 2\Omega)/\pi$

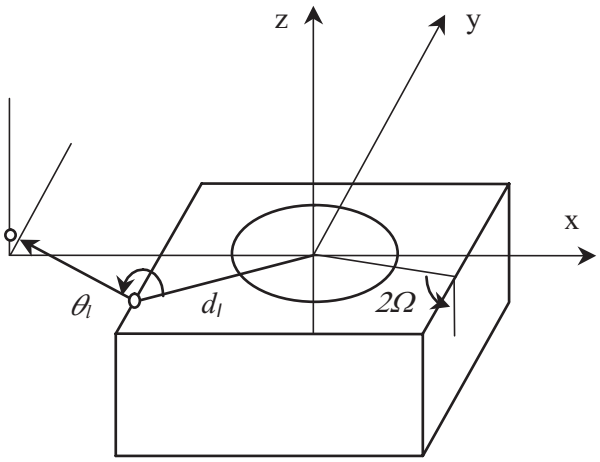

Figure 2.7 - *Depiction of observation angle θ_l and wedge angle 2Ω*

For most loudspeakers, the value of the enclosure wedge angle 2Ω is $\pi/2$. In this case, the directivity function $F_{gtd}(x_l, y_l, \Omega)$ is -0.77 on box surface (θ_l = 0°) and -1.15 on-axis in far-field (θ_l close to 90°). As one can see, the diffraction amplitude becomes infinite close to the shadow boundary. Given that this phenomenon is not physical, Vanderkooy has limited his theory to observation angles $\theta_l <$ 130° [22].

The directivity function $F_{gtd}(\theta_l, \Omega)$ is drawn in figure 2.8 for an angle Ω of π/4.

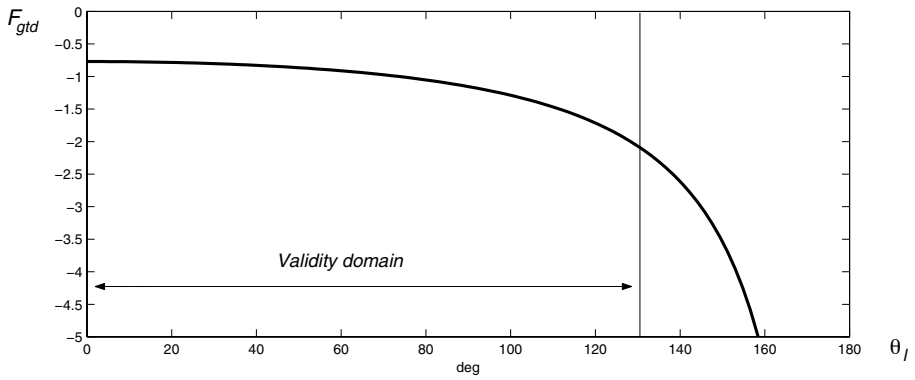

Figure 2.8 - *Directivity function $F_{gtd}(\theta_l, \Omega)$ according to θ_l, for $\Omega = \pi/4$*

In the following, the GTD used for observation angles equal to zero, will be called GTD(0°).

The total sound pressure is given by:

$$\underline{p}(x,y,z) = \underline{p}_{direct} + \sum_{i=1}^{l} \delta \underline{p}_{diffr} \tag{2.21}$$

For observation points located in transition regions (close to shadow boundaries) or for sources located near diffracting edges, the directivity function F_{gtd} of the geometrical theory has to be completed by a transition-region correction factor based on Fresnel integrals. This improved theory, called the Uniform Theory of Diffraction (UTD), allows the diffracted field to be obtained for different types of incident field, whilst removing discontinuities at the boundaries [4, 8, 17, 19]. Let us mention that this theory is valid only in the high-frequency range. Thus, the new directivity function becomes:

$$F_{utd}(x_l, y_l, \Omega) = 2j\sqrt{X_l}\, e^{jX_l} \int_{\sqrt{X_l}}^{\infty} e^{-j\tau^2} \mathrm{d}\tau \;\; F_{gtd}(x_l, y_l, \Omega) \tag{2.22}$$

with $X_l = k s_l \, \sin^2 \lambda_l \, (1 + \cos\theta_l)$ for locally plane waves, s_l being the distance from diffracting edge element "*l*" to observation point, and λ_l the angle of reflection (cone at diffracting elements). These magnitudes are depicted in figure 2.9.

As this integral requires more computation time than approximate expressions, the UTD will be used only for observation points located outside GTD validation domain.

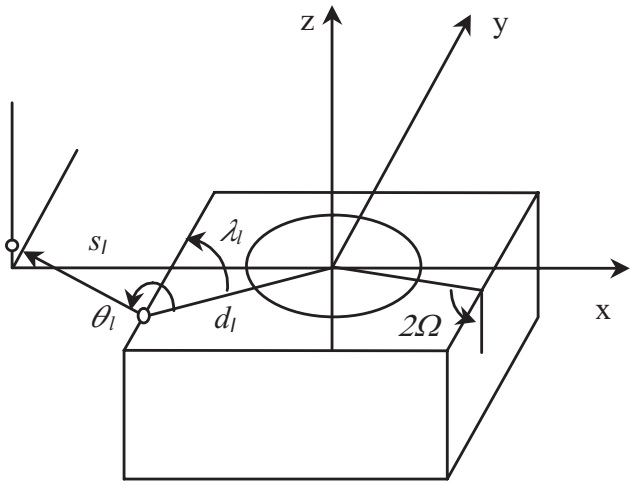

Figure 2.9 - *Depiction of distance s_l and angles θ_l, λ_l and 2Ω*

Figure 2.10 enables the function F_{utd} to be compared to the function F_{gtd} in modulus and phase, for different $L = ks_l \sin^2 \lambda_l$.

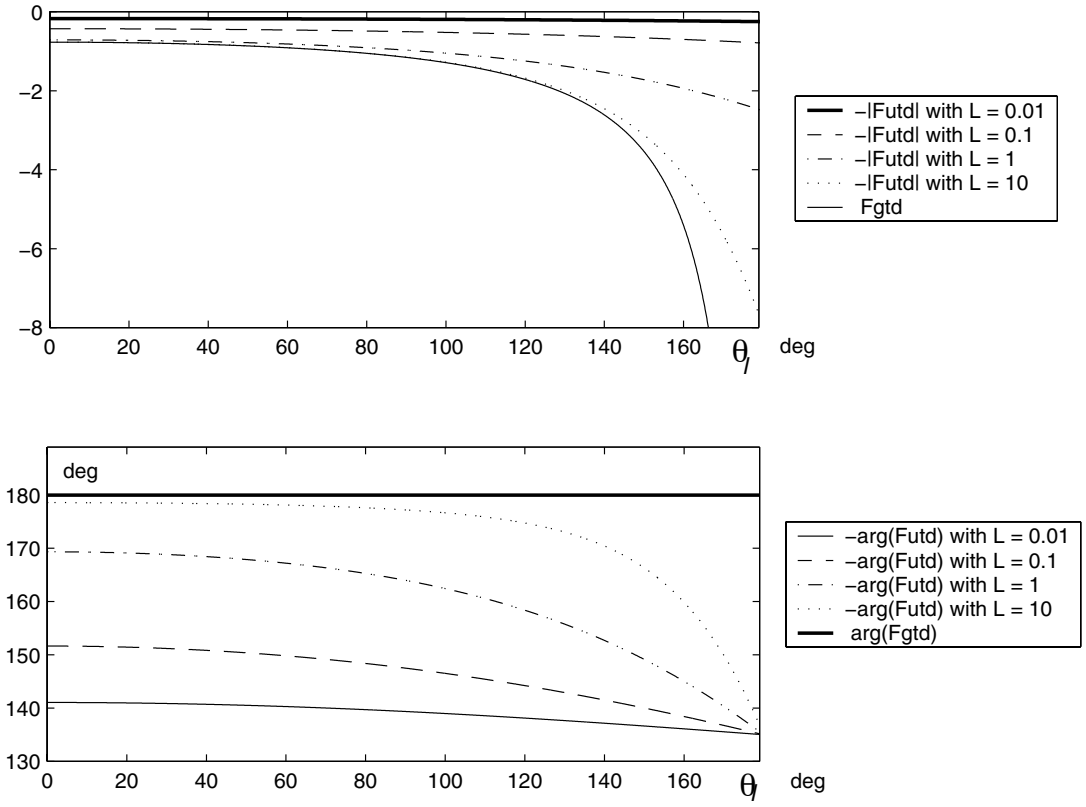

Figure 2.10 - *Comparisons between the directivity function F_{gtd} and F_{utd} according to θ_l, for different values of $L = k\ s_l \sin^2 \lambda_l$*

2.5 Two closed-box loudspeakers

2.5.1 Two adjacent closed-box loudspeakers (finite baffle)

The study of two adjacent closed-box loudspeakers comes down to the one of a limited baffle. The calculations of modifications in loudspeaker behaviour due to mutual effects are carried out using the theory of radiation in an infinite baffle (see Section 2.2) completed with the geometrical theory of edge diffraction for $\theta_l = 0°$.

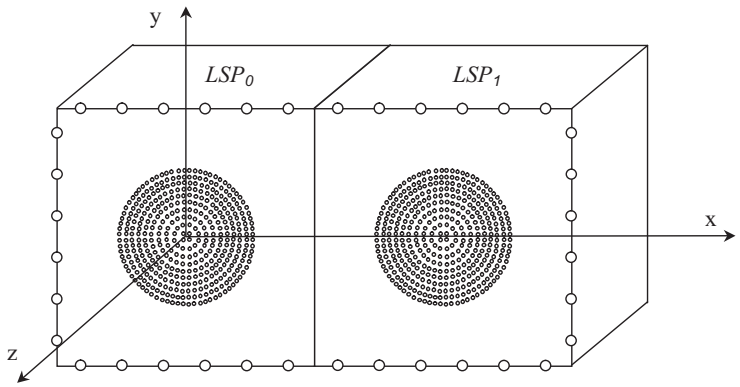

Figure 2.11 - *Depiction of two flat pistons mounted on two adjacent closed boxes*

Without taking into account the interactions, the resulting sound pressure radiated by both loudspeakers becomes:

$$\underline{p}(x,y,z) = \underline{p}_0(x,y,z) + \underline{p}_1(x,y,z) = \underline{p}_{0_{direct}} + \sum_{i=1}^{l} \delta\underline{p}_{0_{diffr}} + \underline{p}_{1_{direct}} + \sum_{i=1}^{l} \delta\underline{p}_{1_{diffr}} \tag{2.23}$$

The additional forces $\underline{F}_{01}$ and $\underline{F}_{10}$ applied on LSP_0, respectively LSP_1 are then given by:

$$\underline{F}_{01} = \frac{S_{d_0}}{m_0} \sum_{i=1}^{m_0} \underline{p}_1(x_{0_i}, y_{0_i}, 0) \qquad \& \qquad \underline{F}_{10} = \frac{S_{d_1}}{m_1} \sum_{j=1}^{m_1} \underline{p}_0(x_{1_j}, y_{1_j}, 0) \tag{2.24}$$

If observation points are located close to shadow boundaries or sources near diffraction points, the total sound pressure may be calculated using the UTD.

2.5.2 Two distant closed-box loudspeakers

In the case of two distant closed-box loudspeakers, the pressure of one loudspeaker has to be calculated in the immediate vicinity of the other one, that is to say close to the shadow boundaries. Thus, as described in Section 2.4, the uniform theory of diffraction has to be used.

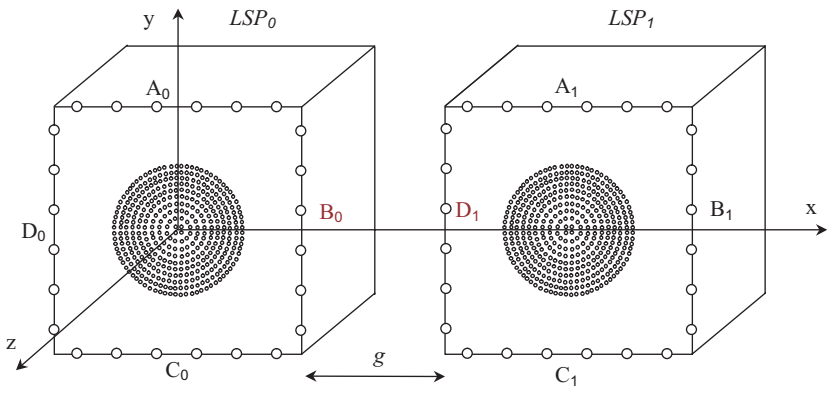

Figure 2.12 - *Depiction of two flat pistons mounted on two distant closed boxes*

In order to save computation time, it may be interesting to calculate this configuration according to GTD(0°), GTD and UTD applied on the eight enclosures edges in four different combinations. The latter, mentioned below, will be then compared during the experimental validations:

1. GTD(0°) used on the eight edges with,
2. GTD used on the six edges A_0, C_0, D_0, A_1, B_1, and C_1 (without diffraction on the remaining two B_0 and D_1),
3. GTD used on the six edges A_0, C_0, D_0, A_1, B_1, C_1, and UTD used on the remaining two B_0 and D_1,
4. and finally, UTD used on the eight edges.

Chapter 3

Calculations of modifications in loudspeaker behaviour

3.1 Aim and process

The aim of this calculation chapter is to give the orders of magnitude of the driver interactions in order to choose the best method of measurement. To do that, different loudspeaker configurations will be analysed according to the theories mentioned in the previous chapter.

In a first stage, the calculations are carried out in the simple and academic case of a single closed-box loudspeaker LSP_0 mounted in an infinite baffle.

In a second stage, the calculations are carried out in the case of two closed-box drivers mounted in an infinite baffle. They enable additionally first order modifications of driver LSP_0 subjected to the sound field of LSP_1 to be predicted, and vice-versa.

In a third stage, the calculations are carried out in the more realistic case of two adjacent and distant closed-box loudspeakers. As in the second stage, they enable the interactions between the two drivers to be obtained in taking into account the diffraction at the boxes edges.

In order to simplify the investigations related to the different cases, all the calculations in this chapter are based on loudspeakers of the same model mounted in identical closed boxes.

These calculations will be validated, afterwards, by a lot of systematic experimentations in which the above set out configurations will be studied (see Chapter 4). As we shall see later, the accuracy of comparisons between calculations and measurements will require the measurement of the TS parameters for each of the loudspeakers individually before introducing them into computation data.

3.2 Loudspeaker data

As we have seen in the modelling chapter, most of loudspeaker calculations start with the determination of parameters linked to the chosen driver, box and power source. The calculations carried out in this chapter, are based on a Tannoy 367-X loudspeaker (fig. 3.1).

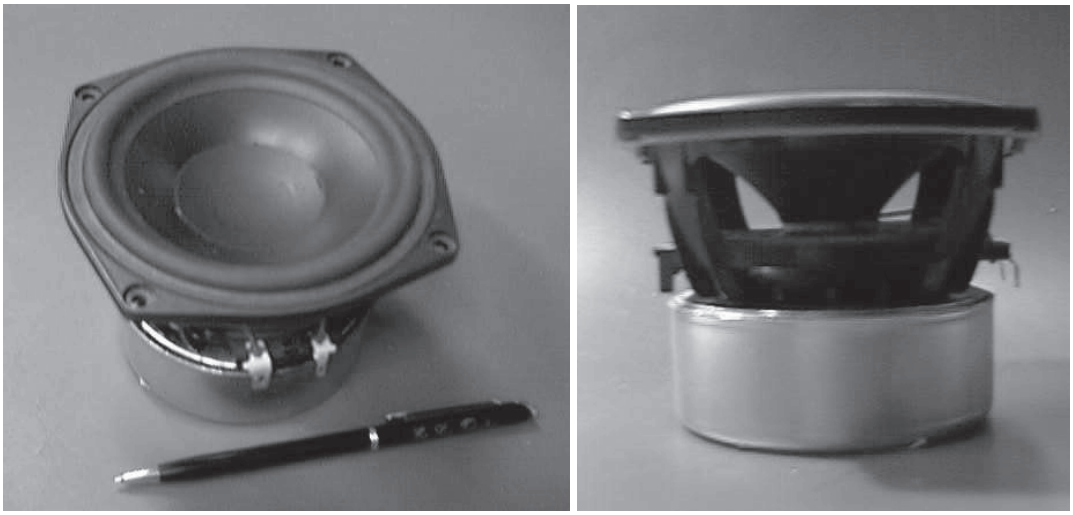

Figure 3.1 - *Pictures of the loudspeaker model used during the whole thesis*

The TS parameters inserted in the calculations come from the measured average of five of those loudspeakers (measurement method explained in Appendix B). These values are given on a temporary basis and their variations will be discussed in the next chapter (see Subsection 4.2.3). They are:

f_s = 68.9 Hz
Q_{es} = 1.34
Q_{ms} = 1.68
Q_{ts} = 0.74
V_{as} = 3.98 dm^3

In a first approximation, R_e is assumed to be independent of voltage, frequency and temperature. The effects of its variations on the results will be also discussed later. The measured average gives:

R_e = 6.9 Ω

These parameters have to be complemented by the loudspeaker diaphragm size (piston radius a in low frequency range) and enclosure net internal volume V_b:

a = 4.5 cm $\rightarrow$ S_d = 63.6 cm^2

V_b = 0.57 dm^3
β = 1

The excitation conditions for the calculations correspond to the arbitrary values:

R_g = 1 Ω
U_g = 1 V (RMS)

Relations (1.33) to (1.36) lead to the TS parameters of the closed-box system:

f_c = 194.7 Hz
Q_{mc} = 4.75
Q_{tco} = 2.4
Q_{eco} = 3.78

According to Section 1.5, the other calculated parameters, necessary to the computations of input impedance and volume velocity, become:

C_{ab} = 4.2 10^{-9} m^3/Pa
Bl = 4.1 Tm
C_{as} = 29.2 10^{-9} m^3/Pa
R_{ae} = 51.6 10^3 Ω_a
R_{as} = 47.1 10^3 Ω_a
α = 7
C_{ac} = 3.65 10^{-9} m^3/Pa
m_{ac} = 182.9 kg/m^4

In the piston domain, that total mass of 7.4 g is made up of three different masses according to the following proportion:

- the moving system mass m_s of about 6.6 g, ie 89 %,
- the box equivalent mass m_b of about 0.5 g, ie 7 %,
- and the equivalent radiation mass m_r of about 0.3 g, ie 4 %.

3.3 One closed-box loudspeaker in an infinite baffle

3.3.1 General points

In the following, n designates the first surface division number enabling the sound pressure to be calculated, when m defines the second one, enabling the force and the radiation impedance to be calculated.

These numbers are chosen according to piston radius and frequency range, so as to correspond as closely as possible to the continuous approach results. However, with computation time to be considered, it is not useful to push the fine tuning too far, but nevertheless far enough so as to ensure sufficient accuracy compared to the calculations and measurements which will be carried out afterwards.

3.3.2 Input impedance and volume velocity

As explained in the introduction, the modifications occurring on a driver subjected to an incident sound field will be analysed later in terms of volume velocity and input impedance. It may therefore be of interest to analyse and understand both these well-known frequency curves. Based on the previous section parameters, volume velocity (equ. 1.14) and input impedance (equ. 1.18) are calculated taking into account the radiation resistance R_{ar} coming from the analytical solution 2.7. This acoustic resistance, generally neglected at this stage of calculations, is nevertheless introduced in the computation code in order to complete the modification studies carried out in the next section.

The equivalent circuits developed in the modelling chapter, showed that electrodynamic driver systems may be represented by an equivalent acoustic resonator (fig. 1.6) made up of acoustic resistance, mass and compliance in series. This circuit enables volume velocity according to excitation signal to be calculated in a simply way (equ. 1.14). The properties of this representation may be copied from those of well-known electrical series-resonant circuits. Then, the volume velocity response may be divided into three parts (below, at and above the resonance frequency) according to the influence of the different components:

- below the resonance frequency, the dominant component proves to be the equivalent compliance, which leads to a variation of volume velocity proportional to the frequency ($\underline{q} \approx j\omega C_{ac}$)
- at the resonance frequency where the mass and compliance influences cancel out each other, the dominant element is the acoustic resistance ($\underline{q} \approx \frac{1}{R_{ac}}$).
- above the resonance frequency, the main role is held by the equivalent mass, which leads to a variation of volume velocity inversely proportional to the frequency ($\underline{q} \approx \frac{1}{j\omega m_{ac}}$)

Figure 3.2 shows the computed volume velocity in modulus and phase, in with the different controlled domains are highlighted. As we can notice, the working of drivers is governed by a lot of laws and components depending on the frequency, which do not make it easy to understand their behaviour. In fact, each component or group of components may become essential, in turn, for a given frequency domain.

Let us analyse also the input impedance in modulus and phase. As previously, figure 3.3 shows the computed curves in modulus and phase with the different controlled domains highlighted.

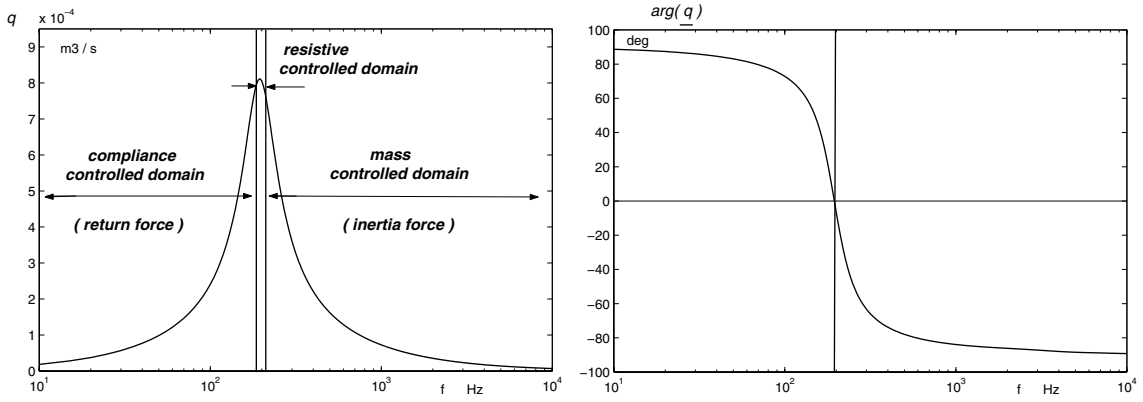

Figure 3.2 - *Computed volume velocity in modulus and phase*

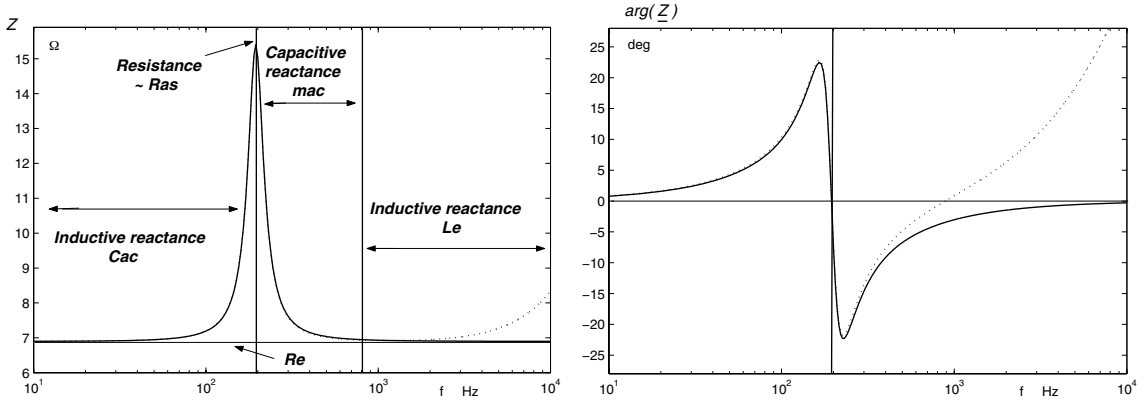

Figure 3.3 - *Computed input impedance in modulus and phase, with (dotted lines) and without (solid lines) taking into account the value of L_e*

According to relation 1.18, the behaviour of the input impedance comes under equivalent electrical resistance, capacitance and inductance. It is not necessary here to prove again the decisive role played by this curve in driver analyses (see Chapter 1 and Appendix B).

3.3.3 Near-field sound pressure

Once the volume velocity is determined, the calculation of the sound pressure radiated by a rigid piston mounted in an infinite baffle may be carried out in different ways depending upon the degree of accuracy required by the application under consideration. In most cases, the distance between the listener and the source is so great compared to the driver size that the computations may be limited to the far field.

The computation of the near-field sound pressure has to be carried out in this work, in order to enable the force exerted by a loudspeaker on the air (see Subsection 3.3.5) to be calculated. Taking into

consideration the boundary conditions of an infinite baffle, the radiated sound pressure may be derived accurately from relation 2.1. Enabling the sound pressure to be calculated anywhere in the half space located in front of the radiating surface, this integral has the disadvantage of requiring a great deal of computation time. In order to accelerate the latter, the continuous approach may be compared to a discrete one (equ. 2.9), in which the piston area is divided into n identical small elements.

Figure 3.4 shows the comparison between the near-field sound pressure calculations resulting from the continuous approach and from the discrete ones (with n = 4 and 400 elements). The modulus and the phase of the sound pressure are calculated on-axis in the immediate vicinity of the piston surface (x = y = 0 and z = 1 μm), in order to prepare the calculation of the force exerted by the driver on the air (see Subsection 3.3.5).

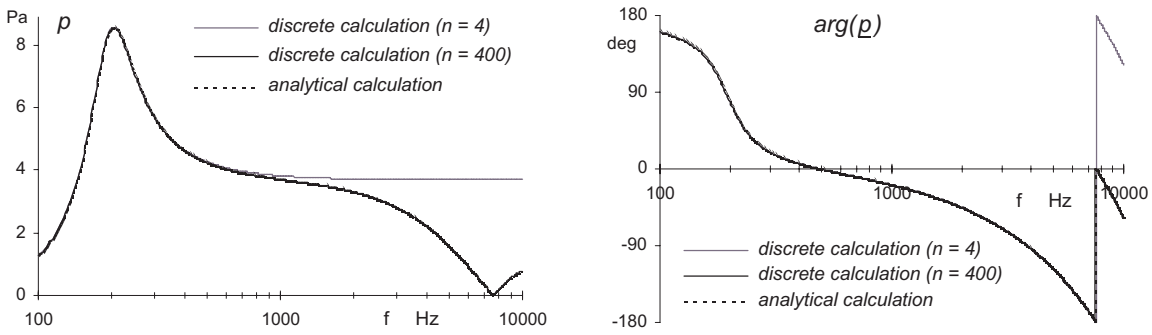

Figure 3.4 - *Comparison of the near-field sound pressure resulting from integral and discrete approaches - modulus and phase calculations carried out on-axis in the immediate vicinity of the piston surface (x = y = 0 and z = 1 μm)*

3.3.4 Error estimations according to *n*

Within the framework of this thesis, the near-field sound pressure calculation does not constitute an end in itself, but only an intermediate stage in view of calculating the force exerted by a piston on another one. That is why the comparison between the analytical approach and the discrete one does not enable the suitable number of division elements to be chosen, but contributes only to have a first idea of the tendency. In our case and for values of ka less than $\sqrt{2}$, the modulus error remains less than 8 % for n = 4 and less than 0.8 % for n = 400, when the phase error does not exceed 0.005 degrees for both divisions. It should be noted moreover that these error calculations are very difficult to define because of the sound pressure non uniformity. Let us now analyse the differences between analytical and discrete approaches according to the acoustic force and radiation impedance, which offer the advantage of being independent of the observation point.

3.3.5 Reaction force and radiation impedance

The calculation of the medium reaction force exerted on the piston results from the integration of the radiated sound pressure on the whole surface of its membrane (equ. 2.3). Given that the calculation of this double surface integral requires large computational time, it is advisable to use Rayleigh analytical solution 2.4. The latter enables directly the acoustic radiation mass and resistance to be obtained, following relation 2.7.

The existence of this attractive and accurate analytical solution makes the discrete approach seemingly useless. However, the latter will nevertheless be studied with the aim of choosing both surface divisions, which will be applied afterwards when calculating the force exerted by a piston on another one, a case for which no analytical solution exists. The purpose here will therefore be to define both numbers n and m, comparing the discrete results and the analytical ones issued from the Rayleigh solution, in order to apply those by default to the calculations of the interaction forces between two pistons (see Section 3.4.1).

Figure 3.5 shows the results of the force calculations in modulus and phase. Compared with continuous approach results, the curves enable increased precision according to the second surface division (m = 4 or 36) to be highlighted, for the first one n set to 400 surface elements.

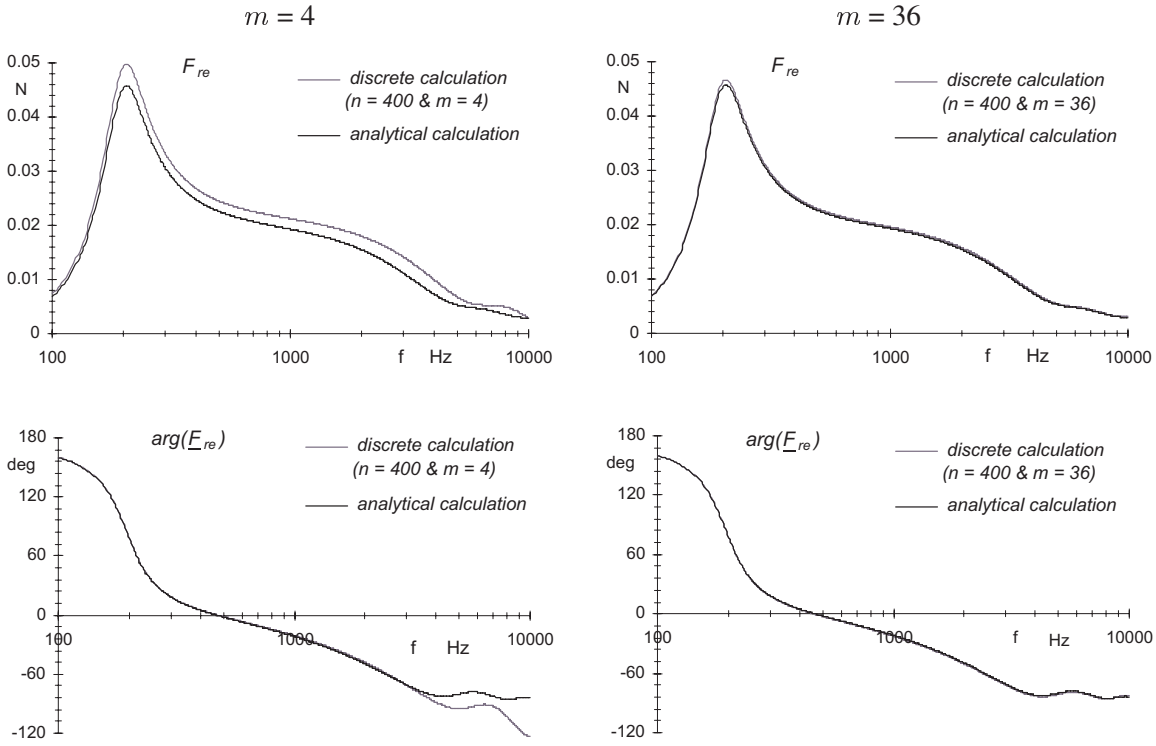

Figure 3.5 - *Computed medium reaction force in modulus and phase - comparison of analytical solution (Bessel and Struve functions) with discrete results according to n = 400 and m = 4 and 36*

Figure 3.6 is given, as a rough guide, for those readers who may be more familiar with the radiation impedance curves than with those of the reaction force. As with the reaction force, this figure enables the analytical (Bessel and Struve) approach with the discrete one to be compared, for n = 400 and m = 4 or 36.

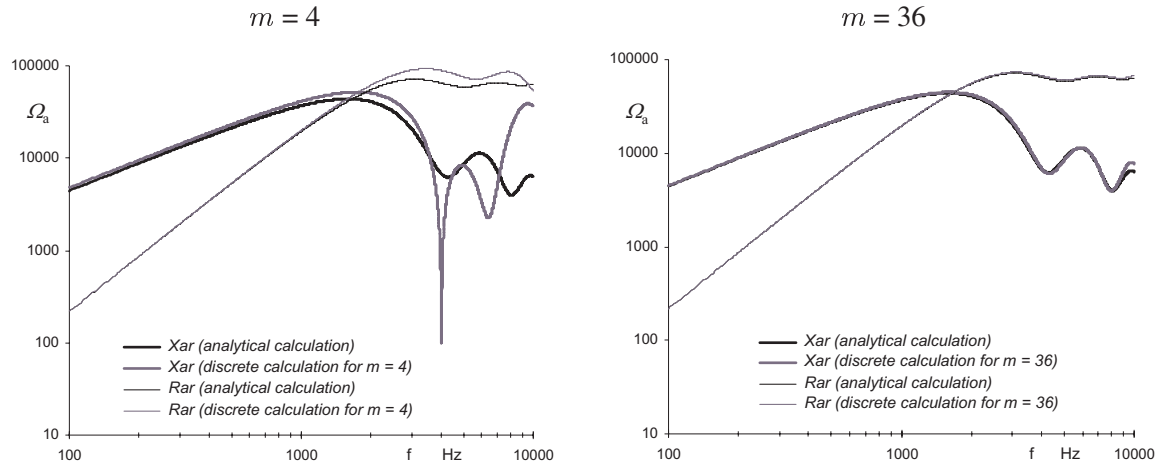

Figure 3.6 - *Computed radiation impedance (R_{ar} and X_{ar}) - comparison of analytical solution with discrete results according to n = 400 and m = 4 and 36*

3.3.6 Error discussion

After analysing the best compromise between an acceptable degree of accuracy and time-saving considerations, the first division number was set to 400 elements and the second one to 36.

In order to justify this choice, figure 3.7 shows the force differences in percent and degrees between the analytical calculations and the discrete ones, computed with n = 400 and m = 36. These differences are in the order of 2 percent and 0.8 degree for $ka \leq \sqrt{2}$, corresponding to a frequency of about 1.6 kHz. This accuracy is tolerable in view of the orders of magnitude calculated in the next section, where the force variations under the influence of another loudspeaker may reach ± 19 % and ± 10 degrees. These values correspond to the case where both drivers are identical and located close together (separated by a distance of $3a$).

As for the radiation impedance calculations, figure 3.8 gives the X_{ar} and R_{ar} differences in percent between both approaches, also for n = 400 and m = 36. The differences observed for $ka \leq \sqrt{2}$ are larger for the reactive part than for the resistive one, generally neglected in this range of frequency. The X_{ar} errors are less than 3 %, when the R_{ar} ones are less than 1.3 %. As with the reaction force calculations, these errors have now to be compared with the radiation impedance modifications occurring when the loudspeaker is subjected to the sound field radiated by another loudspeaker (see Section 3.4.1). Both drivers are again identical and separated by a distance of $3a$. Considering variations of $\pm 16\%$ for X_{ar} and 100% for R_{ar}, the error calculations are again judged to be acceptable.

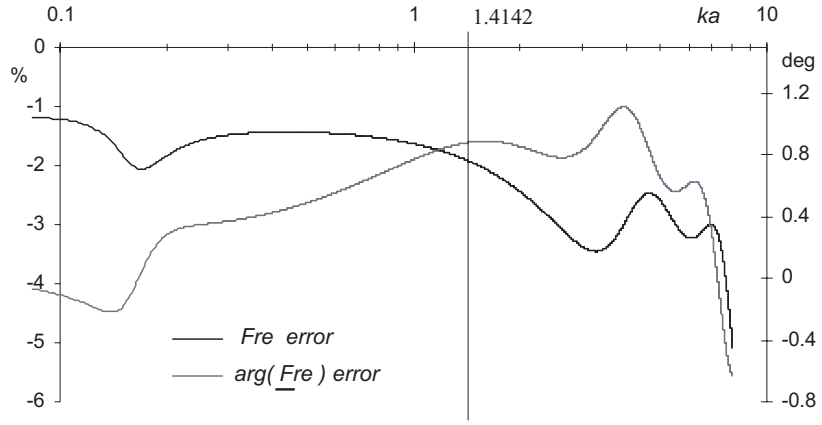

Figure 3.7 - *Error calculations of the reaction force carried out according to the discrete approach (n=400 and m=36) in comparison with the continuous one (Bessel and Struve)*

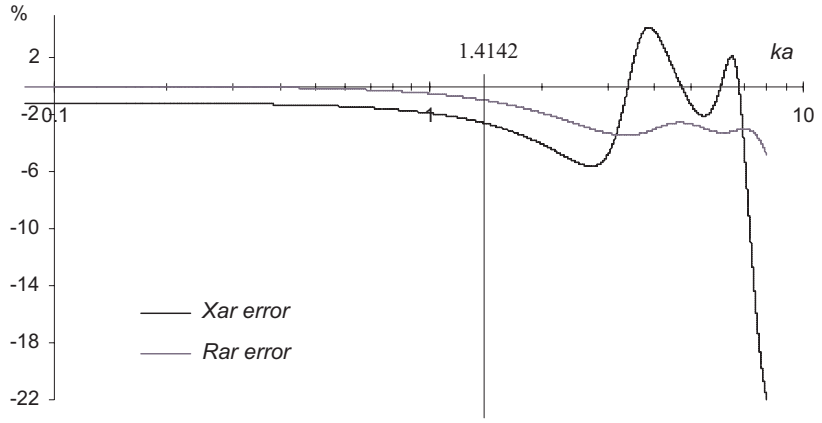

Figure 3.8 - *Error calculations of the radiation resistance and reactance carried out according to the discrete approach (n=400 and m=36) in comparison with the analytical one*

In turn, the measurements will also confirm the compromise made between time saving and accuracy related to surface subdivisions.

3.4 Two closed-box loudspeakers in an infinite baffle

In a first step, the driver modifications are calculated for a distance between source centres set to three radii (smallest realistic value) and for both driver excitations set to 1 V RMS in-phase. The consequences of the variation of these three variables (distance, excitation ratio and excitation phase difference) will be studied in a second step.

3.4.1 Resulting modifications

The LSP_1 surface divisions (n_1 and m_1) depend not only on piston size and frequency range, but also on the distance between pistons centres. The division n_1, chosen equal to n_0, enables the sound pressure to be calculated anywhere, in particular at LSP_0 surface (fig. 3.9).

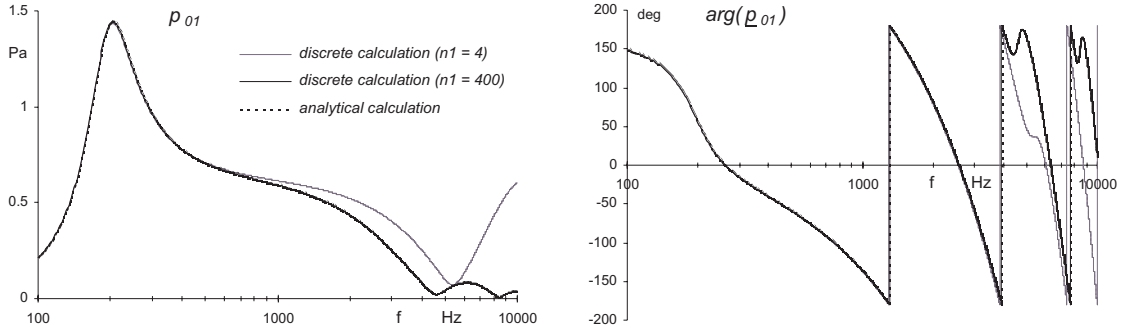

Figure 3.9 - *LSP_1 sound pressure calculated in modulus and phase in the immediate vicinity of LSP_0 piston surface (x = y = 0 and z = 1 μm) - comparison between continuous approach (integral) and discrete ones (n_1 = 4 and 400)*

The third LSP_0 surface division m_1 enables the LSP_1 force $\underline{F}_{01}$ applied to LSP_0 to be calculated. This force corresponds to $\underline{F}_{ext}$ drawn in Figure 1.9. According to the previous results and to the complexity of the double surface integral, m_1 is chosen equal to m_0. Thus, the modifications of the force (fig. 3.11), radiation impedance (fig. 3.12), input impedance (fig. 3.13) and volume velocity (fig. 3.14) are calculated with n_0 = 400, m_0 = 36, n_1 = 400, m_1 = 36.

The action force necessary to the LSP_0 to move the air becomes ($\underline{q}$ constant):

$$\underline{F}'_0 = -\left(\underline{F}_{re_0} + \underline{F}_{01}\right) \tag{3.1}$$

According to the frequency, the modifications of the LSP_0 action force are calculated in percent and degrees, in accordance with:

$$F_{0_{mod}} = 100\ \frac{F'_0\ -\ F_{re_0}}{F_{re_0}} \tag{3.2}$$

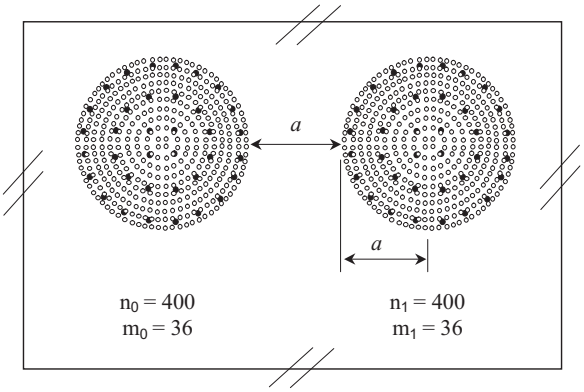

Figure 3.10 - *Depiction of the double surface division of the two pistons mounted in an infinite baffle*

$$arg(\underline{F}_0)_{mod} = arg(\underline{F}'_0) \; - \; arg(\underline{F}_{re_0}) \tag{3.3}$$

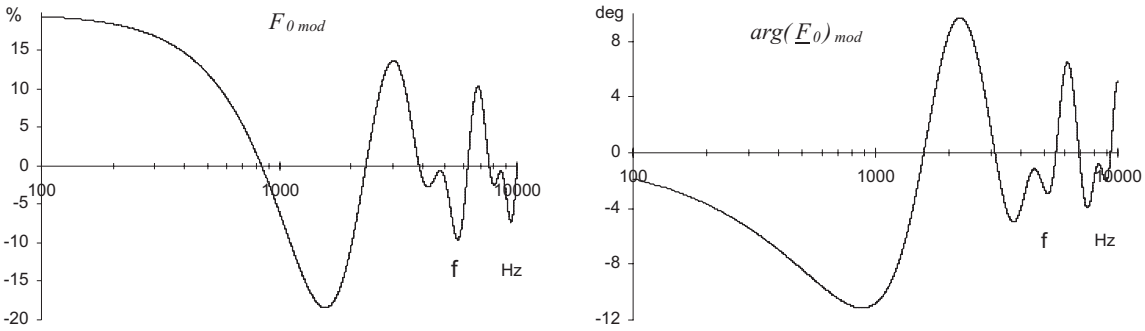

Figure 3.11 - *Modification of LSP_0 action force - calculations in modulus (%) and phase (deg)*

The calculation of $\underline{F}_{01}$ enables the radiation impedance to be obtained according to equation 2.15. The equivalent radiation impedance $\underline{Z}'_{ar_0}$ is calculated according to equation 2.11. Let us now calculate the modifications in percent occurring on R_{ar_0}, X_{ar_0} and m_{ar_0}:

$$R_{0_{mod}} = 100 \; \frac{R'_{ar_0} \; - \; R_{ar_0}}{R_{ar_0}} \tag{3.4}$$

$$X_{0_{mod}} = 100 \; \frac{X'_{ar_0} \; - \; X_{ar_0}}{X_{ar_0}} \tag{3.5}$$

$$m_{0_{mod}} = 100 \ \frac{m'_{ar_0} \ - \ m_{ar_0}}{m_{ar_0}} \tag{3.6}$$

Figure 3.12 shows the reactive and resistive parts of LSP_0 radiation impedance taking into account or not the disruptions due to LSP_1. The modification values $R_{0_{mod}}$ and $X_{0_{mod}}$ are also plotted.

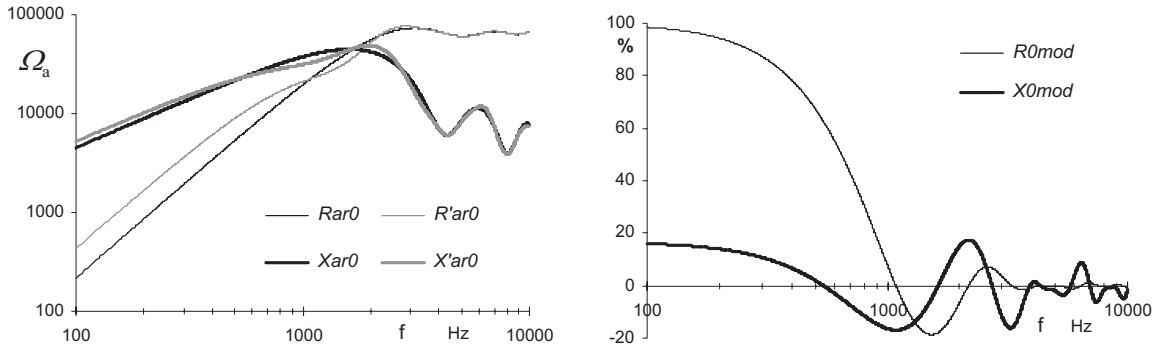

Figure 3.12 - *Reactive and resistive parts of LSP_0 radiation impedance taking into account or not the disruptions due to LSP_1 - modifications in $\%$*

Considering that the two loudspeakers LSP_0 and LSP_1 are identical and identically driven, they are both modified in the same way. Thus, in order to lighten notations in this subsection, the loudspeaker identifications (0 or 1) will be omitted here.

The calculations of the input impedance $\underline{Z}$ (equ. 1.18) and volume velocity $\underline{q}$ (equ. 1.14) are carried out now taking into account the radiation impedance $\underline{Z}_{ar}$ (deduced from relation 2.10) coming from the four membrane subdivisions (fig. 3.10). When the loudspeaker is subjected to an incident sound field, the same computations are carried out for the modified input impedance $\underline{Z}'$ and volume velocity $\underline{q}'$, replacing $\underline{Z}_{ar}$ by $\underline{Z}'_{ar}$. The modifications in percent and degrees are calculated as:

$$Z_{mod} = 100 \ \frac{Z' \ - \ Z}{Z} \tag{3.7}$$

$$arg(\underline{Z})_{mod} = arg(\underline{Z}') \ - \ arg(\underline{Z}) \tag{3.8}$$

$$q_{mod} = 100 \ \frac{q' \ - \ q}{q} \tag{3.9}$$

$$arg(\underline{q})_{mod} = arg(\underline{q}') \; - \; arg(\underline{q}) \tag{3.10}$$

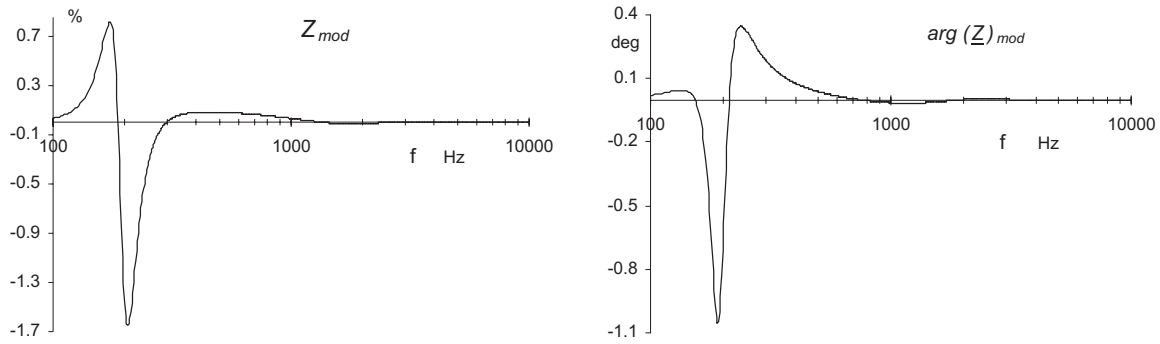

Figure 3.13 - *Input impedance modifications, in modulus (%) and phase (degree)*

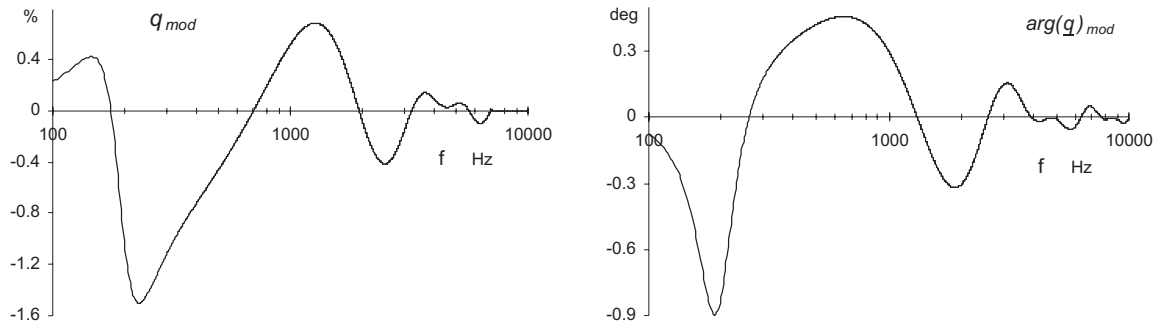

Figure 3.14 - *Volume velocity modifications, in modulus (%) and phase (degree)*

The results show that the closer the frequency is to the system resonance, the greater the modifications become. This is due to the fact that the mechanical impedance $\underline{Z}_{mg}$ (fig. 1.8 to 1.10) has its minimum at the resonance.

The comparisons of modifications between input impedance and volume velocity, according to the frequency, show that the orders of magnitude are similar at the system resonance, but this is not the case away from resonance. The volume velocity modifications are then higher than those of input impedance.

The orders of magnitude of the results are so significant, that the modifications of input impedance and volume velocity ought to be measurable.

The volume velocity modifications give directly the change in sound pressure, due to the fact that the latter corresponds exactly to the former in the case of relative modification calculations (in %, dB or degree). The sound pressure modifications are then identical to those of figure 3.14, that is in the

order of -1.5 to 0.6 % and -0.9 to 0.4 degrees. As these values are constant anywhere in half-space, the calculations can be given any coordinates x, y and z.

Let us now calculate the sound pressure radiated by both loudspeakers together without and with interaction. Whilst the sound pressure level difference ΔL_p can not be measured, it may be computed in order to have an idea of its order of magnitude in dB:

$$\Delta L_p = 20 \log \frac{|\underline{p}'_0 + \underline{p}'_1|}{20\ 10^{-6}} \ - \ 20 \log \frac{|\underline{p}_0 + \underline{p}_1|}{20\ 10^{-6}} \tag{3.11}$$

$$arg(\underline{p})_{mod} = arg(\underline{p}'_0 + \underline{p}'_1) \ - \ arg(\underline{p}_0 + \underline{p}_1) \tag{3.12}$$

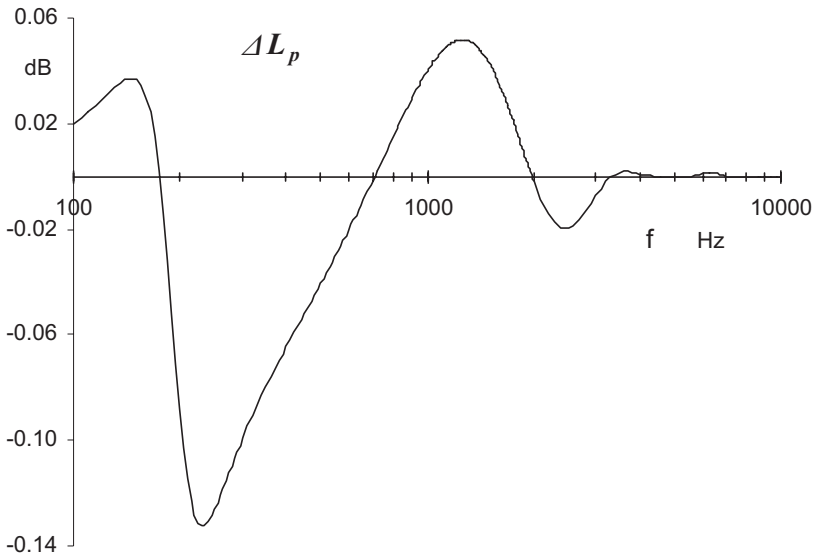

Figure 3.15 - *Modifications of the total sound pressure level (dB) radiated by both loudspeakers*

The equivalence between the modifications of the volume velocity of each loudspeaker and the resulting sound pressure radiated by both loudspeakers together, is valid as far as both systems are defined by the same values of parameters and are identically driven in amplitude and phase.

Until now, the LSP_0 behaviour modifications were calculated for one given configuration and settings. Whilst these calculations are sufficient to obtain orders of magnitude, they are not sufficient to analyse and study incident sound field actions more accurately. This is why the calculations must be completed with various parameters settings.

3.4.2 Modification calculations according to excitation ratio

This subsection and following ones treat the variations of $\underline{Z}$ and $\underline{q}$ modifications according to the excitation ratio U_1/U_0, excitation phase difference ϕ and distance r between loudspeaker centres.

Figures 3.16 and 3.17 show the input impedance and volume velocity modifications in modulus and phase, according to excitation ratio ($\frac{U_1}{U_0}$ = 0.1, 0.5, 1, 1.5, 2, 3) and frequency (f from 100 to 500 Hz). ϕ is set to 0° and r to $3a$ (smallest realistic value).

In accordance with the equivalent mechanical circuit drawn in figure 1.9, $\underline{F}_{ext}$ variations entail identical changes on the velocity $\underline{v}_e$. This means that the fluctuations of the excitation ratio entail similar variations in the modifications of loudspeaker behaviour. This theory is confirmed by the curves of figures 3.16 and 3.17.

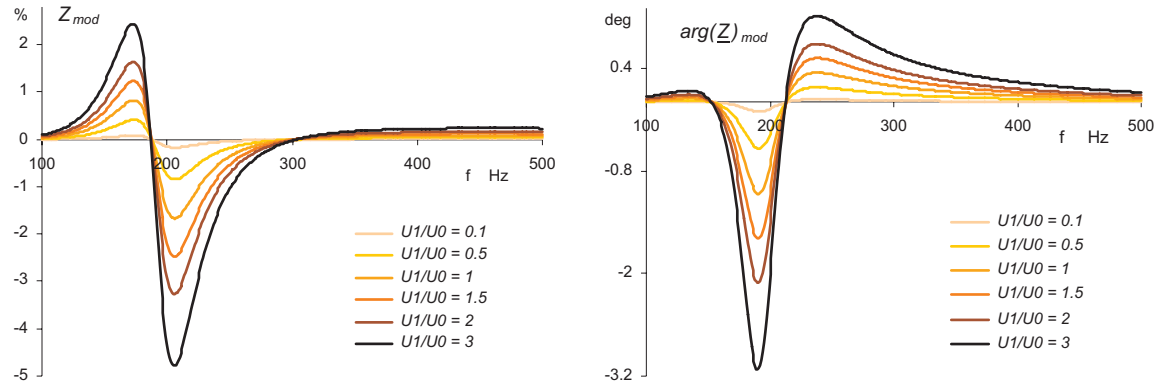

Figure 3.16 - *Input impedance modifications (modulus-phase) according to excitation ratio and frequency*

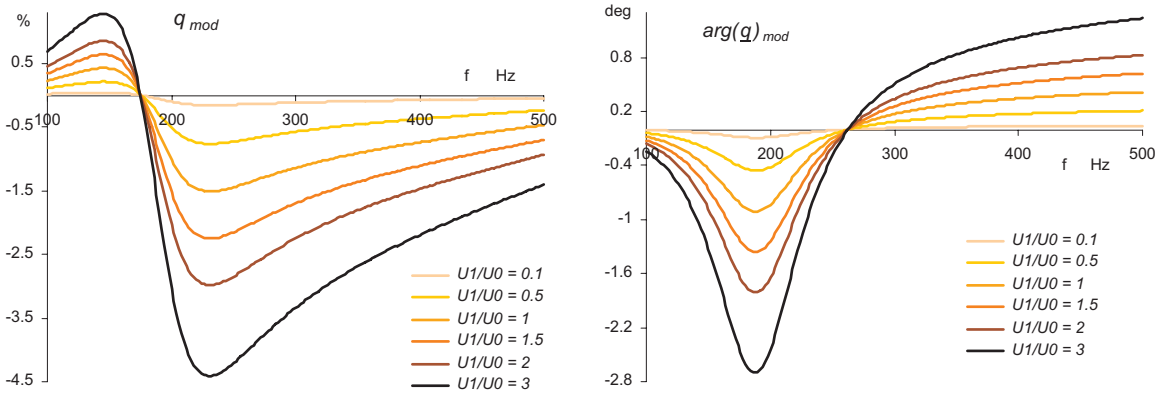

Figure 3.17 - *Volume velocity modifications (modulus-phase) according to excitation ratio and frequency*

For information, the sound pressure radiated by the two loudspeakers together are also calculated according to excitation ratio. Figures 3.19 and 3.20 show the sound pressure difference (with and without interaction) for two loudspeakers driven by different excitation amplitudes. The calculations are carried out at the points A and B, according to figure 3.18.

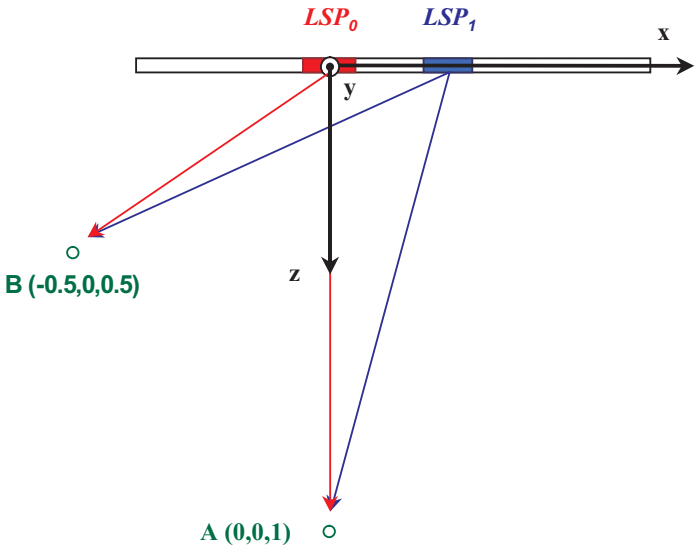

Figure 3.18 - *Sound pressure calculation points (A and B)*

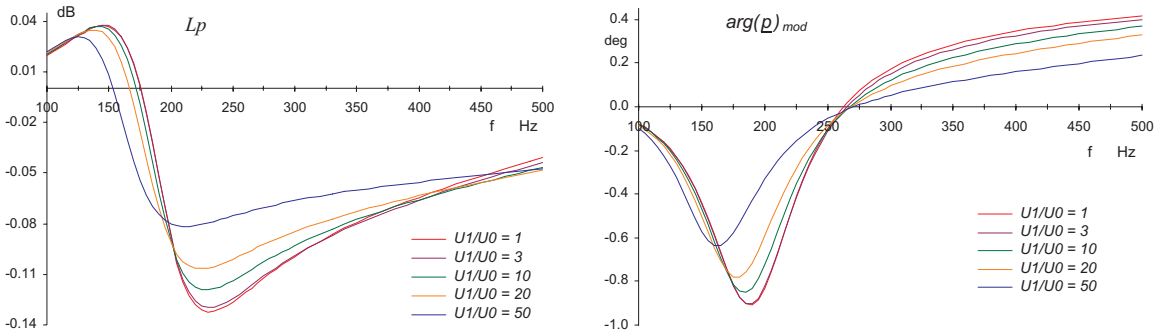

Figure 3.19 - *Modifications of the sound pressures radiated by both loudspeakers together for different excitation ratios - calculations at point A*

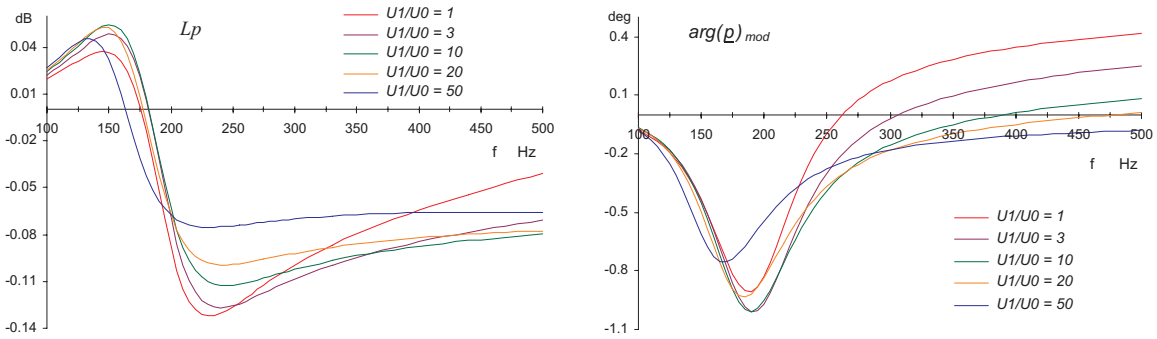

Figure 3.20 - *Modifications of the sound pressures radiated by both loudspeakers together for different excitation ratios - calculations at point B*

As was assumed, figures 3.19 and 3.20 confirm that the sound pressure modifications are dependent on the observation point, as far as the loudspeakers are described by different parameters or are driven in a different way.

3.4.3 Modification calculations according to excitation phase difference

In order to analyse loudspeaker behaviour modifications independently of the observation point, this subsection is going to focus only on input impedance and volume velocity modifications.

Figure 3.21 shows the input impedance modifications in modulus and phase, according to excitation phase difference (ϕ from 0° to 180° every 30°) and frequency (f from 100 to 500 Hz). $\frac{U_1}{U_0}$ is set to 1 and r to $3a$ (smallest realistic value).

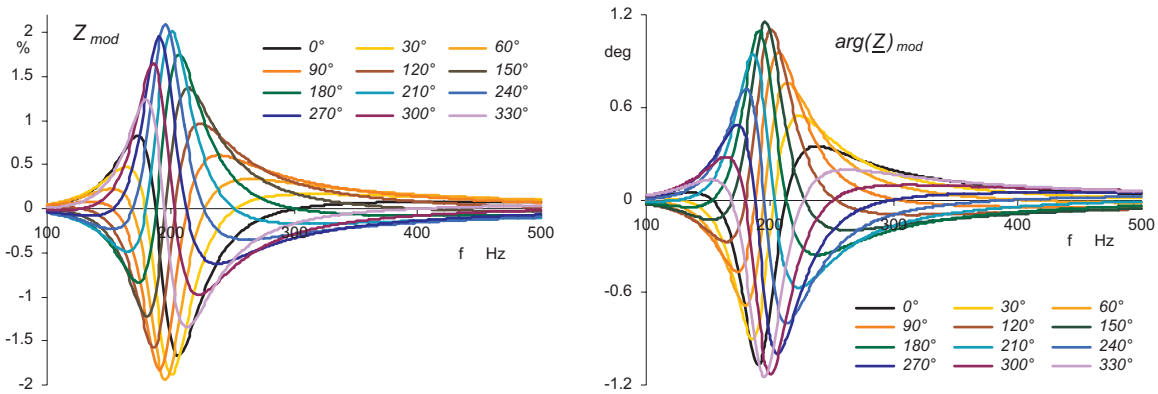

Figure 3.21 - *Input impedance modifications (modulus-phase) according to excitation phase difference and frequency*

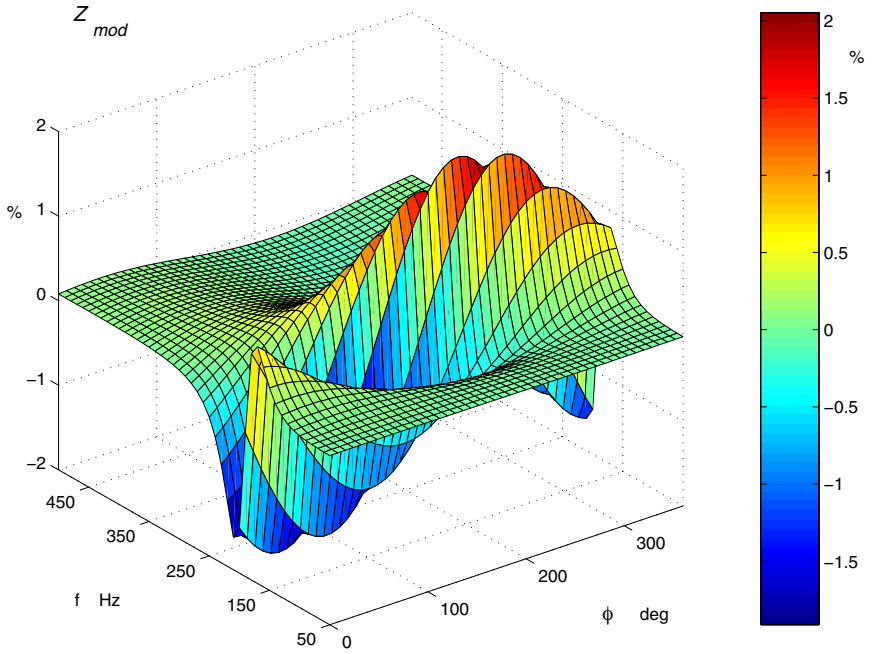

Figure 3.22 - *Input impedance modifications (modulus) according to excitation phase difference and frequency*

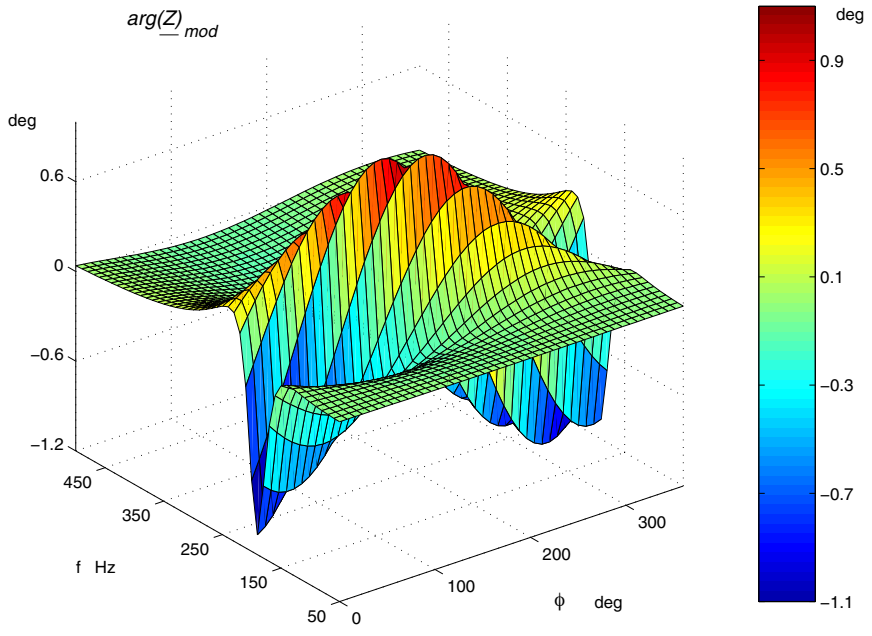

Figure 3.23 - *Input impedance modifications (phase) according to excitation phase difference and frequency*

In order to have a better idea of the modifications according to both parameters f and ϕ, the curves of figure 3.21 are displayed in 3D views (fig. 3.22 and 3.23). The calculations are carried out every 5 Hz from 50 to 500 Hz, and every 4 deg from 0 to 360 deg.

Let us now apply the same process to the case of the variations in volume velocity modifications. As for the input impedance, the study starts with a figure showing the volume velocity modifications in modulus and phase according to ϕ, for $\frac{U_1}{U_0} = 1$ and $r = 3a$ (fig. 3.24).

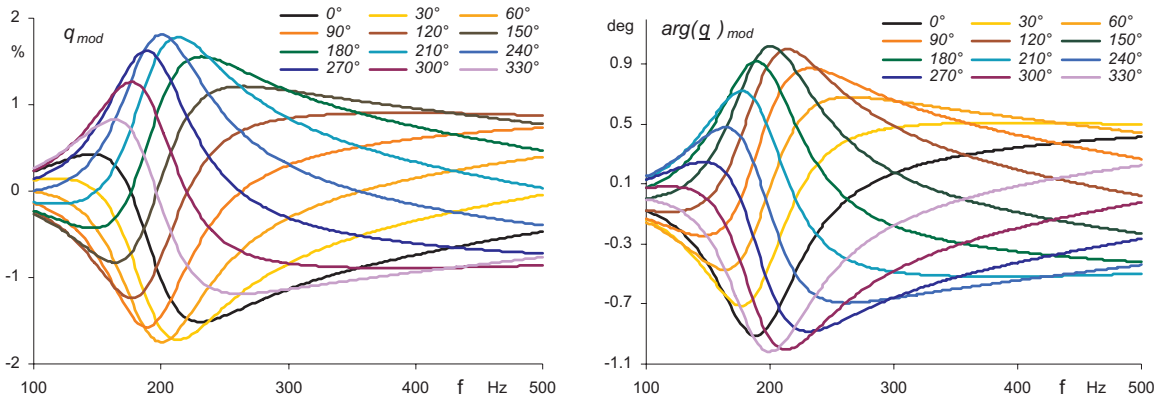

Figure 3.24 - *Volume velocity modifications (modulus-phase) according to excitation phase difference and frequency*

In order to have a better idea of the modifications according to both parameters f and ϕ, the curves of figure 3.24 are also displayed in 3D views (fig. 3.25 and 3.26). The calculations are carried out every 5 Hz from 50 to 500 Hz, and every 4 deg, from 0 to 360 deg.

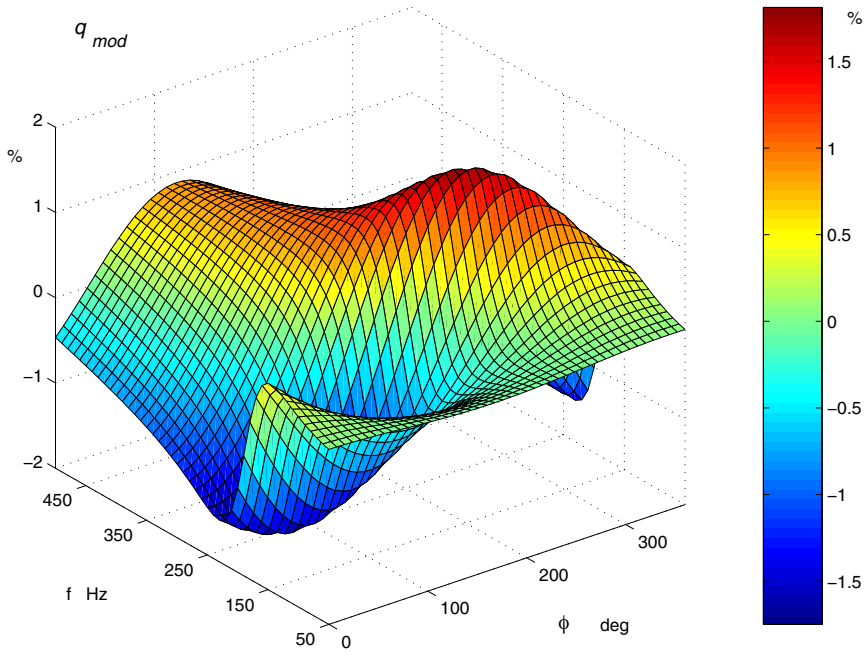

Figure 3.25 - *Volume velocity modifications (modulus) according to excitation phase difference and frequency*

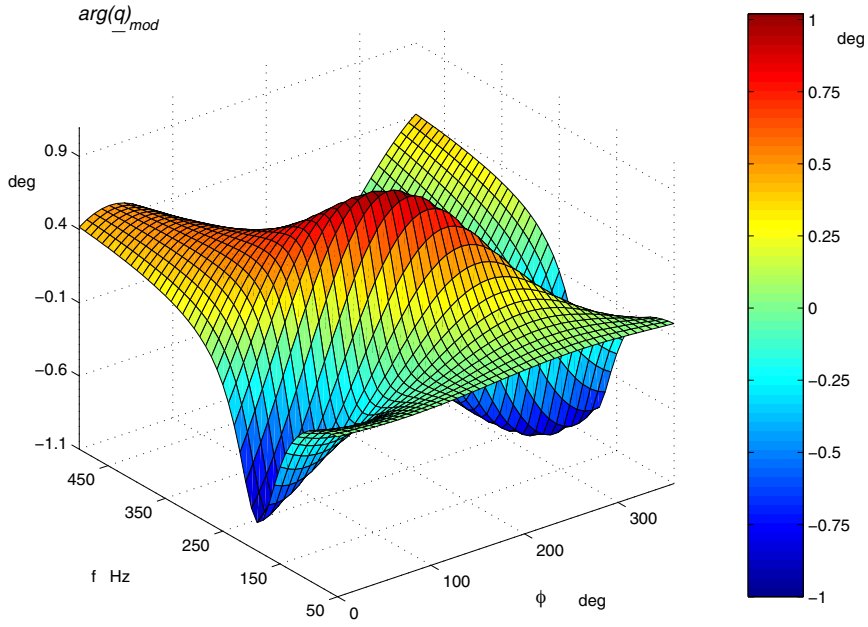

Figure 3.26 - *Volume velocity modifications (phase) according to excitation phase difference and frequency*

3.4.4 Modification analysis according to excitation phase difference

Let us now take a closer look at the previous subsection curves. Taking ϕ = 0° curve as reference, figure 3.27 shows for five given frequencies, the input impedance variation functions in modulus $F_m(\phi, f)$ and phase $F_p(\phi, f)$, according to ϕ.

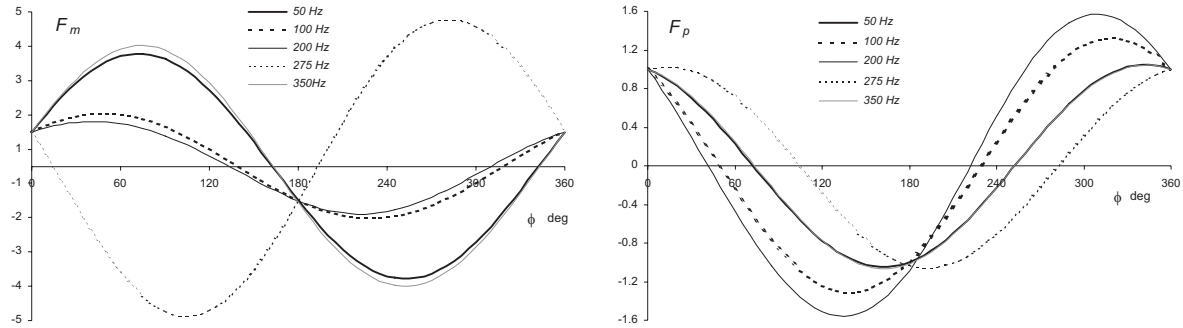

Figure 3.27 - *Functions F_m and F_p calculated for f = 50, 100, 200, 275 and 350 Hz*

The analysis of these curves calculated every 5 Hz enables the variation functions $F_m(\phi, f)$ and $F_p(\phi, f)$ to be determined. They have been identified as:

$$F_m(\phi, f) = \cos(\phi) + G(f)\ \sin(\phi) \tag{3.13}$$

$$F_p(\phi, f) = \cos(\phi) - G(f)^{-1}\ \sin(\phi) \tag{3.14}$$

These equations enable the function $G(f)$ to be calculated frequency by frequency. The result is plotted in figure 3.28 (blue curve). According to the latter, $G(f)$ has been identified as being determined by the reference conditions (black curves of figure 3.21). The zeros correspond to modulus extrema and the discontinuities to modulus zeros. Conversely and due to the fact that $G(f)$ is inverted in F_p, the zeros correspond to phase zeros and the discontinuities to phase extrema. In other words:

$$G(f) = 1.65\ \frac{arg(\underline{Z}(0°))_{mod}}{Z(0°)_{mod}} \tag{3.15}$$

Figure 3.28 shows the comparison between the function $G(f)$ calculated:

- at first from equations 3.13 and 3.14,
- secondly from the function identified in retrospect (equ. 3.15).

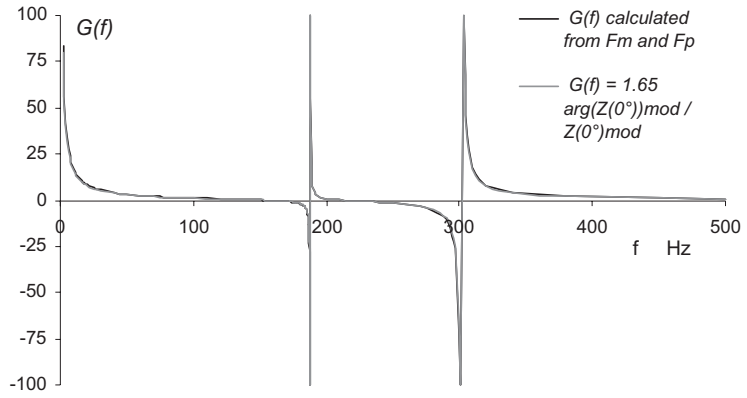

Figure 3.28 - *Function $G(f)$ calculated from the curves of figure 3.21 and from the identified function of equation 3.15*

Let us now analyse in the same way the variations of $\underline{q}$ modifications (fig. 3.24, 3.25 and 3.26). The modification functions have been again identified taking again the $\phi = 0°$ curve as reference. According to phase difference and frequency, the variation functions in modulus $H_m(\phi, f)$ and phase $H_p(\phi, f)$ of the volume velocity modifications are identified as:

$$H_m(\phi, f) = \cos(\phi) - K(f)^{-1}\ \sin(\phi) \tag{3.16}$$

$$H_p(\phi, f) = \cos(\phi) + K(f)\ \sin(\phi) \tag{3.17}$$

The function $K(f)$ is determined by the reference conditions at $0°$ (black curves of figure 3.24), in the same way as $G(f)$, ie:

$$K(f) = \frac{-q(0°)_{mod}}{1.65\ arg(\underline{q}(0°))_{mod}} \tag{3.18}$$

Figure 3.29 shows the comparison between the function $K(f)$ calculated:

- at first from equations 3.16 and 3.17,
- secondly from the function identified in retrospect (equ. 3.18).

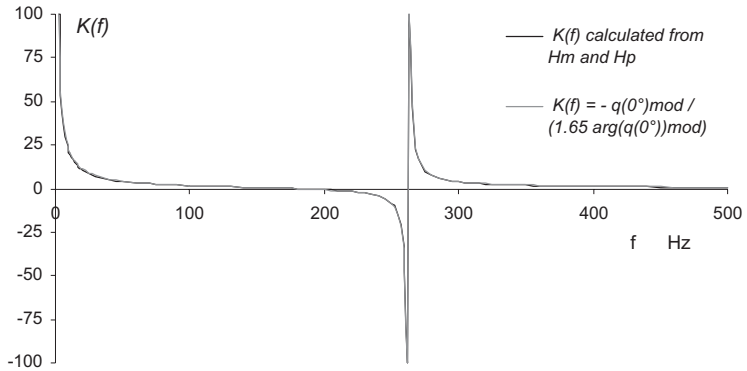

Figure 3.29 - *Function $K(f)$ calculated from the curves of figure 3.24 and from the identified function of equation 3.18*

3.4.5 Modification calculations according to distance between loudspeaker centres

As mentioned in Subsection 3.4.3, this subsection focuses only on input impedance and volume velocity, in order to calculate their modifications according to the distance r between the loudspeaker centres, independently of the observation point.

Thus, figures 3.30 and 3.31 show $\underline{Z}$ and $\underline{q}$ modifications in modulus and phase, according to distance between piston centres ($r = 2a, 3a, 4a, 5a, 6a, 8a, 10a$), and frequency ($f$ from 100 to 500 Hz). ϕ is set to 0° and $\frac{U_1}{U_0}$ to 1.

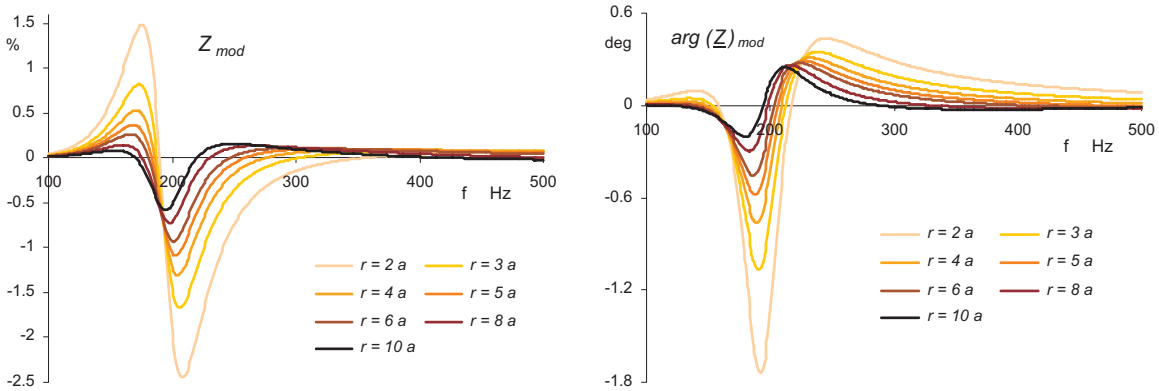

Figure 3.30 - *Input impedance modifications (modulus-phase) according to distance r and frequency*

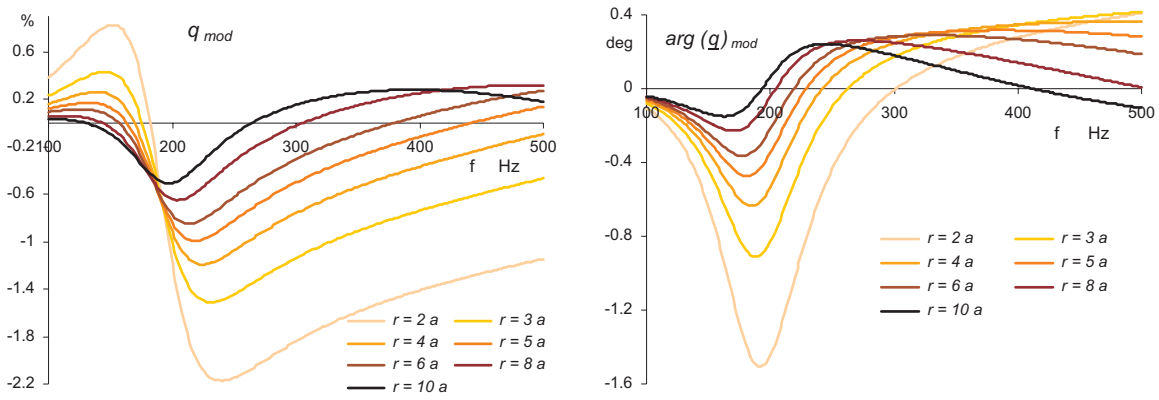

Figure 3.31 - *Volume velocity modifications (modulus-phase) according to distance r and frequency*

3.4.6 Modification analysis according to distance between loudspeaker centres

As in Subsection 3.4.4, let us take a closer look at the curves plotted in Subsection 3.4.5.

Unlike the two previous parameters (U_1/U_0 and ϕ), the variation function according to the distance between source centres is not obvious to determine. Figure 3.32 shows for six given frequencies, the volume velocity variation functions in modulus $F_m(r, f)$ and phase $F_p(r, f)$, according to r.

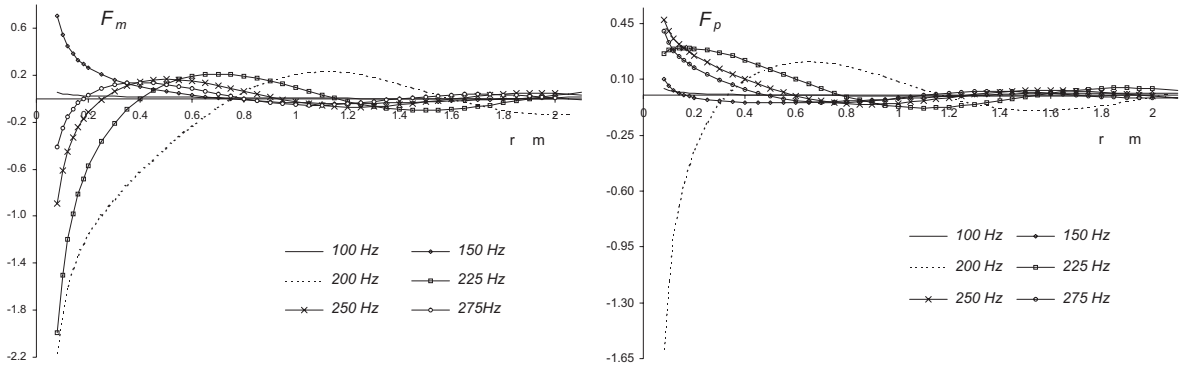

Figure 3.32 - *Functions F_m and F_p calculated for f = 100, 150, 200, 225, 250 and 275 Hz*

An analytical solution was proposed by R.L. Pritchard [11]. However, let us analyse these curves numerically. Calculated every 5 Hz, they enable the variation functions F_m and F_p to be approximated in terms of Bessel functions:

$$F_m(r,f) = \frac{-a_m\ J_1(b\ r + c_m)}{r^{0.9}} \tag{3.19}$$

$$F_p(r,f) = \frac{-a_p\ J_1(b\ r + c_p)}{r^{0.9}} \tag{3.20}$$

where b, a_m, c_m, a_p, c_p are the variables represented in figure 3.33:

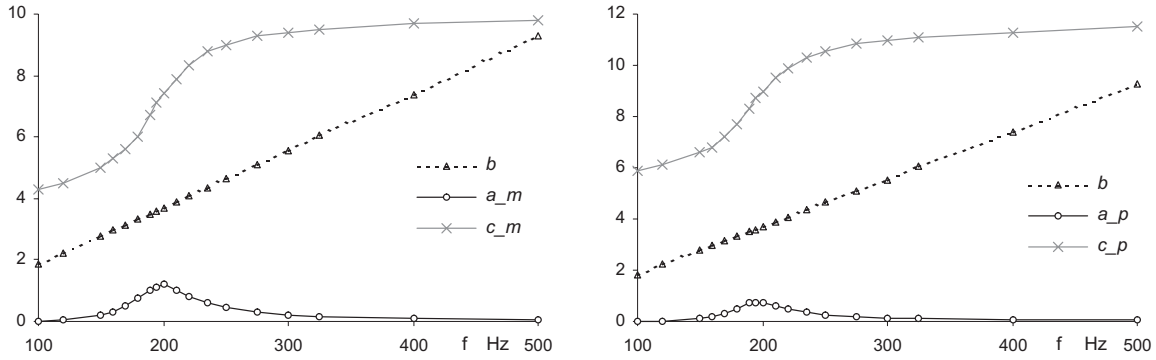

Figure 3.33 - *Variables b, a_m, c_m, a_p, c_p of the functions $F_m(r,f)$ and $F_p(r,f)$*

These variables are very much like:

- a linear function of the frequency for b,
- a function of Z for a_m and a_p, and
- a function of $arg(\underline{Z})$ for c_m and c_p.

The volume velocity variation functions $H_m(r,f)$ and $H_p(r,f)$ may be also approximated by equations 3.19 and 3.20, where b, a_m, c_m, a_p, c_p are the variables represented in figure 3.34. As for the input impedance, these variables are very much like:

- a linear function of the frequency for b,
- a function of q for a_m and a_p, and
- a function of $arg(\underline{q})$ for c_m and c_p.

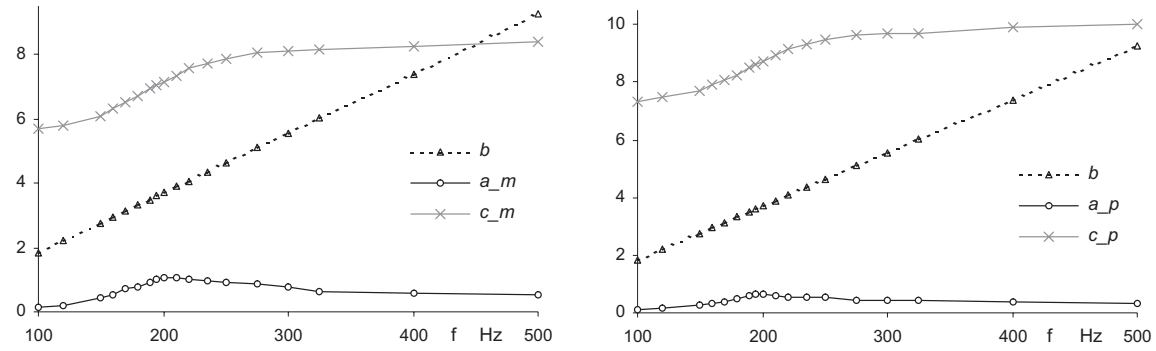

Figure 3.34 - *Variables b, a_m, c_m, a_p, c_p of the functions $H_m(r, f)$ and $H_p(r, f)$*

3.4.7 Iteration number

Mentioned in Subsection 1.7, the numerical computations of $\underline{Z}$ and $\underline{q}$ modifications have to be iterated several times in order to tend toward the solutions. This is explained by the fact that after the first computation, enabling the modified volume velocities $\underline{q}'_{0,1}$ to be found, each loudspeaker radiates a modified sound pressure, which in turn, is going to affect the other one. This is translated into a second calculation leading to the new modified volume velocities $\underline{q}''_{0,1}$, and so on. While this operation may be reproduced indefinitely, the differences between two consecutive calculations will tend rapidly toward zero. The iteration number will depend on the tolerance margin chosen regarding to the required accuracy.

Let us now calculate the difference of $\underline{Z}$ and $\underline{q}$ modifications according to the iteration number. Figure 3.35 shows the Z_{mod} and $arg(\underline{Z})_{mod}$ calculated differences between iterations 0-1, 1-2, 2-3, and 3-4, for three frequencies. The two loudspeakers are identical, separated by $r = 3a$ and excited according to U_1/U_0 = 10. Figure 3.36 shows the same results according to q_{mod} and $arg(\underline{q})_{mod}$ calculations.

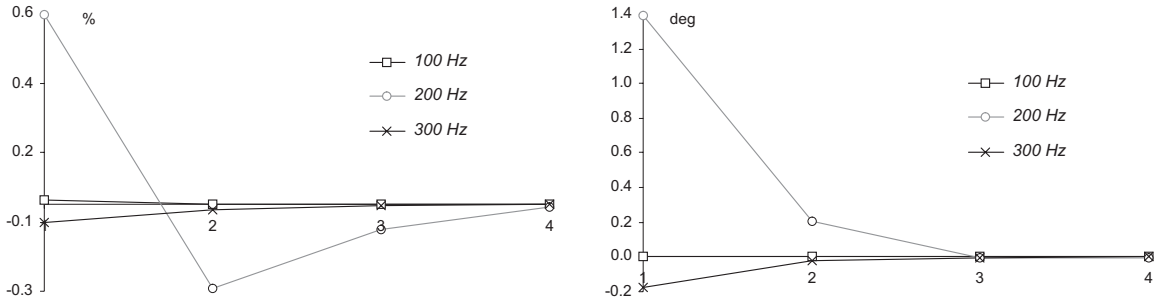

Figure 3.35 - *Z_{mod} and $arg(Z)_{mod}$ differences between 0-1, 1-2, 2-3, and 3-4 iterations*

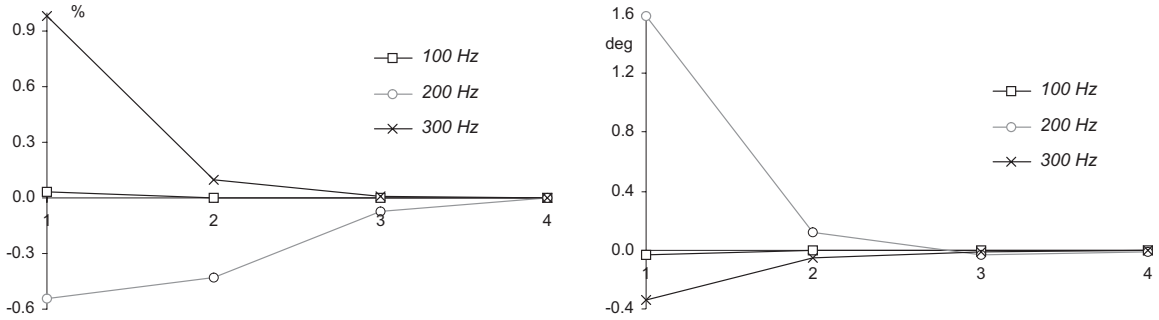

Figure 3.36 - *q_{mod} and $arg(q)_{mod}$ differences between 0-1, 1-2, 2-3, and 3-4 iterations*

As we can see, the differences, tending towards zero when the number of iterations increases, depend directly on the frequency. In Chapter 4, this number is calculated in such a way that the calculated differences fit into the chosen tolerance margin for whatever frequency.

3.5 Diffracion by a closed box

The calculations of closed-box loudspeakers differ from those in baffles because of the need to take into account the diffractions of the enclosure edges.

The sound pressure of a loudspeaker mounted in an infinite baffle is first calculated in order to refer to a customary radiation example. Then, the sound pressure of the same loudspeaker mounted in a closed box can be computed according to the three diffraction methods (see Section 2.4):

1. GTD(0°)
2. GTD
3. UTD

In order to display the different validation domains of the three methods, figure 3.38 shows sound pressure iso-curves in modulus (Pa) and phase (deg) computed near the system resonance (200 Hz) and close to the front panel and piston surface at (z = 1 mm). The latter is divided into 400 elements and the enclosure edges into 24 secondary sources.

Calculated according to the above diffraction methods, figure 3.38 enables the near-field sound pressure to be compared, as:

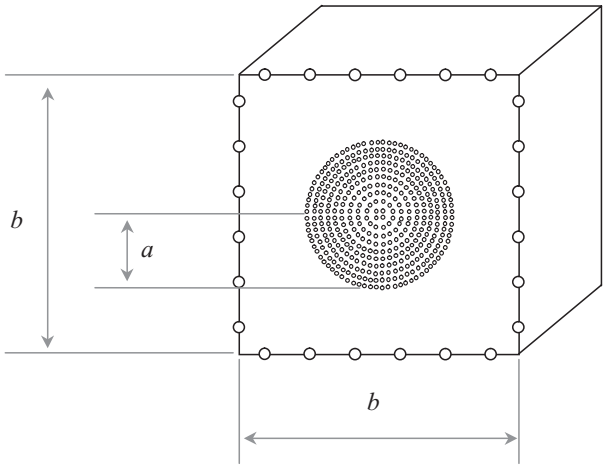

Figure 3.37 - *Depiction of a piston of radius a divided into 400 elements and mounted on a close box of front size b × b, the edges of which are divided into 24 secondary sources)*

1. Figure 3.38 A.
   The calculation of a piston mounted in an infinite baffle is given first, as a reference for the three following calculations of a piston mounted in a closed box.

2. Figure 3.38 B.
   The calculation using the GTD(0°) enables the 24 secondary sources spread on the edges to be easily observed. It is obvious that this result is not valid close to the enclosure edges. Nevertheless, it can be used, as we shall see later, anywhere else in space with a good degree of accuracy.

3. Figure 3.38 C.
   The figure shows very clearly that this method is not valid for observation points located close to the shadow boundaries. We can see that the sound pressure tends to infinity outside the enclosure edges ($\theta_l \cong 180°$ for z $\cong$ 0). The phase results are also interesting because they point out that the phase is reversed at the enclosure edges.

4. Figure 3.38 D.
   Compared with the radiation of a driver mounted in an infinite baffle (fig. 3.38 A), the sound pressure calculated with the aid of the UTD appears to be the most realistic. The reversal phase phenomenon does not appear as clearly as in the case C (figures 3.39 and 3.40 show a drop in phase of about 15 degrees for z = 1 mm). Furthermore, the diffraction is observed here as a kind of break in the radiation field, instead of secondary sources discontinuities.

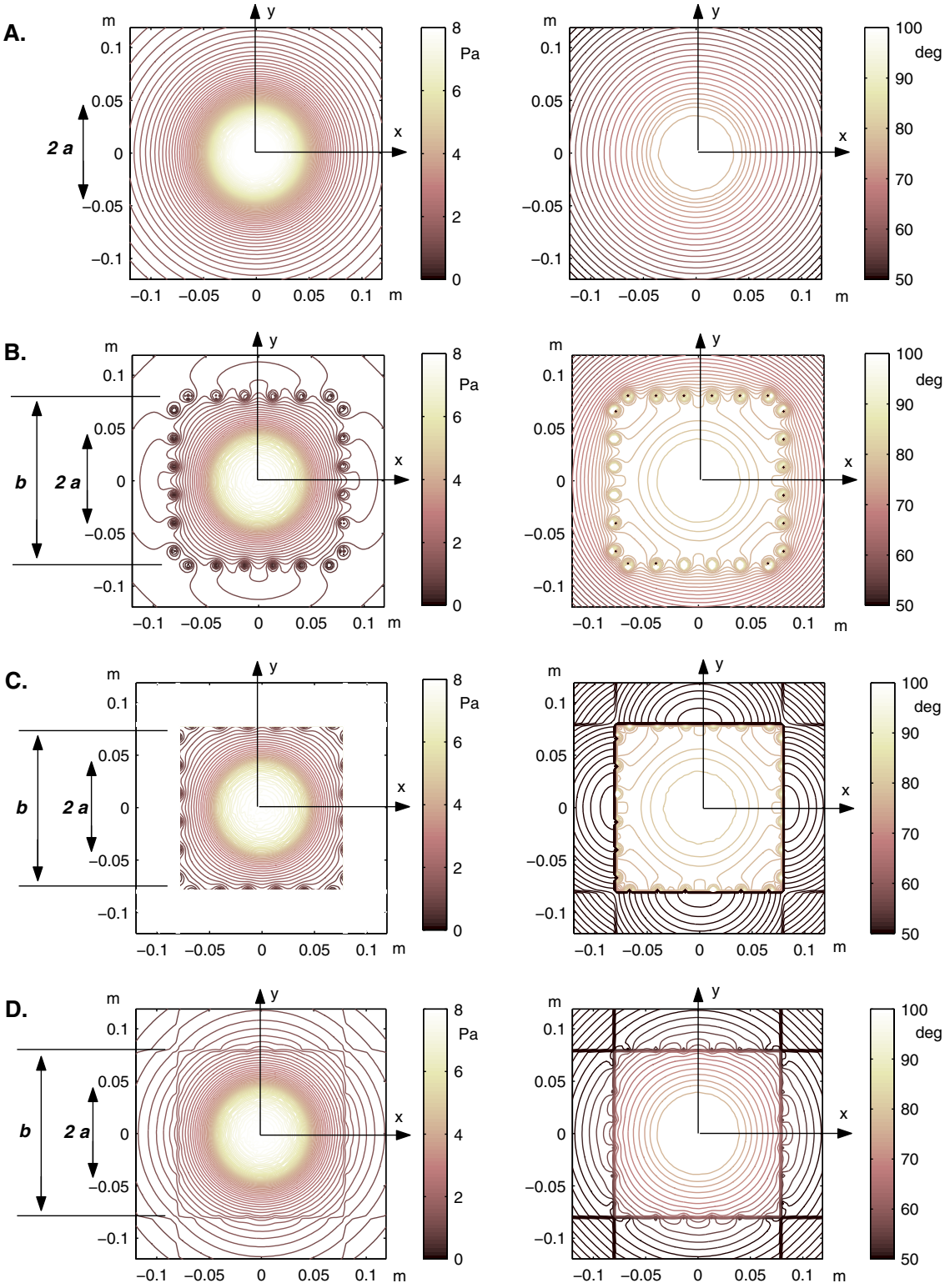

Figure 3.38 - *Sound pressure iso-curves calculated at 200 Hz and at z = 1 mm of a piston ($\oslash = 2a$) in an infinite baffle (A) and in a closed box (front size of $b \times b$) according to GTD with $\theta_l = 0°$ (B), GTD dependent on θ_l (C) and UTD dependent on θ_l (D)*

Whilst figure 3.38 represents the sound pressure on a section located just closed to the baffle (z = 1 mm), it remains difficult to compare the different diffraction methods. To do that, the sound pressure is calculated in modulus and phase according only to the coordinate x, for z = 1 mm. On the one hand, figure 3.39 shows the sound pressure at $y = 0$, that is to say without computing the sound pressure directly on piston or edges elements centres. On the other hand, figure 3.40 shows the sound pressure computed at $y = b/12$ in order to carry out the calculations on two secondary sources centres.

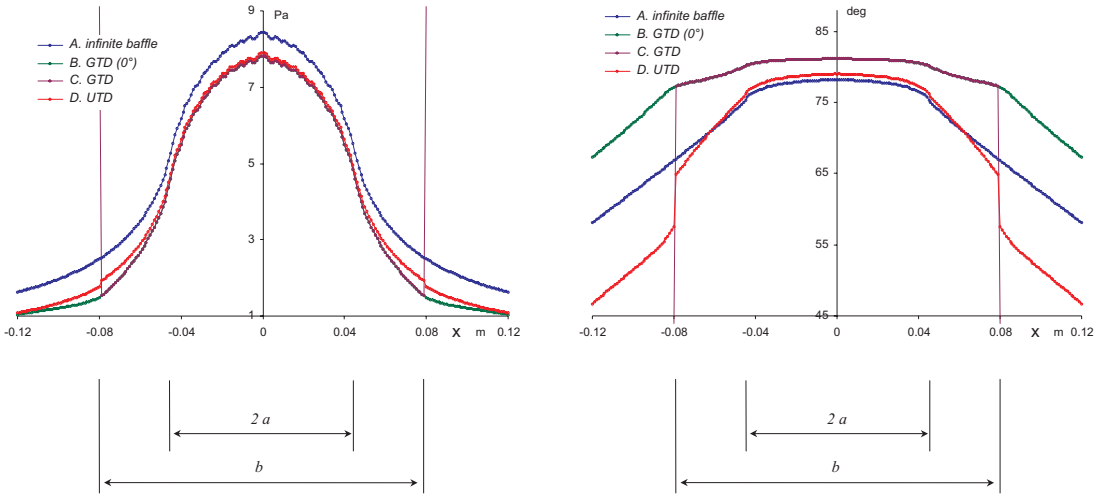

Figure 3.39 - *Sound pressures calculated according to x, at $y = 0$ and $z = 1$ mm - $2\pi st$ radiation compared to GTD(0°), GTD and UTD*

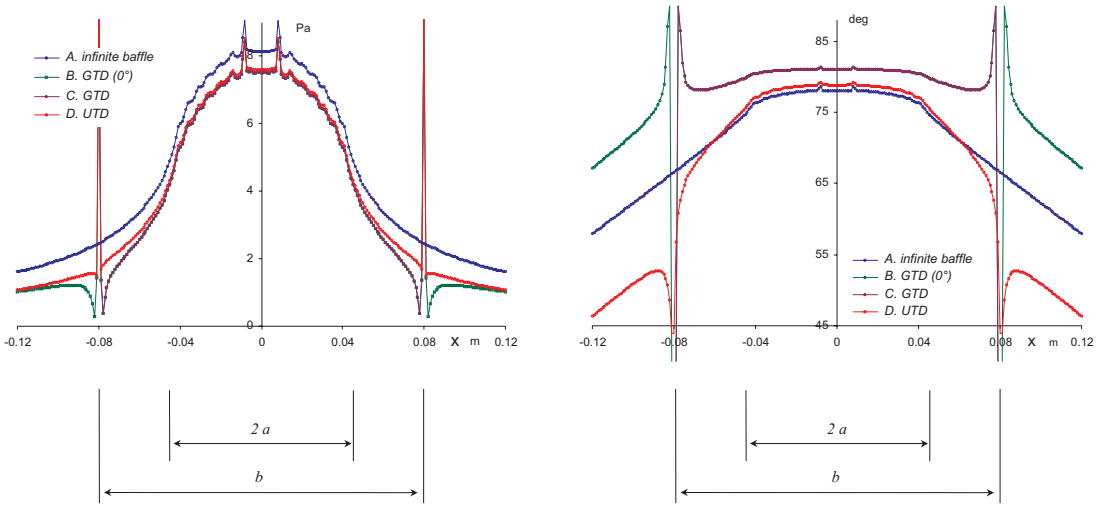

Figure 3.40 - *Sound pressures calculated according to x, at $y = b/12$ and $z = 1$ mm - $2\pi st$ radiation compared to GTD(0°), GTD and UTD*

In order to supplement the latter study concerning the space validation domains of the UTD and GTD, the same has to be done for the frequency validation domains. Figures 3.41 and 3.42 show comparisons between the radiations of a closed-box loudspeaker mounted:

- in an infinite baffle (2πst),
- without baffle and without taking into account diffraction at enclosure edges (4πst),
- without baffle but with taking into account enclosure edges diffraction calculated according to both diffraction methods GTD and UTD.

The calculations versus frequency are carried out on-axis at z = 1 m ($\theta_l \cong 85.5°$) in figure 3.41 and at z = 1 cm ($\theta_l \cong 7°$) in figure 3.42.

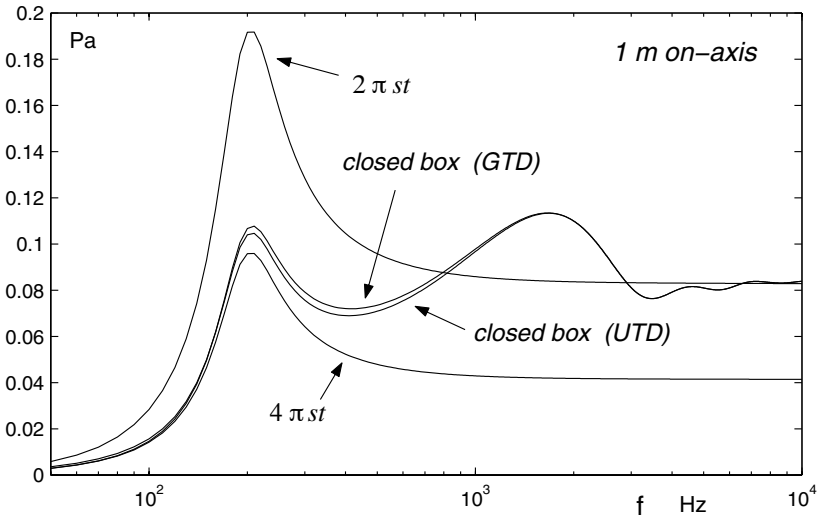

Figure 3.41 - *Comparison of the on-axis sound pressure radiated by a closed-box loudspeaker mounted in an infinite baffle with the sound pressure radiated by the same closed-box loudspeaker taking into account (GTD & UTD) or not (4πst) the diffraction at the edges - calculation at z = 1 m*

As required, the sound pressure curves on-axis ($\theta_l < 90°$) show good similitudes between both theories of diffraction. Furthermore, the far-field curves (at z = 1 m) fit with the common sense concerning the radiation behaviour of a closed-box loudspeaker:

- low frequency range: as the external box dimensions are very small in comparison to the wavelength λ, the driver does not "see" the enclosure and radiates as if it were mounted in 4πst.
- high frequency range: as the wavelength λ is small compared to the front panel of the box, each little radiating surface of the piston "sees" the front panel as if it were an infinite baffle.

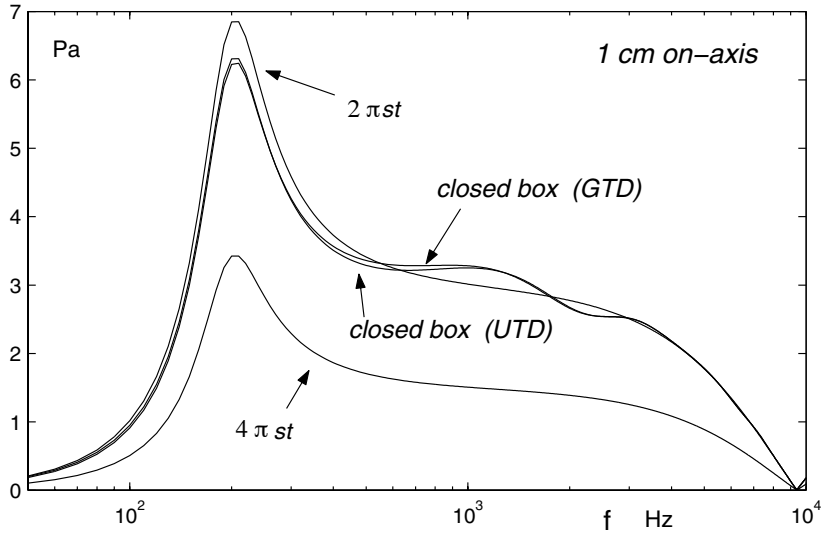

Figure 3.42 - *Same as figure 3.41 but calculated at z = 1 cm*

The near-field curves on-axis (at 1 cm) show a sound pressure behaviour close to that of a driver radiating in 2πst. By the same token, as the observation distance is very small compared to the box front panel dimensions, the observation point "sees" the front panel as an infinite baffle.

Figure 3.44 shows the comparison of the same calculation methods mentioned previously, but with the difference that the computations are carried out this time out-of-axis at x = - 4 a, y = 0, and z = 1 cm. That means that θ_l is contained between 2 and 175 degrees, as shown in figure 3.43.

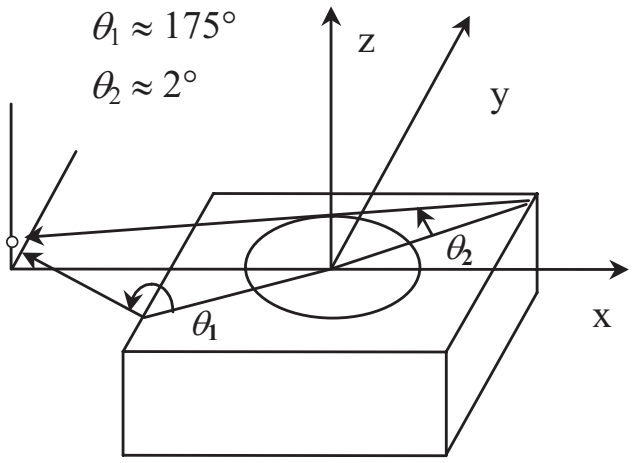

Figure 3.43 - *Depiction of the observation angles θ_1 = 175° and θ_2 = 2°*

For observation points located close to shadow boundaries (when z $\rightarrow$ 0), the observation angles θ_l tend to 180° for the diffraction occurring at the edge located between the driver and the observation point. Conversely, the angles tend to 0° for the diffraction occurring at the other edges.

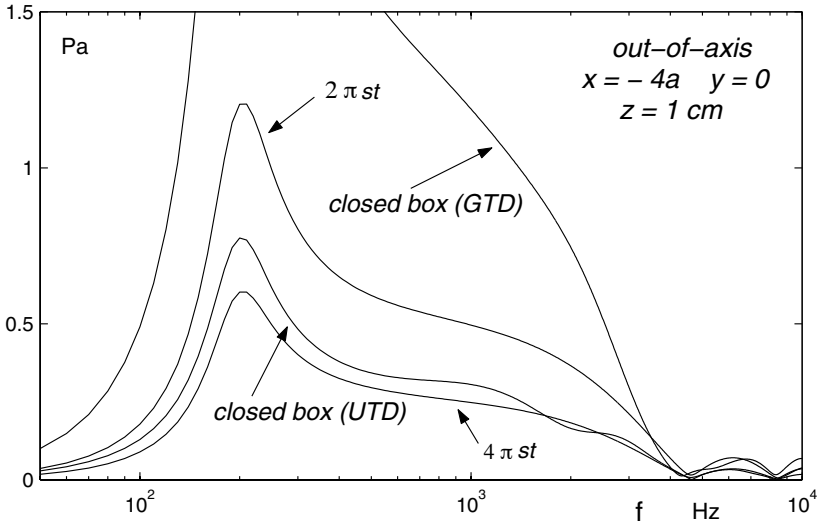

Figure 3.44 - *Same as figure 3.41 but calculated out-of-axis at z = 1 cm*

In this case, the curves calculated according to GTD and UTD differ considerably (fig. 3.44): when the GTD curve tends to infinity (for z $\rightarrow$ 0) in which case it is unusable, the UTD curve appears to approach common sense. The observation point located close to the front panel surface "sees" thus the loudspeaker system as a whole, as if it radiates in 4πst (fig. 3.43).

In conclusion, the UTD will be applied whenever $ks_l(\sin^2 \lambda_l)(1 + \cos\theta_l) < 1$ (fig. 2.9), that is to say in the two following cases:

- when observation points are located close to shadow boundaries (at least one $\theta_l > 130°$)
- when sources are located near diffraction edges ($\lambda_l \cong 0°$)

3.6 Diffraction of two adjacent and distant closed-box loudspeakers

Let us apply the diffraction calculations carried out in the previous section to the case of two identical adjacent and distant closed-box loudspeakers (fig. 2.11 and 2.12).

Taking into account first order interactions between LSP_0 and LSP_1, figures 3.45 and 3.46 show the total sound pressure at 200 Hz, radiated by two adjacent closed-box loudspeakers in the immediate vicinity (z = 1 mm) of their piston and box front panel surfaces. As the closed-box loudspeakers are mounted side by side, the diffraction calculation comes down to the case of two pistons mounted in a limited baffle. Figures 3.45 and 3.46, representing sound pressure modulus and phase iso-curves, enable GTD(0°) and UTD to be displayed. Given that the GTD (dependent on θ_l) gives very bad results close to the shadow boundaries, this method is left aside in these figures.

The pistons surfaces are divided into 400 radiating elements and the finite baffle edges into 36 secondary sources. Both loudspeakers have the same excitation in amplitude (1 V RMS) and phase.

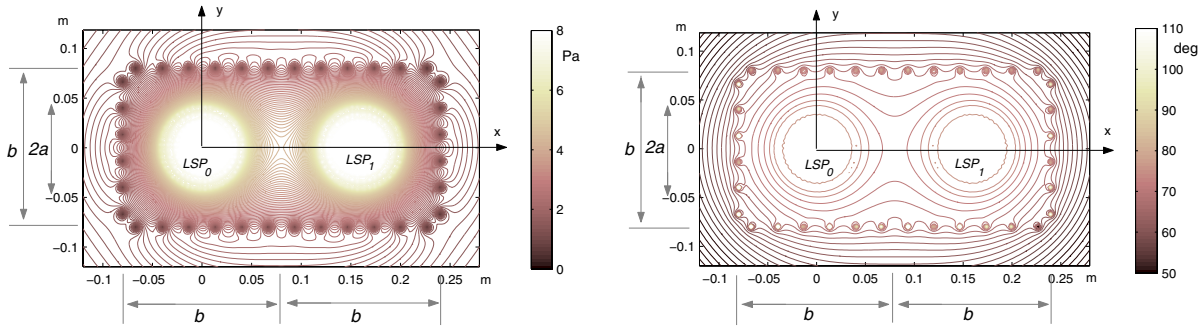

Figure 3.45 - *Sound pressure in modulus and phase of two adjacent loudspeakers calculated according to GTD(0°)*

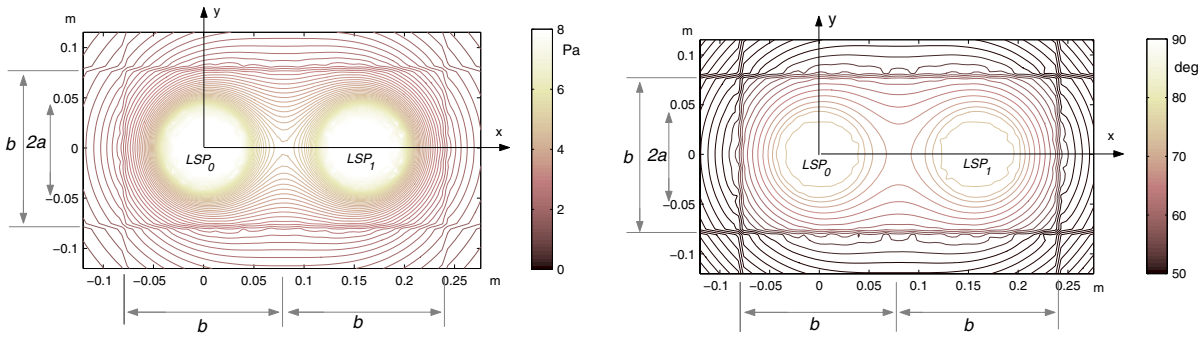

Figure 3.46 - *Sound pressure in modulus and phase of two adjacent loudspeakers calculated according UTD*

For an easier comparison of diffraction methods, the sound pressure is plotted in figure 3.47 according only to the coordinate x, for $y = 0$ and $z = 1$ mm.

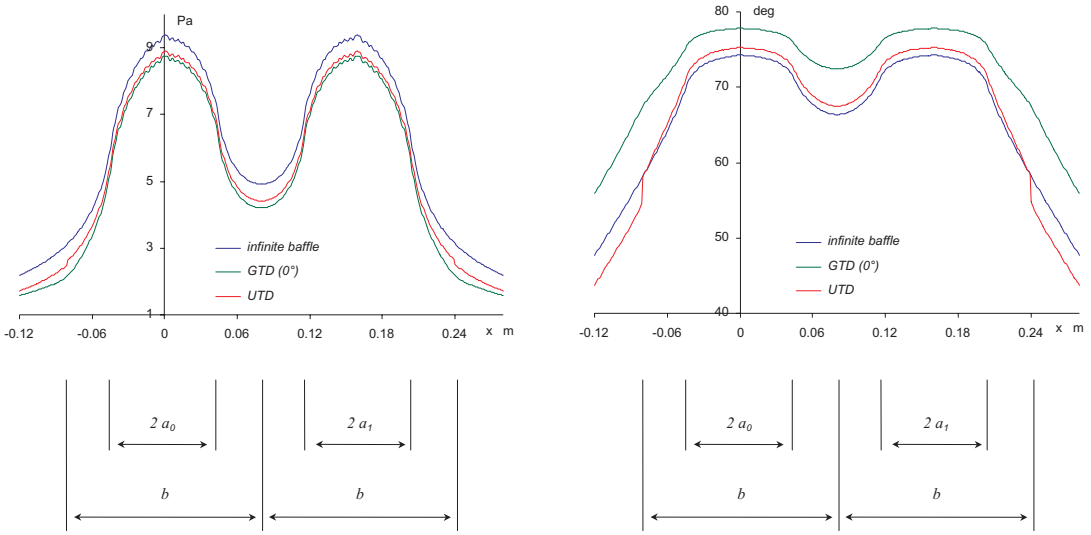

Figure 3.47 - *Sound pressure of two adjacent closed-box loudspeakers - calculation according to x with $y = 0$ and $z = 1$ mm - comparisons between $2\pi st$ radiation, GTD(0°) and UTD methods*

As we can see, the results of calculations based on GTD(0°) and UTD are relatively close to those of two loudspeakers mounted in an infinite baffle. This is explained by the fact that calculation points are chosen very close to the box surfaces, taking care to avoid coordinates (x,y) of secondary source centres.

Let us now apply the iso-curves calculations in the case of two closed-box loudspeakers separated by a distance g as depicted in figure 2.12. The pistons surfaces are divided into 400 elements and the boxes edges into 24 secondary sources each.

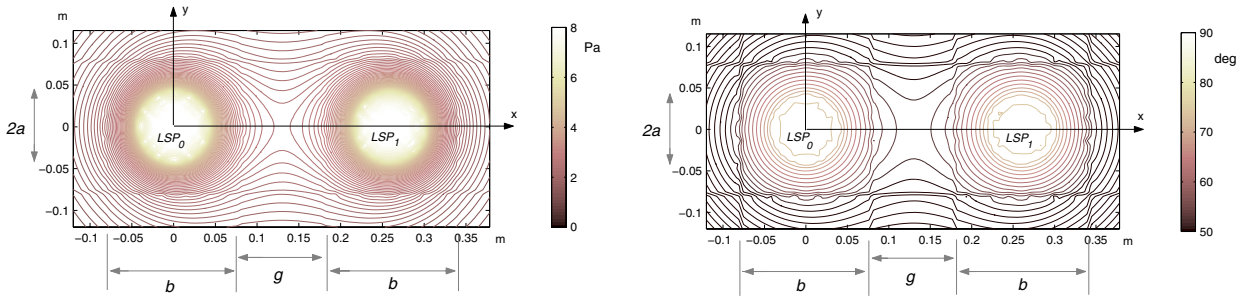

Figure 3.48 - *Sound pressure (modulus - phase) of two distant closed-box loudspeakers (10 cm apart) calculated according to UTD*

As previously, the sound pressure is also plotted (fig. 3.49) according to the coordinate x, for $y = 0$ and $z = 1$ mm.

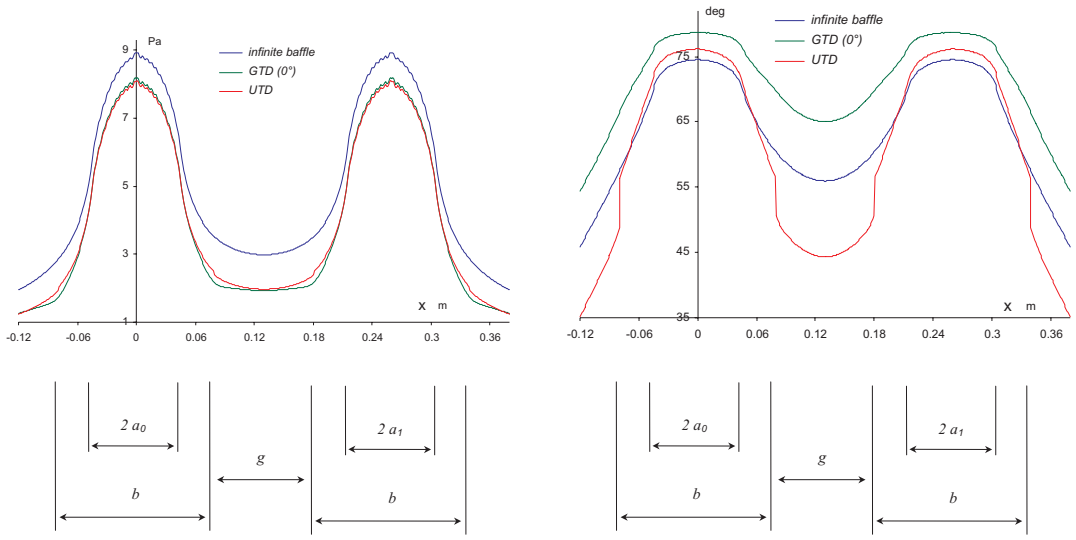

Figure 3.49 - *Sound pressure of two closed-box loudspeakers separated by a distance $g = 10$ cm - calculation according to x with $y = 0$ and $z = 1$ mm - comparisons between $2\pi st$ radiation, GTD(0°) and UTD methods*

Let us now calculate the loudspeaker behaviour modifications according to the frequency and the distance g. Figures 3.50 to 3.52 show $LSP_{0,1}$ medium reaction force, input impedance and volume velocity modifications. Figure 3.53 shows the modifications of the sound pressure radiated by the two loudspeakers together at $x = 0$, $y = 0$ and $z = 1$ m (equ. 3.11). The case of two adjacent loudspeakers is calculated according to both methods GTD and UTD.

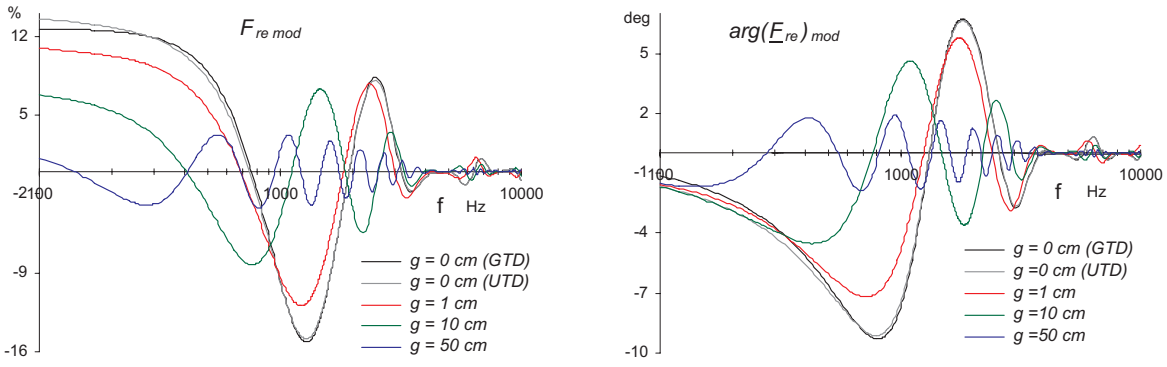

Figure 3.50 - *Modifications of $LSP_{0,1}$ medium reaction force in modulus and phase according to frequency and distance g - GTD and UTD methods*

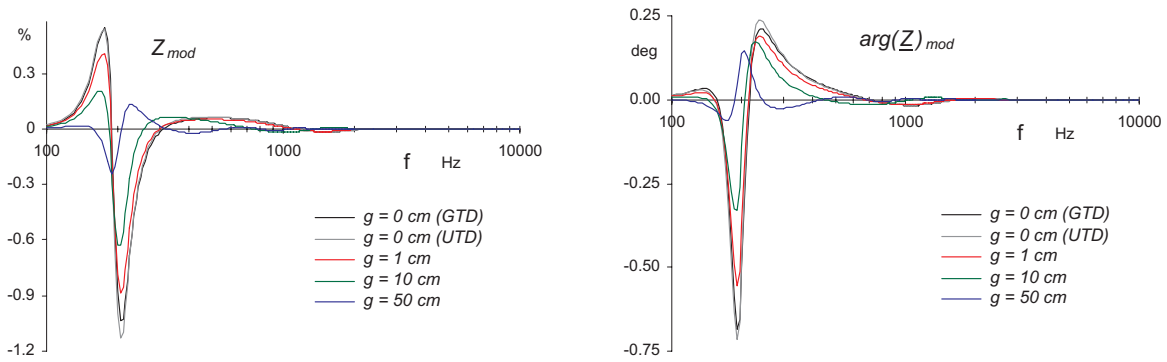

Figure 3.51 - *Modifications of $LSP_{0,1}$ input impedance in modulus and phase according to frequency and distance g - GTD and UTD methods*

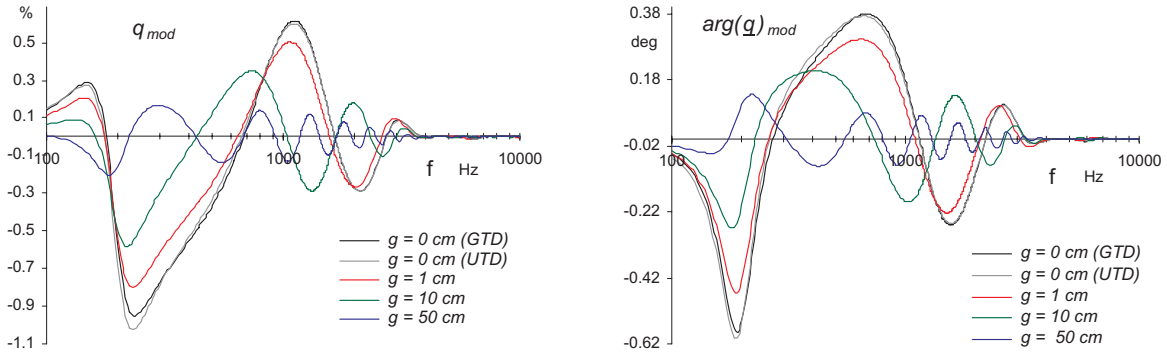

Figure 3.52 - *Modifications of $LSP_{0,1}$ volume velocity in modulus and phase according to frequency and distance g - GTD and UTD methods*

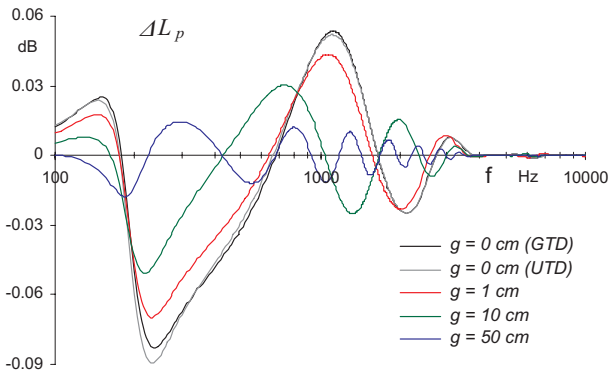

Figure 3.53 - *Differences of the total sound pressure level ΔL_p with and without interaction, at 1 m on-axis according to frequency and distance g - GTD and UTD methods*

All these curves are given in order to keep in mind the modification orders of magnitude related to the different quantities, as well as to observe the different modification laws of decrease.

3.7 Conclusion

Based on the various theories described in Chapter 2, this calculation part has enabled the orders of magnitude of interactions between two loudspeakers to be computed, with a view to choosing the best method of measurement.

This chapter started with the calculations of the input impedance and volume velocity of one closed-box loudspeaker mounted in an infinite baffle. Based on the equivalent acoustical and electrical circuits described in Chapter 1, these calculations were carried out according to the measured parameters of a chosen loudspeaker model. Once the volume velocity was determined, numerical computations of the near-field sound pressure and the medium reaction force were compared to analytical calculations in order to set the two numbers of surface divisions, which were then introduced as default values in the calculation of the force exerted by a loudspeaker on another one.

The interaction computations between two closed-box loudspeakers mounted in an infinite baffle were then carried out by means of first order modifications in volume velocity and input impedance. The resulting orders of magnitude led to the assumption that the input impedance and volume velocity modifications ought to be measurable. Furthermore and in order to analyse incident sound field actions more accurately, it was necessary to complete these calculations with the study of the modifications varying according to different parameters such as the excitation ratio, the excitation difference of phase and the distance between pistons centres.

Finally, the calculation codes developed in the case of two closed-box pistons mounted in an infinite baffle were applied to the more realistic configuration of two closed-box pistons mounted without any baffle. In this case, the computations were modified in order to take into account the effects of diffraction at the enclosure edges. The latter were calculated according to three different methods, that is, the geometrical theory of diffraction independent of the observation angle (GTD(0°)), the geometrical theory of diffraction dependent on the observation angle (GTD), and the unified theory of diffraction (UTD).

The sound pressure radiated by a closed-box loudspeaker was calculated first at different observation points using the GTD and UTD methods. In order to assess the results, the latter were then compared to the calculations of the same closed-box loudspeaker radiating in 2πst and 4πst.

The comparisons of the diffraction methods led to the conclusion that the UTD ought to be applied whenever the observation points were located close to the shadow boundaries or the sources near the diffraction edges. However, as this method requires more computation time than the GTD, the latter will be used in all the other cases.

Chapter 4

Experimental validations

4.1 Aim and process

The aim of this chapter is to validate the previous calculations, by means of three experiments: two closed-box loudspeakers mounted first in an IEC baffle, secondly side by side and finally separated by a distance g.

A method is first proposed in order to determine the measurements set-up (see Subsection 4.2.1), validate the choice of modification study by means of volume velocity and input impedance (see Subsection 4.2.2), discuss the TS parameters (see Subsection 4.2.3) and propose the experiment configurations (see Subsection 4.2.4).

Finally, the measurement results are compared with the calculations for all cases experimented. These comparisons lead to discussions about calculation methods and measurement uncertainties.

4.2 Method

4.2.1 Measurement principles

In order to obtain experimentally the loudspeaker input impedance $\underline{Z}$ and volume velocity $\underline{q}$, it is essential to determine initially which kinds of measurements have to be carried out and which quantities have to be measured.

As the complementarity between measurements carried out using pure tones and white noise enables the calculation validations to be carried out respectively according to the excitation phase difference and frequency, both these kinds of measurements will be treated.

In the case of measurements using pure tones, the loudspeakers are driven by a two-channel sine wave generator allowing their excitations to be varied in modulus as well as in phase. With the aim of measuring only the modifications in loudspeaker behaviour due to the incident sound field, the experimentations must free themselves of any additional effects relating to time-dependent perturbations,

which may be of the same order of magnitude than the effects to be measured. Then, in order to no longer have to take into account the LSP_0 temperature drifts, the LSP_1 is excited by tonebursts.

In the case of measurements using white noise, the loudspeakers are driven through the medium of a PC-based (see Appendix A).

Let us see now which quantities have to be captured. It is very obvious which quantities are required to obtain the input impedance, ie the input voltage $\underline{U}$ and current $\underline{I}$, but it is more problematic to find an effective measurement method suitable for the volume velocity. In our case, two methods afford a real interest:

- the measurement of the diaphragm velocity $\underline{v}$ enables $\underline{q}$ to be calculated according to relation 2.5.
- the measurement of the in-box sound pressure $\underline{p}_{in}$ enables $\underline{q}$ to be calculated, according to the relation:

$$\underline{q} = j\omega C_{ab}\, \underline{p}_{in} \tag{4.1}$$

This last measurement method is applicable in so far as the box behaves like an acoustic compliance, meaning that the acoustic mass m_{ab} and resistance R_{ab} can be neglected (see Appendix B).

In both cases, obtaining the measured volume velocity requires some calculations involving estimated parameters: the projected membrane surface for the first one, and the net enclosure volume for the second one. Some preliminary results lead us to think that the first method will give more accurate results than the second one. Nevertheless, the second method will be preferred for practical reasons.

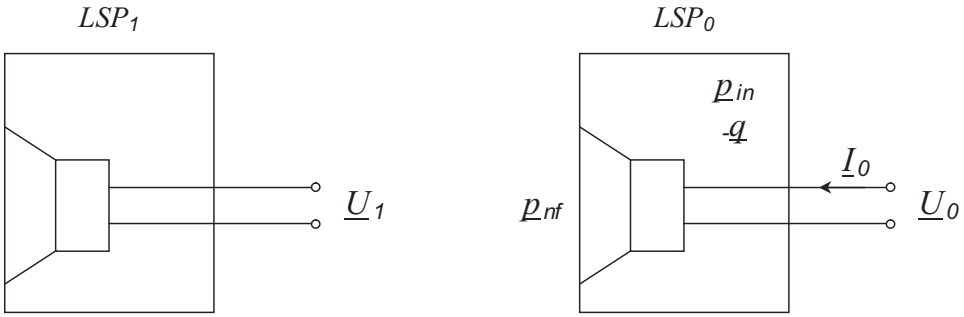

Figure 4.1 - *LSP_0 and LSP_1 measured quantities*

Summing up the measured quantities $\underline{U}_1$, $\underline{U}_0$, $\underline{I}_0$, $\underline{p}_{in}$, and $\underline{p}_{nf}$, figure 4.1 shows that the modification measurements will be carried out essentially on the loudspeaker LSP_0, subjected to the LSP_1. The

LSP_0 near-field sound pressure $\underline{p}_{nf}$ is added to the other quantities in order to control the excitations in the case of measurements carried out using pure tone excitations, and check the sound level in the case of measurements carried out using white noise.

4.2.2 Preliminary experiment

The aim of this preliminary experiment is to turn the attention on every potential measurement difficulty, to determine the measurement set-up, and to validate the choice of the measurement types. It seems essential, in this preliminary stage, to get rid of any diffraction and significant mutual effects likely to distort the results. The measurement principle is thus chosen in order to reduce the mutual effects to a minimum by virtue of great volume velocity differences.

The chosen configuration (fig. 4.2 and 4.3), made up of two different closed-box loudspeakers mounted face-to-face at a distance of one meter, will also enable the orders of magnitude of modifications occurring at a loudspeaker (LSP_0) subjected to an incident sound field to be predicted (see Appendix A for equipment list).

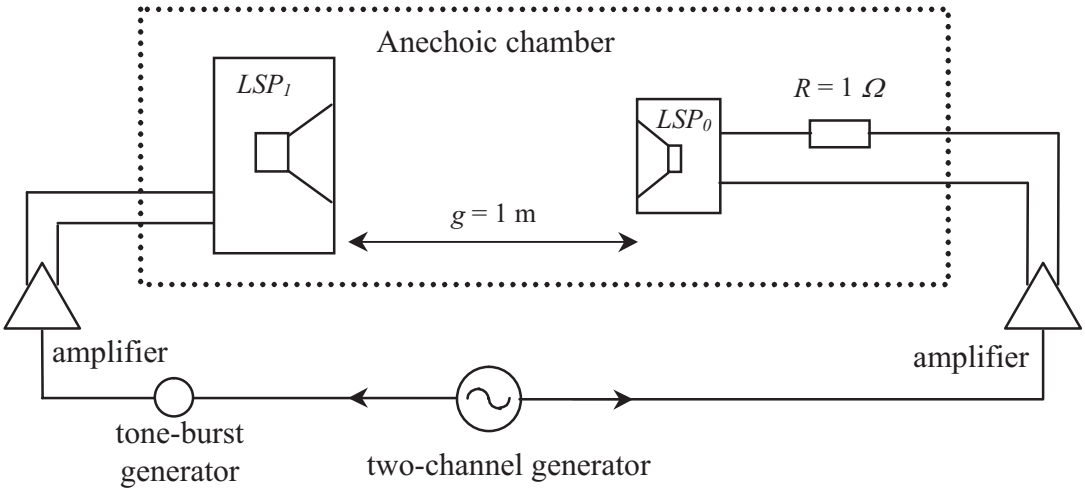

Figure 4.2 - *Assembly diagram of a closed-box loudspeaker (LSP_0) subjected to the sound field of another loudspeaker (LSP_1) located in far-field - pure tone excitations*

The incident sound field is delivered by the closed-box system LSP_1, made up of four PHL loudspeakers. The secondary source LSP_0 is a specimen of the loudspeaker used in the calculation part (see Section 3.2), and mounted in a small closed box of external dimensions: 0.1 x 0.16 x 0.16 m^3 (fig. 4.4).

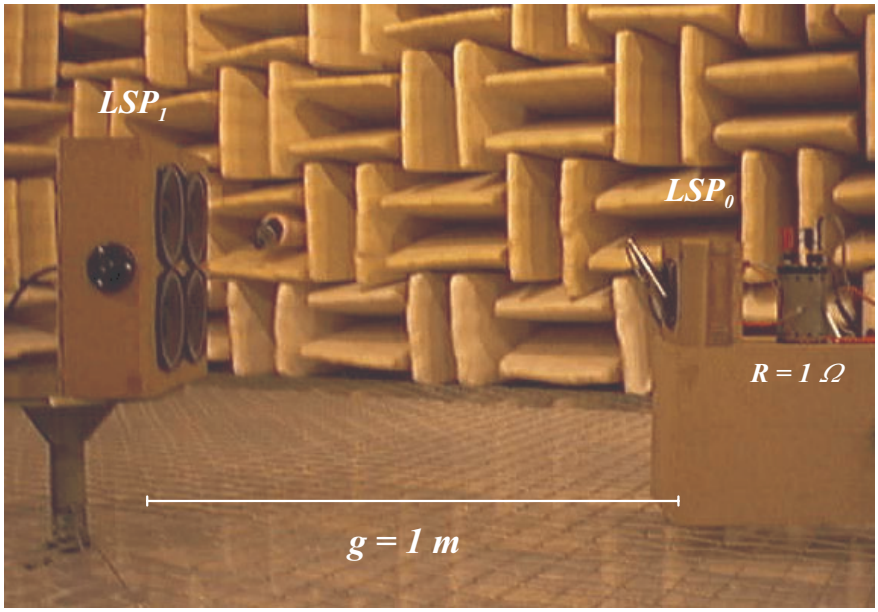

Figure 4.3 - *Picture of two different closed-box loudspeakers mounted face-to-face at a distance of 1 m*

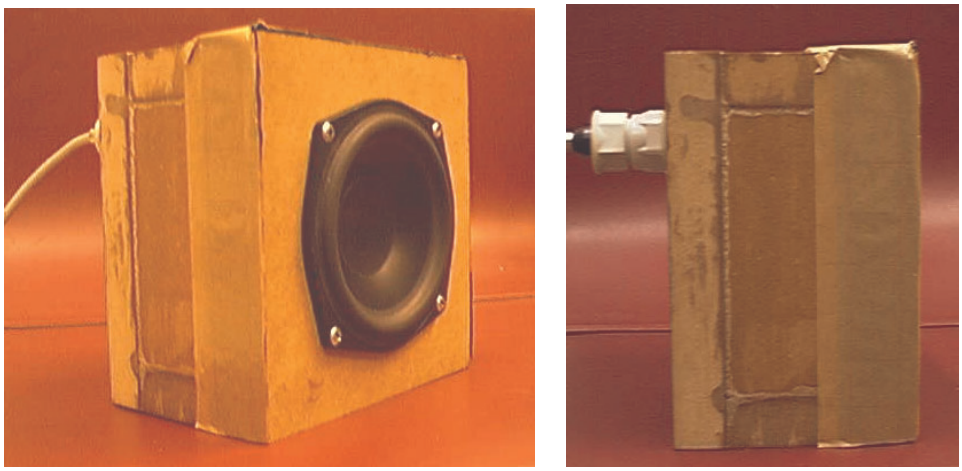

Figure 4.4 - *LSP_0 closed-box loudspeaker made up of a driver (see Section 3.2) mounted in a small enclosure of external dimensions: 0.1 x 0.16 x 0.16 m^3) - 1/2" microphone inside the box*

In order to measure the greatest modifications of input impedance and volume velocity, a first frequency of 200 Hz is chosen close to the LSP_0 resonance. A second one, of 1 kHz, is chosen more than two octaves higher so as to notice the expected decrease of modifications.

In order to reduce the mutual effects to a minimum, the $LSP_{0,1}$ excitation levels are individually adjusted so as to obtain the same sound pressure level $L_{p_{nf}}$ of 120 dB in the immediate vicinity of LSP_0 membrane (at outer suspensions level). The difference of phase between input voltages is set so as to minimize the near-field sound pressure at p_{nf} location.

This setting determines the reference state (0°). The measurements are then carried out in out-of-phasing LSP_1 input voltage from 0° to 180° in 10° steps. The quantities $\underline{U}_0$, $\underline{I}_0$ and $\underline{p}_{in}$ are recorded during 10 seconds and converted in *.wav* under the software *CoolEditPro*, before to be post-processed under *Matlab*.

Figure 4.5 shows the variations over time of the LSP_0 input impedance modulus with and without an incident sound field (tone bursts of one second every two seconds) at 200 Hz and 1kHz. These measurements correspond to the reference state.

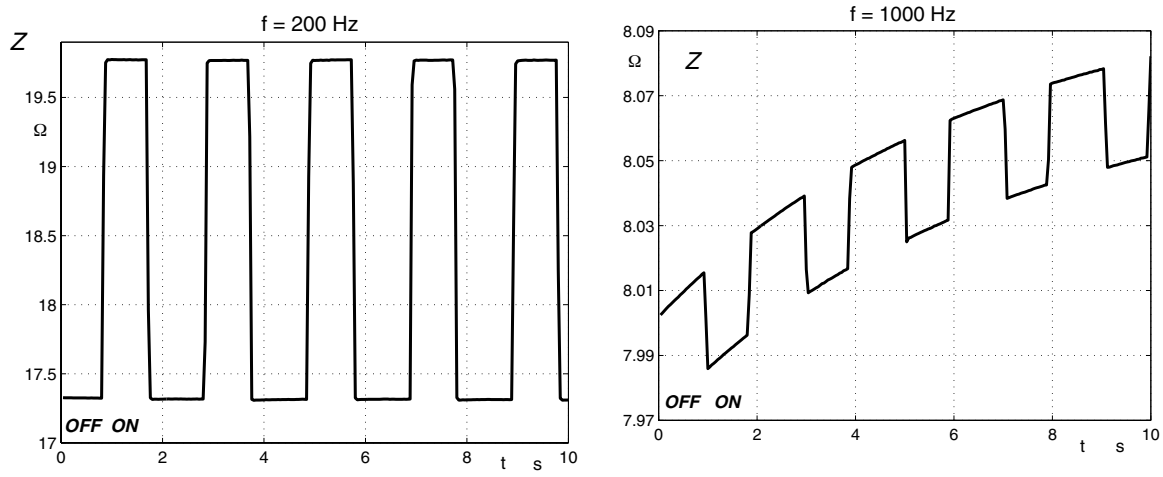

Figure 4.5 - *Variation over time of LSP_0 input impedance (reference state of 0°)*

As was expected the modifications at 200 Hz, in the order of 15 %, are much more significant than those at 1 kHz, which are only in the order of 0.4 %.

Additionally, the second graph is quite representative of the rise of the voice-coil resistance due to increasing temperature. However, the input resistance differences, with and without external sound field, remain unchanged in time.

Let us now plot the LSP_0 input impedance modifications corresponding to the differences between the on/off states shown in figure 4.5, and this versus the excitation difference of phase ϕ. Figures 4.6, and 4.7 show the input impedance modifications in modulus and phase versus ϕ, for 200 and 1000 Hz. The phase difference is calculated by cross-correlation, according to the *Matlab XCORR* function (see Appendix A.3).

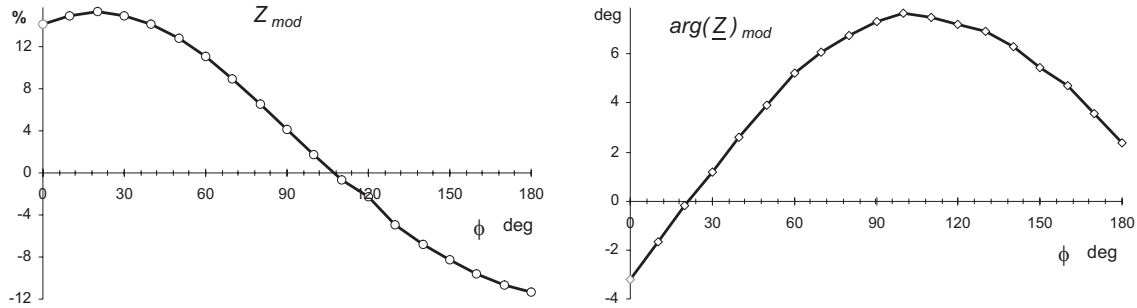

Figure 4.6 - *Modulus and phase modifications at 200 Hz of the LSP_0 input impedance, versus difference of phase*

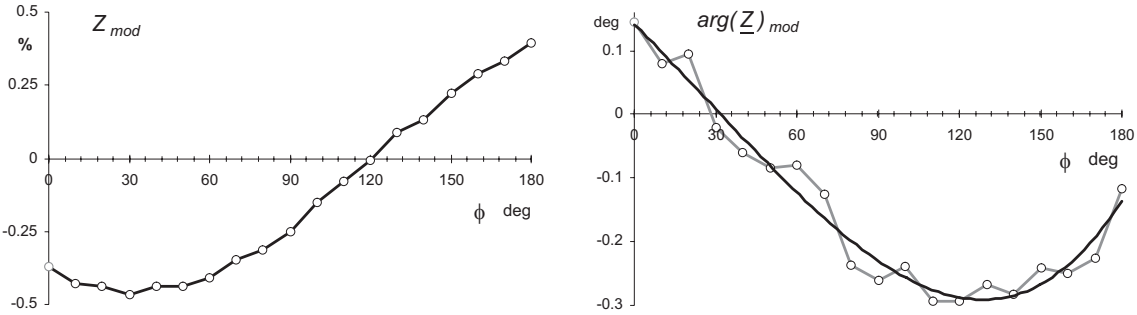

Figure 4.7 - *Modulus and phase modifications at 1000 Hz of the LSP_0 input impedance, versus difference of phase*

The orders of magnitude of phase modifications at 1000 Hz being very small, the cross-correlation calculations show some inaccuracies. A polynomial approximation of order 4 is thus also plotted in figure 4.7.

Let us do the same for the $\underline{p}_{in}$ modifications in modulus versus ϕ. The calculations are again carried out at 200 and 1000 Hz (fig. 4.8).

These results show that the effects of an incident sound field on a closed-box loudspeaker can be easily measurable in terms of input impedance $\underline{Z}$ and sound pressure $\underline{p}_{in}$ modifications. They thus valid the measurement set-up. Furthermore, they also enable the sinusoidal tendency of modification variations according to ϕ to be highlighted, which closely matches the expected variations calculated in Sections 3.4.3 and 3.4.4.

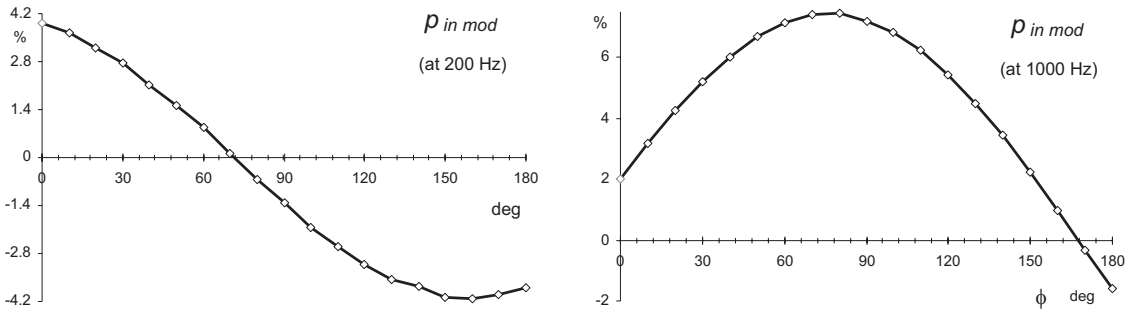

Figure 4.8 - *Modulus modifications of LSP_0 inner sound pressure versus difference of phase, at 200 and 1000 Hz*

4.2.3 Description and TS parameters

From this subsection, the two loudspeaker systems LSP_0 and LSP_1 will be as identical as possible (fig. 4.9), which does not mean that their parameters will be exactly the same. These small differences could not be neglected when accurately comparing measurement results with predictions. The parameters of both closed-box loudspeakers will thus be first measured and then introduced individually in calculation sheets.

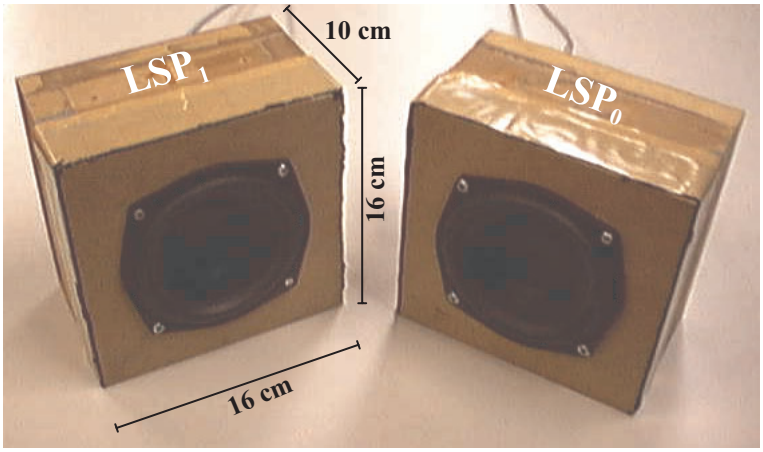

Figure 4.9 - *Picture of LSP_0 and LSP_1*

As explained in Appendix B, the choice of the TS parameters measurement fell on the delta compliance method, in which the parameters are determined from measurements of electrical input impedances. According to an excitation voltage of 50 mV (RMS), an example of these measured parameters is given for both loudspeaker systems in the above mentioned appendix.

As the accuracy of those parameters is essential and also due to the fact that, in the next sections, the loudspeakers will be driven by different excitation amplitudes with a maximum value of 2 V, it appears to be vital to measure the parameters at increasing input voltages.

Figures 4.10 and 4.11 show the resonance frequencies f_s and f_c of both loudspeakers according to the input voltage. They are measured without any warming up and after a warming up period of 30 minutes, carried out with the same input voltage used during the parameters measurement.

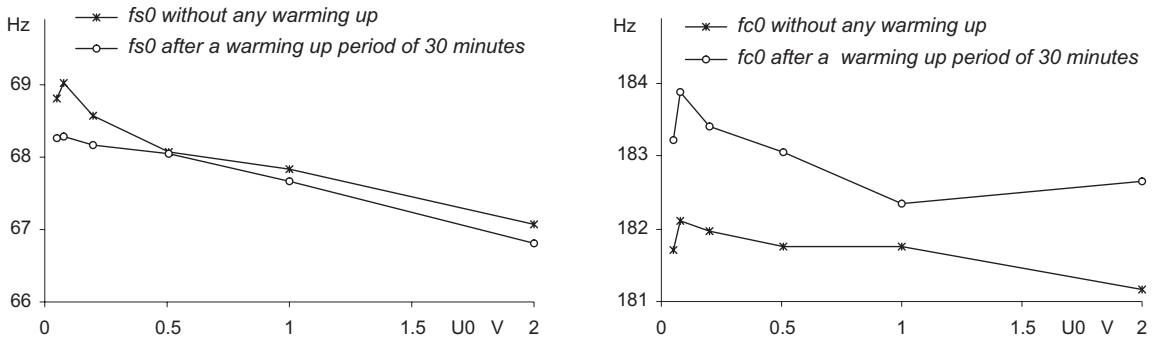

Figure 4.10 - *Resonance frequencies of the LSP_0 measured in free and closed-box assemblies according to the input voltage - measurements with and without any warming up*

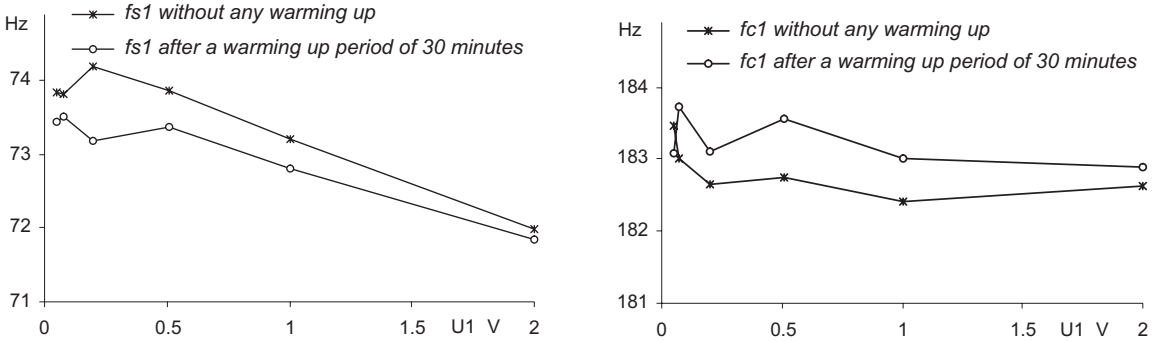

Figure 4.11 - *Resonance frequencies of LSP_1 measured in free and closed-box assemblies according to the input voltage - measurements with and without any warming up*

The shape of the curves related to the free assemblies appears to confirm that the resonance frequency f_s decreases with the increasing excitation. This main tendency is much less marked in the closed-box systems curves. This observation tends to prove that the mechanical compliance C_{ms}, corresponding to the inner and outer suspensions, increases with the membrane displacement. This effect is of course less manifest when the driver is mounted in a small enclosure due to the fact that the value of the acoustic suspension related to the enclosure volume overcomes the increase in C_{ms}. In order to justify that the resonance frequency is mainly determined by the enclosure [12], let us calculate the values of C_{ac}, C_{ab} and α, according to Section 1.5:

$$C_{ac_0} = 36.9\ 10^{-9}\ \mathrm{m}^3/\mathrm{Pa} \quad C_{ab_0} = 42.9\ 10^{-9}\ \mathrm{m}^3/\mathrm{Pa} \quad \alpha_0 \cong 6.1$$

$$C_{ac_1} = 35.9\ 10^{-9}\ \mathrm{m}^3/\mathrm{Pa} \quad C_{ab_1} = 42.9\ 10^{-9}\ \mathrm{m}^3/\mathrm{Pa} \quad \alpha_1 \cong= 5.1$$

Without going further into detail, we can admit that the driver may not be regarded as a linear nor invariant system. While it is possible to do away with this non-linear behaviour by introducing into the calculation data TS parameters that correspond to the input voltage, it is more difficult to take into account their time variations due to the voice-coil warming up and the ageing of the driver. Therefore, due to the difficulty in monitoring the latter phenomena and because their orders of magnitude are higher than those of the measurement inaccuracies, their valuation will give the tolerance margins necessary for the error calculations.

The other required parameters are:

- the membrane radius $a = 4.5 \pm 0.1$ cm,
- the net internal box volume $V_b = 0.585 \pm 0.05$ dm^3 (see Appendix B.3),
- the source resistances $R_{g_0} = 1.8 \pm 0.1\ \Omega$ and $R_{g_1} = 0.8 \pm 0.1\ \Omega$ (see Appendix C), and
- the estimated compliance factor $\beta = 1$ (no filling material).

4.2.4 Experiment configurations

Now that the expected orders of magnitude of loudspeaker modifications have been highlighted, that the feasibility of measurement process has been proved and that most of the possible difficulties have been delimited, the study can focus on the validation part comparing measurement results with calculations. Three experiments have been chosen starting with a simple academic case and ending with a more realistic one, corresponding for example to the case of loudspeakers mounted in an array:

- Experiment 1: two closed-box loudspeakers mounted in an IEC baffle, corresponding to the calculation case of loudspeakers mounted in an infinite baffle (see Section 4.3)
- Experiment 2: two adjacent closed-box loudspeakers, corresponding to the calculation case of loudspeakers mounted in a limited baffle (see Section 4.4)
- Experiment 3: two distant closed-box loudspeakers (see Section 4.5)

Finally, a supplementary experiment was carried out by means of two closed-box loudspeakers mounted face-to-face. An elementary analysis of this case showed that it involves phenomena beyond the scope of this thesis. It was decided not to go into the subject in any greater depth. The assumptions and ideas of investigation are nevertheless given in Appendix E, as well as the comparisons between measurements and calculations.

4.3 Two closed-box loudspeakers mounted in an IEC baffle

4.3.1 Aim

This first experiment is necessary to validate the calculations carried out in the simple case of two pistons mounted in an infinite baffle (see Section 3.4). The loudspeakers LSP_0 and LSP_1 are those represented in figure 4.9.

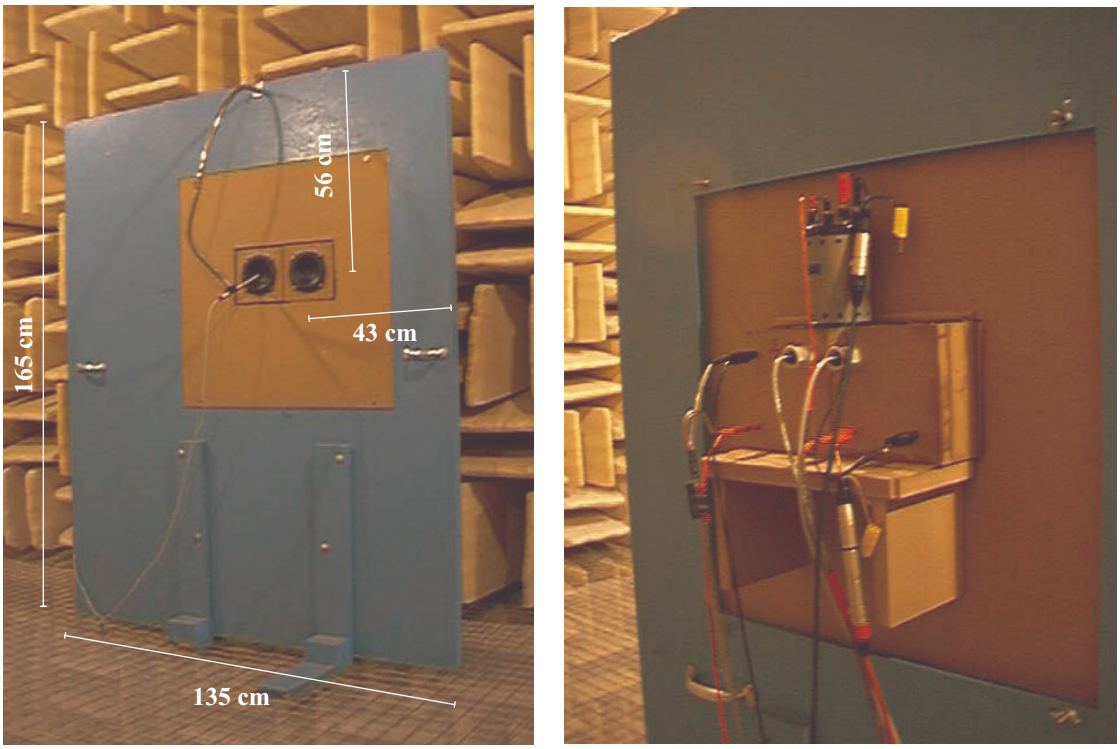

Figure 4.12 - *Two adjacent closed-box loudspeakers mounted in an IEC baffle (135 x 165 cm) - front and back views*

With the aim of validating the calculations according to input voltage (difference of phase and amplitude), the measurements are first carried out using pure tone excitations (200 Hz) in accordance with the preliminary experiment (see Subsection 4.2.2).

Then, with a view to validate also the calculations according to the frequency, the measurements are also carried out using white noise excitations.

As previously, the equipment lists are given in Appendix A for both measurement methods.

4.3.2 Measurements using pure tone excitations at 200 Hz

The measurement process and measured quantities are the same as those used in the preliminary experiment (fig. 4.1).

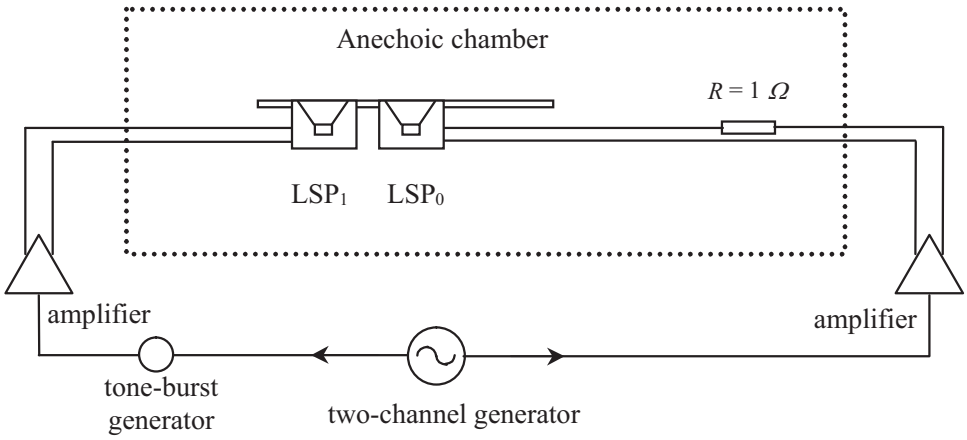

Figure 4.13 - *Assembly diagram of two closed-box loudspeakers mounted in an IEC baffle and driven in pure tones*

LSP_0 and LSP_1 are driven in order to produce separately the same sound pressure level $L_{p_{nf}}$ at LSP_0 outer suspensions level. The reference state is set up following the next operation sequence:

1. $L_{p_{nf}}$ = 90 dB with U_0 = 0.075 V and U_1 = 0 V
2. $L_{p_{nf}}$ = 90 dB with U_0 = 0 V and U_1 = 0.51 V
3. $L_{p_{nf}}$ = 52 dB (minimum level) with U_0 = 0.075 V, U_1 = 0.51 V and ϕ = 36 deg

It is worth noting here that the amplifiers were wired completely out-of-phase. Thus, the ϕ reference value is in reality -144 degree, as it can be seen in figure 4.14. Instead of repeating the measurements, it was decided to go on with this wiring for the rest of the thesis. Therefore and in order to correspond to the measurements, LSP_0 and LSP_1 excitations are introduced into calculation sheets according to a π phase shifting. Thus, it is worth noting here that all the measurement and calculation results given in this chapter will be upside-down relative to those of Chapter 3.

Figure 4.14 shows the near-field sound pressure level $L_{p_{nf}}$ according to excitation phase differences ϕ (every 10 degrees). The measured curve is compared to the two calculated ones, according to 0 and 2 iterations (see Subsection 3.4.7). The iteration number will be set by the calculations of $\underline{Z}$ and $\underline{q}$ modifications.

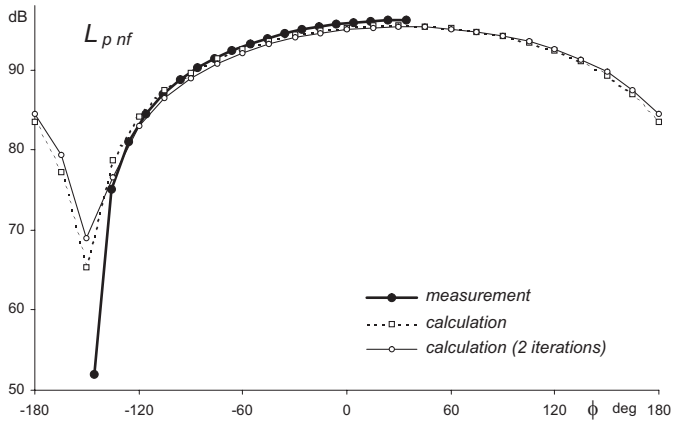

Figure 4.14 - *Sound pressure level $L_{p_{nf}}$ radiated by the two loudspeakers together according to ϕ - comparisons between measurements and calculations (0 and 2 iterations)*

In order to obtain the measured phase, the post-processing is again carried out by cross-correlation of input voltage U_0 and current I_0, using the *Matlab* function *XCORR*. As an example, figure 4.15 shows the post-processed input impedance in modulus and phase for the reference state of ϕ = -144 deg, $\underline{Z}$ and $\underline{Z}'$ being respectively the LSP_0 input impedance without and with LSP_1 action.

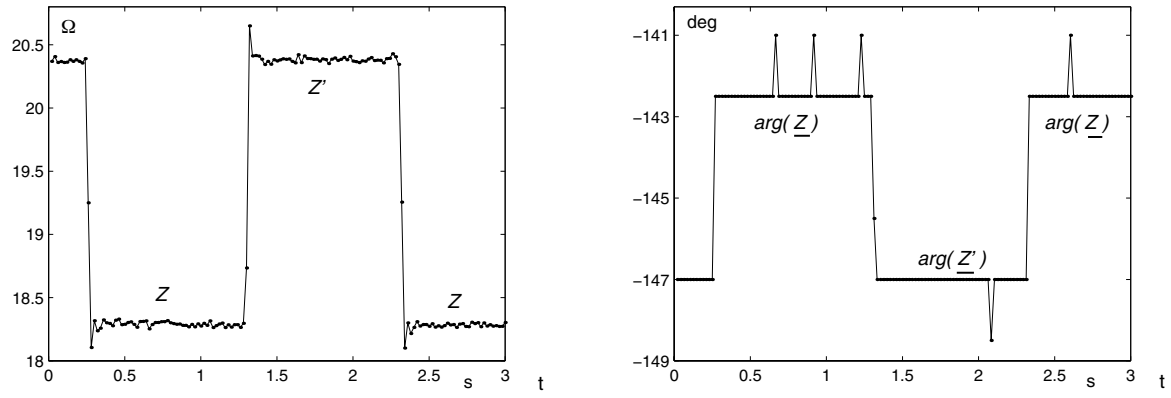

Figure 4.15 - *LSP_0 input impedance over time in modulus and phase, with and without LSP_1 action*

This post-processing is also carried out for the other measurements (every 10 degrees) in order to compute the input impedance modifications over phase difference, according to relations 3.7 and 3.8. Figure 4.16 shows thus the post-processing results compared to the calculated $\underline{Z}$ modifications in modulus and phase, according to ϕ.

The iteration number is considered to be acceptable when the difference between two consecutive iterations is bounded by $\pm 10^{-4}$ ($\pm 0.01\%$) for the modulus and $\pm$ 0.01 degree for the phase. These

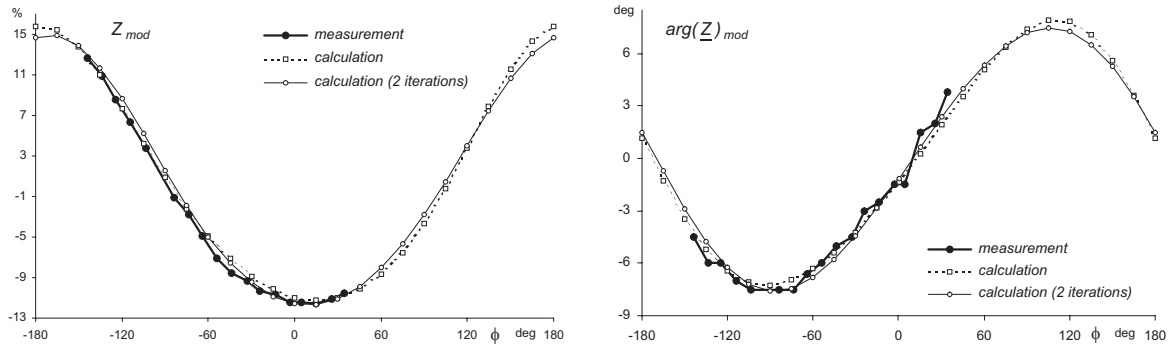

Figure 4.16 - *LSP_0 input impedance modifications in modulus and phase according to ϕ - calculations with 0 and 2 iterations*

values were chosen with regard to the fact that they may be considered negligible compared with modification orders of magnitude, measurement uncertainties and other disturbing effects such as voice-coil warming up,... The retained number of iterations corresponds thus to the last but one operation. In the present case, two iterations are sufficient.

Let us proceed in the same way for the volume velocity modifications. Figure 4.17 shows the post-processed volume velocity in modulus and phase for the reference state (ϕ = -144 deg), $\underline{q}$ and $\underline{q}'$ being respectively the LSP_0 volume velocity without and with LSP_1 action.

The phase is again post-processed by cross-correlation of in-box sound pressure $\underline{p}_{in}$ and input voltage U_0. Unlike electrical measurements, the acoustical measurements appear to be corrupted by ambient noise. This will be discussed later. Consequently, the phase plot of figure 4.17 also shows the tolerance margin defined by m_i and m_s, in which $\underline{q}$ phase values are located, as well as the averages of points.

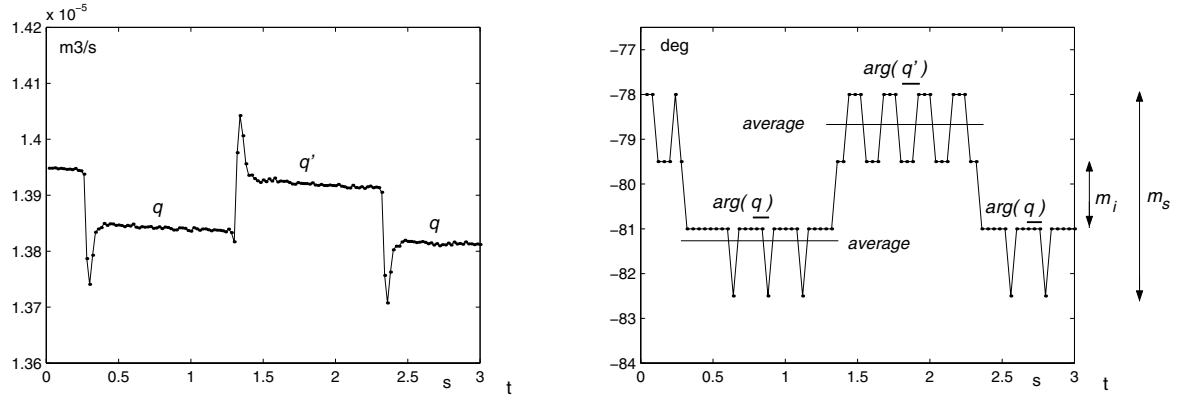

Figure 4.17 - *LSP_0 volume velocity over time in modulus and phase, with and without LSP_1 action*

As the phase values $arg(\underline{q})$ are difficult to be post-processed in an accurate way, the measured modification $arg(\underline{q})_{mod}$ is calculated, according to relation 3.10, taking into account the $arg(\underline{q})$ and $arg(\underline{q}')$ average values shown in figure 4.17.

As done before for the input impedance and according to relation 3.9, figure 4.18 shows the measured and calculated $\underline{q}$ modifications in modulus and phase according to ϕ. The measured phase modifications are completed with the tolerance margin boundaries m_i and m_s and with a supplementary curve coming from time shifting post-processing.

In the same way as with the input impedance, the number of iterations necessary to calculate $\underline{q}$ modifications is also 2.

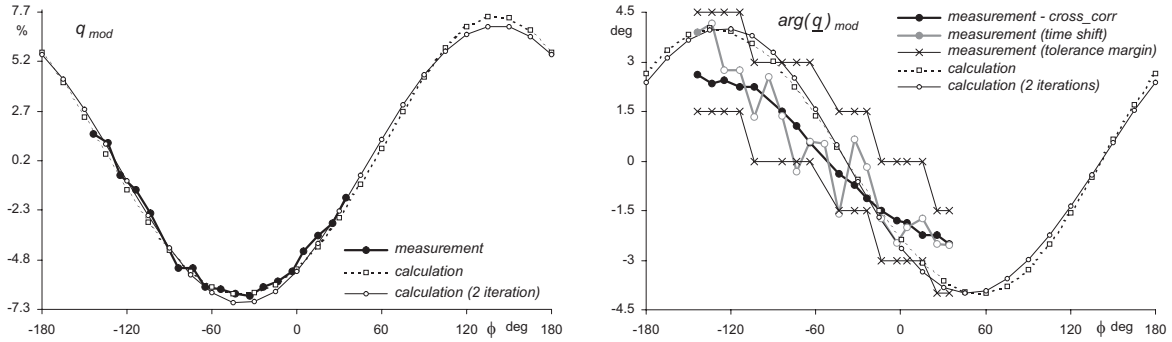

Figure 4.18 - *LSP_0 volume velocity modifications in modulus and phase according to ϕ - calculations with 0 and 2 iterations*

In order to end this pure tone analysis, let us also compare the calculated and measured input impedance modifications, when LSP_1 input voltage is doubled, without changing any other settings or parameters (fig. 4.19).

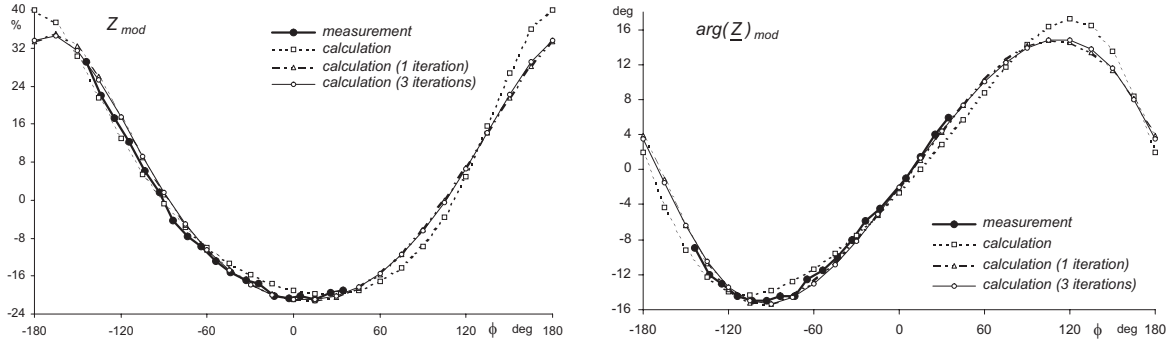

Figure 4.19 - *LSP_0 input impedance modifications in modulus and phase according to ϕ, with U_1 doubled - calculation with 0, 1 and 3 iterations*

This figure highlights two important points. Firstly, the amplitude and phase curves show modifications virtually twice as high as the ones of figure 4.16, corroborating the predictions calculated in Subsection 3.4.2. Secondly, the comparisons between measurements and calculations without and with iterations seem to justify interaction computations of higher order than one.

Finally, these results call for some comments. Figures 4.16, 4.18 and 4.19 show satisfactory similarities between measured and calculated results. The small differences come, for the most part, from ambient noise, post-processing inaccuracy, and uncertainties on measured TS parameters. To a lesser degree, they can also come from the calculation hypotheses (piston modelling, uniform membrane velocity, membrane subdivision, loudspeaker radius).

According to the equations of Appendix D, it is possible to compute the errors made on the TS parameters by estimating the possible post-processing errors made on f_- ($\pm$ 0.1 Hz), f_+ ($\pm$ 0.1 Hz) and z_0 ($\pm$ 0.5). By considering every realistically conceivable combination of the modified parameters f_s, Q_{es} and Q_{ms}, the error calculations have to be carried out 64 times for each driver, that comes altogether (for two drivers) to 4096 calculated cases. To this figure can be added the measurement error of the net internal volume V_b, estimated at $\pm$ 0.05 dm^3, which offers the advantage of showing the same error for the two closed boxes. Thus the error calculations should be ideally repeated 8192 times in order to find the worst cases.

Without calculating all these cases, the computations were nonetheless carried out 128 (64x2) times for each driver. As these results give a great number of curves surrounding the measurement ones, it appears not really interesting to show them here. Furthermore, the resulting resonance frequencies variations appear to be smaller than those mentioned in Subsection 4.2.3. Thus, it is rather worthwhile to give examples of $\underline{Z}$ modification variations according to three parameters, ie $V_b \pm 0.05\ \mathrm{dm}^3$, $f_{c0} \pm 1$ Hz (realistic variations according to Subsection 4.2.3), and $R_{e0} \pm 1\ \Omega$. Figure 4.20 shows the comparisons between these new modification curves and the reference one coming from figure 4.16. As previously, these curves are computed according to 2 iterations.

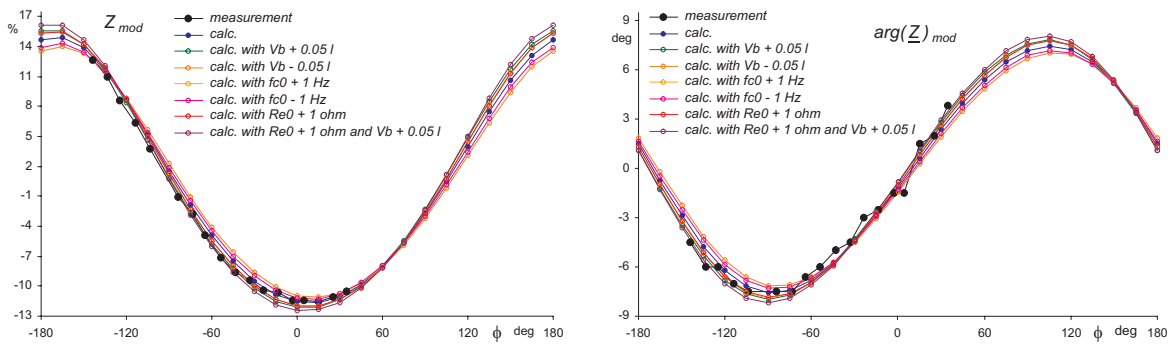

Figure 4.20 - *LSP_0 input impedance modifications in modulus and phase according to ϕ - comparisons between the reference curve of figure 4.16 and six curves according to measurement error of V_b, and variations of f_{c0} and R_{e0} (2 iterations)*

This figure shows that the variations of input impedance modifications due to the errors made on these three significant parameters are in the order of the differences between measurements and calculations. Given, as well, that the interfering noise can not be taken into account in the calculations and that the resulting post-processing accuracy depends on a few settings such as undersampling frequency, averaged points number or cross-correlation windows lengths, the calculations are considered as being validated.

4.3.3 Measurements using white noise excitations

In order to carry out measurements using white noise excitations, the two-channel generator is replaced by a computer, as described in Appendix A. The measured quantities are otherwise the same as previously (fig. 4.1).

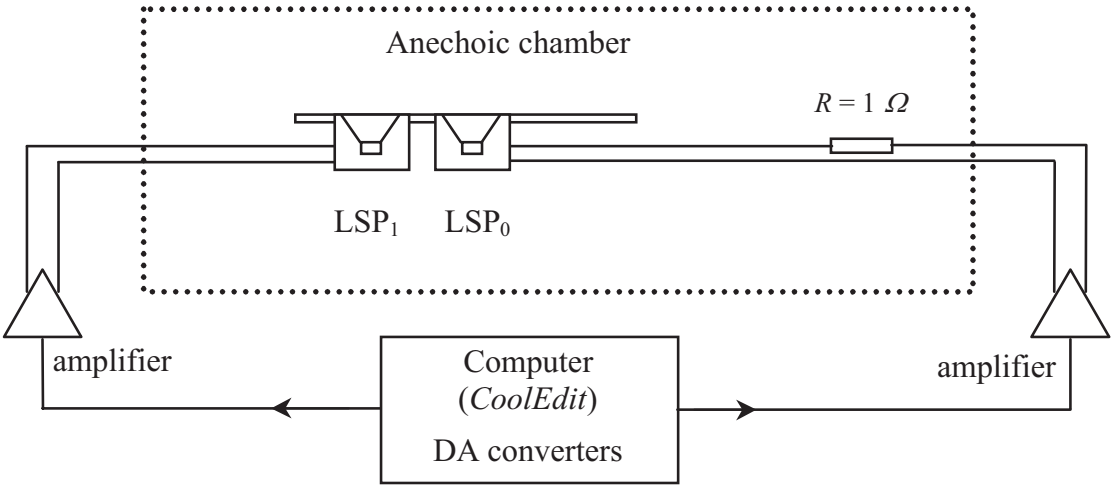

Figure 4.21 - *Assembly diagram of two closed-box loudspeakers mounted in an IEC baffle and driven in white noise*

The measurements are carried out at four different excitation voltage ratios, ie 100, 10, 2 and 1, with $u_1(t)$ always set at 2 V RMS. In order to lighten the presentation of results, the input impedance and volume velocity modifications will be given only for ratio values of 10 and 1, the two other ratios having nothing more to contribute, except that they confirm the results of the chosen ones.

All the measured quantities are recorded during 30 seconds, according to the excitations sequences drawn in figure 4.22, showing the input voltages $u_1(t)$ and $u_0(t)$ generated by the PC-based.

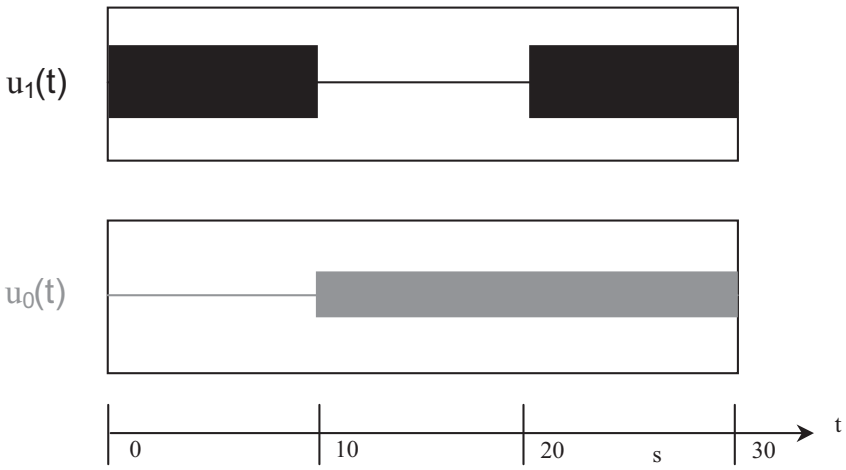

Figure 4.22 - *Drawing of the excitations sequences*

The recorded waves $u_0(t)$, $i_0(t)$ and $p_{in}(t)$ are then post-processed. After an under-sampling, the input impedance and volume velocity are computed according to the frequency, using the *Matlab TFE* transfer functions (see Appendix A.3):

$$[\underline{Z}, f] = \textit{TFE}\ (i_0(t), u_0(t), \textit{NFFT}, F_s\ , \textit{WINDOW}, \textit{NOVERLAP})$$

$$[\underline{q}, f] = j\omega\ C_{ab}\ u_0\ \ \textit{TFE}\ (u_0(t), p_{in}(t), \textit{NFFT}, F_s\ , \textit{WINDOW}, \textit{NOVERLAP})$$

In order to obtain $\underline{Z}$ and $\underline{q}$ without and with LSP_1 disturbances, these computations are carried out twice, respectively from 10 to 20 s and from 20 to 30 s. The values of *NFFT*, F_s , *WINDOW* and *NOVERLAP* are set case by case. The modifications of $\underline{Z}$ and $\underline{q}$ in modulus and phase are then deduced from relations 3.7, 3.8, 3.9 and 3.10.

Let us now compare measurement results with calculations. The accuracy of the latter requires some preliminary measurements; then, in addition to the TS parameters of each driver (see Subsection 4.2.3), the measured excitation ratio is also introduced in calculation data, because it differs from the theoretical value, due to the excitation setting inaccuracy and to the different values of TS parameters between both loudspeakers, notably the value of R_g (see Appendix C).

The signals $u_0(t)$ and $u_1(t)$ have thus also to be post-processed using the *TFE* transfer function. With the aim of making the calculations easier, the modulus and the phase of this function are approximated in polynomial series of order 25. Figure 4.23 enables this function to be compared, for both ratios, with the theoretical value of 10 (respectively 1) for the modulus, and 0 for the phase.

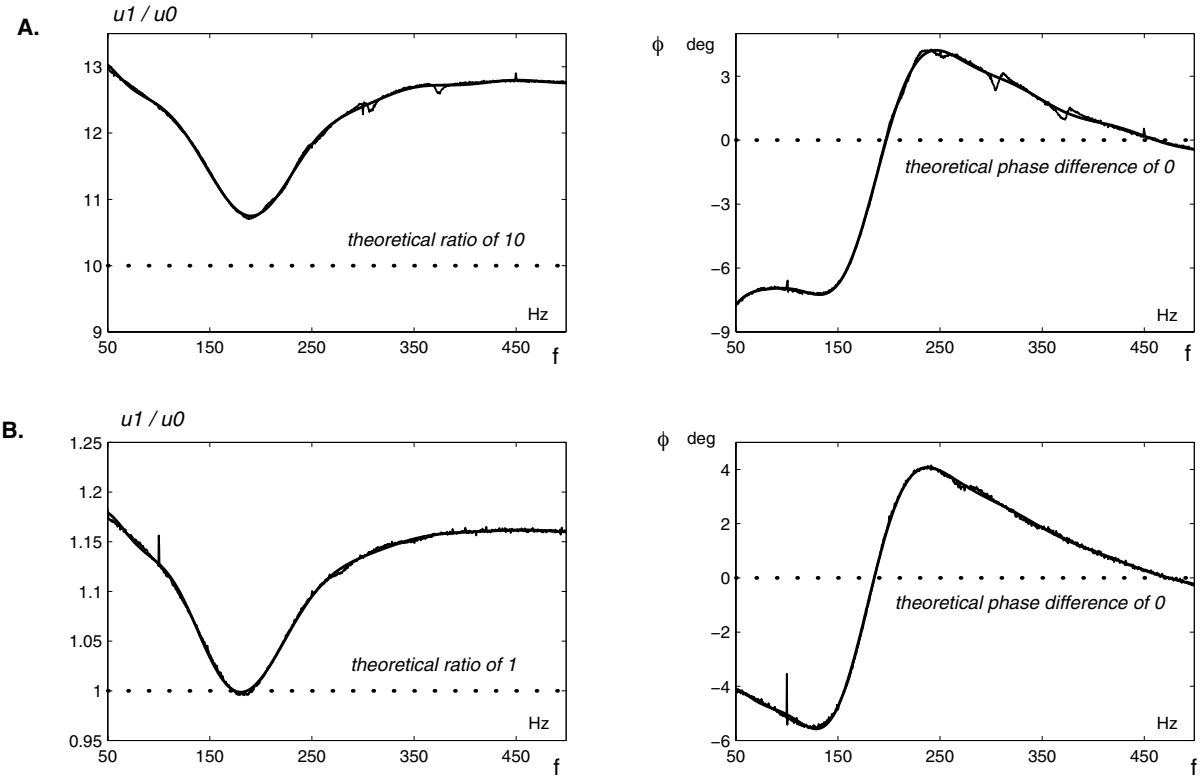

Figure 4.23 - *Comparison between expected (black dots) and measured excitation differences for the two retained settings: ratio of 10 (A.) and 1 (B.) - plots of excitation ratios and differences of phase ϕ, according to TFE results (blacke curves) and polynomial approximations of order 25 (grey curves)*

Figures 4.24 and 4.25 show the measured and calculated modifications of $\underline{Z}$ and $\underline{q}$, according to the frequency, for the excitation ratios of 10 and 1. Whilst the measured and calculated curves follow the same tendency and have similar orders of magnitude, the comparisons show nevertheless significant differences due, to a large extent, to various approximations, among which, those appearing to come from the IEC baffle, given that the latter is not infinite in practice. The frequencies of 206 and 252 Hz, corresponding to the finite baffle dimensions (165 x 135 cm), are drawn in the figures.

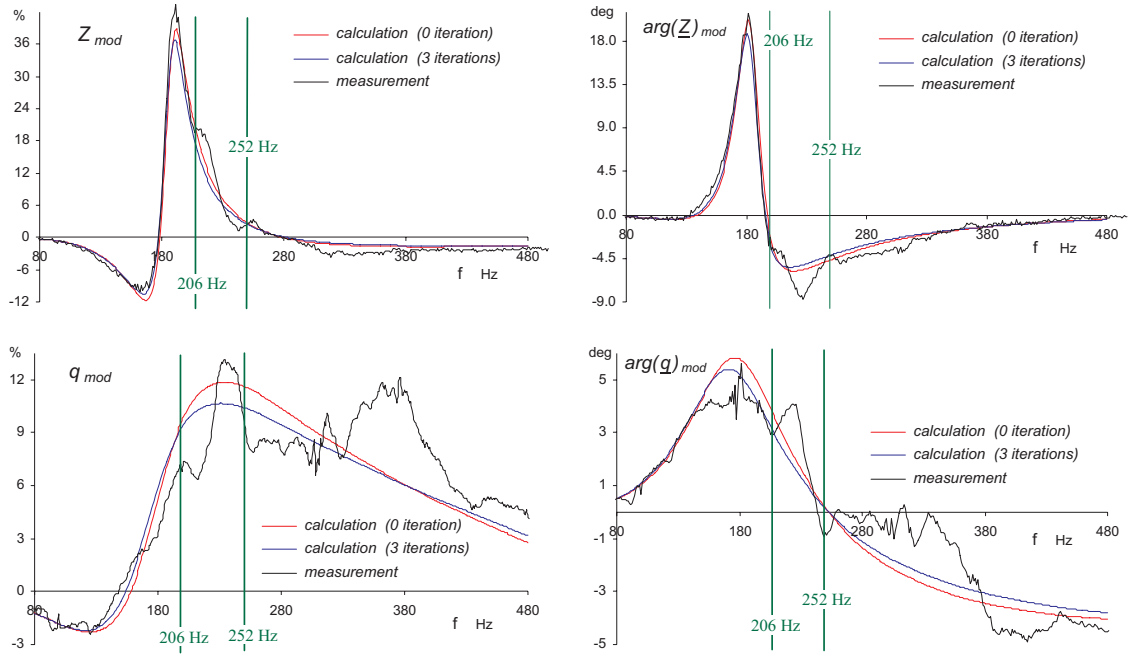

Figure 4.24 - *Comparisons between measured and calculated modifications of input impedance and volume velocity in modulus and phase for an excitation ratio of 10*

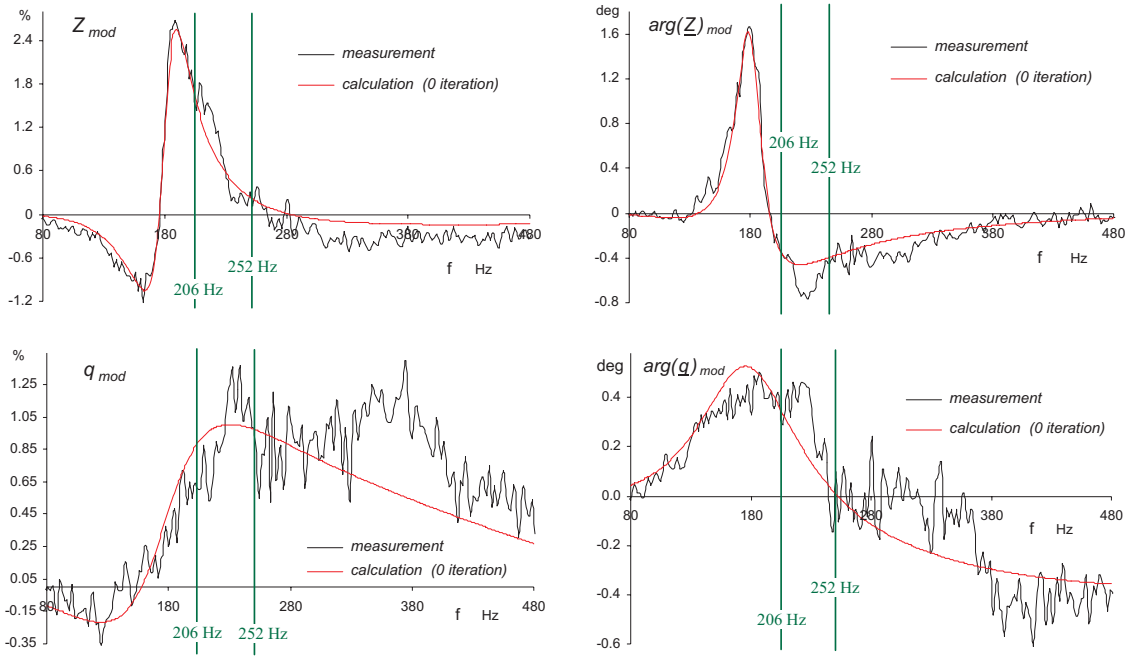

Figure 4.25 - *Comparisons between measured and calculated modifications of input impedance and volume velocity in modulus and phase for an excitation ratio of 1*

Dwelling more on figures 4.24 and 4.25, two interesting phenomena can be observed. At first, and contrary to what was observed in Section 3.4, the orders of magnitude of input impedance and volume velocity modifications, are totally different at the system resonance. Whilst the $\underline{Z}$ modifications are greater than the $\underline{q}$ modifications at the resonance, the tendency is reversed on both sides of the resonance. Secondly, the iteration number, calculated according to the previous subsection prescriptions (tolerance margin of $\pm$ 0.01 %, ie $\pm 10^{-4}$) for the modulus and $\pm$ 0.01 degree for the phase), increases with the excitation ratio. This confirms the observation made in the experiment using a pure tone.

Figure 4.26 shows the differences calculated between the third and fourth iterations of the $\underline{Z}$ and $\underline{q}$ modifications given in figure 4.24. As we can see, the differences are smaller for the $\underline{q}$ calculations, due to the lower modification values at the resonance. Although the iteration numbers are the same here for $\underline{Z}$ and $\underline{q}$ modification computations, it is expected that these numbers can be lower for the $\underline{q}$ calculations than they are for the $\underline{Z}$ calculations. They will depend on the modification values of $\underline{Z}$ and $\underline{q}$ (see Section 4.5 and Appendix E).

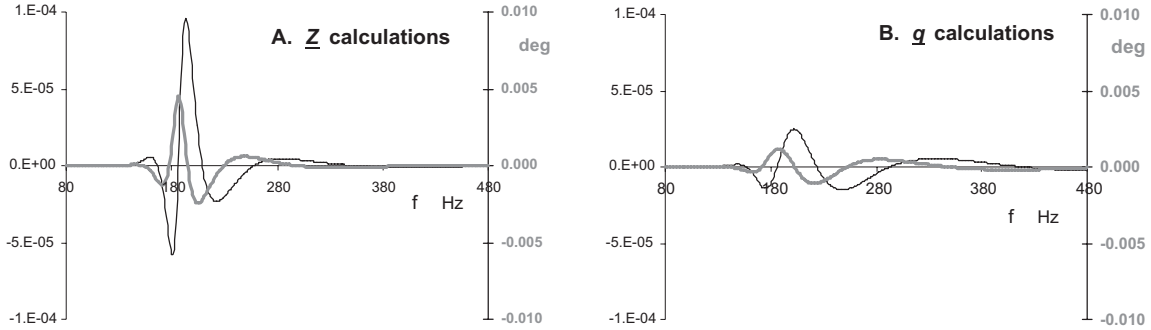

Figure 4.26 - *Differences between the third and fourth iterative calculations of the input impedance (A) and volume velocity (B) modifications in modulus (black curves) and phase (grey curves)*

Finally, it is of course obvious to note that the smaller the modifications are, the more inaccurate the post-processed results are. In order to validate calculations by experiments, all the next measurements will be carried out according to an excitation ratio of 10.

4.4 Two adjacent closed-box loudspeakers

4.4.1 Aim

The radiation of two side-by-side closed-box loudspeakers can be considered the same as that of loudspeakers mounted in the same finite baffle, the dimensions of which correspond to the two front panels of the enclosures. This configuration enables the previous one to be connected to the next one. In other words, this assembly acts as a link between the case of two closed-box loudspeakers mounted in an infinite baffle and that of two separated closed-box loudspeakers.

4.4.2 Measurement process

The measurement process is the same as in Subsection 4.3.3, where the loudspeakers are driven by white noise. The equipment list is again given in Appendix A.

A first series of measurements were carried out putting the closed-box loudspeakers on a 2 m rail, as shown in figure 4.27. While this assembly did away with most reflections, the post-processed results were unexploitable due to some interferences, regardless of excitation ratio.

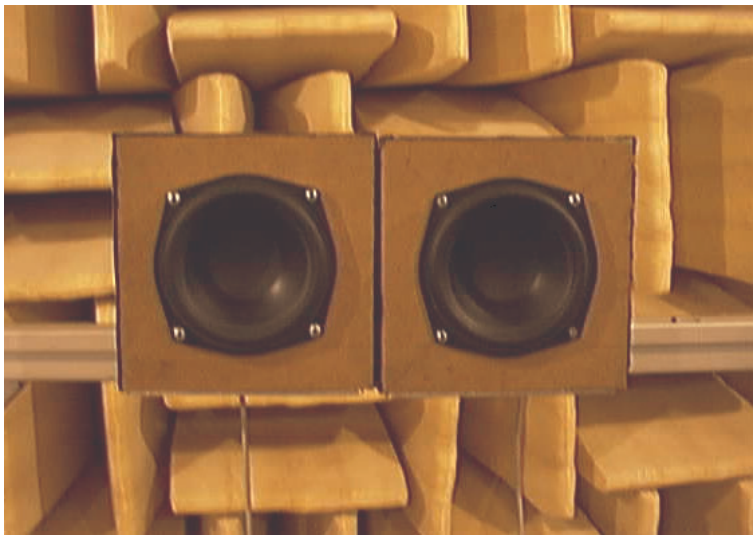

Figure 4.27 - *Picture of two side-by-side closed-box loudspeakers mounted on a rail*

It was then decided to put the loudspeakers simply on one of the immovable stands belonging to the anechoic chamber, taking care to avoid any significant surface reflection disturbances (fig. 4.28). Furthermore and in order to avoid also any mutual vibrations between the enclosures, the latter are separated by about 0.5 mm.

Figure 4.28 - *Picture of two side-by-side closed-box loudspeakers mounted on an immovable stand*

4.4.3 Measured and calculated results

As explained in Subsection 4.3.3, the TS parameters and the measured excitation ratio are once again introduced in the calculation data sheets. While the measurements and computations were carried out according to the three excitation ratios of 1, 2 and 10, this section will give only the results related to the last one corresponding to the greater LSP_0 modifications. As mentioned in the previous section, the greater the excitation ratio is, the more accurate the comparisons between measurements and computations are.

In order to be aware of the edges diffraction effects, measurement results are first compared to computations carried out in 2πst (infinite baffle) and 4πst. Figures 4.29 and 4.30 show these comparisons in terms of input impedance and volume velocity modifications according to the frequency.

As previous calculations and common sense could suggest, the measured modification results are more or less located between the curves computed in 2πst (baffled) and 4πst. Compared to computation results, let us note in passing that the measured curves show a slight shifting toward the high frequencies (especially visible on the phase curves). In order now to get closer to measurement results, the computations can be improved by taking into account the edge diffraction effects.

In accordance with the theoretical method developed in Subsection 2.5, the geometric theory of diffraction is thus introduced into the computation sheets. To do that, the reduced baffle made up of the two adjacent enclosures front panels is divided into a discrete number of secondary sources. For want of a contradictory theory, these sources are placed at regular intervals on the six diffracting edges, taking care to avoid the four panels corners. An example of edges partition is given in figure 2.11 in the case of 36 elements, ie 6 by edge.

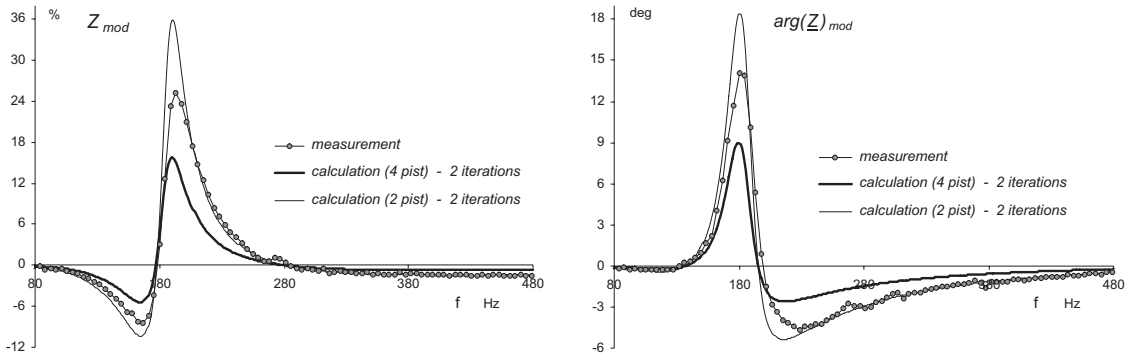

Figure 4.29 - *LSP_0 input impedance modifications - comparisons between measurements and calculations in 2π and 4π steradian*

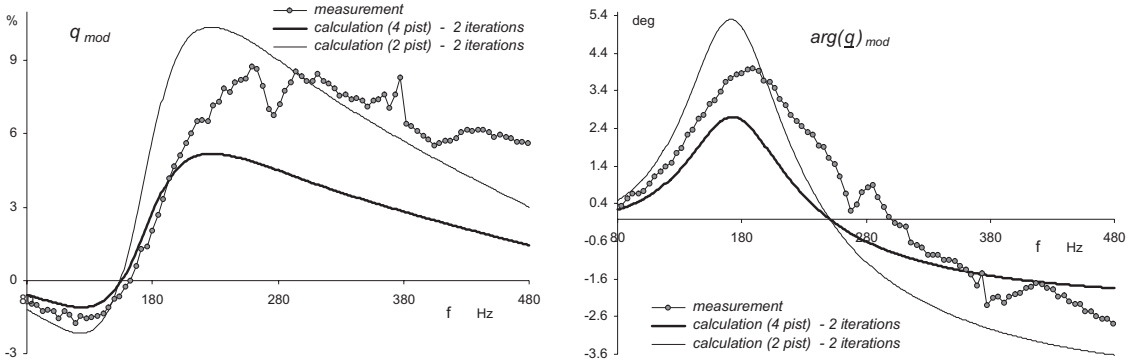

Figure 4.30 - *LSP_0 volume velocity modifications - comparisons between measurements and calculations in 2π and 4π steradian*

In order to be consistent with the determination of the computed iteration number, the edge division number will be set in the same way. Carried out according to a source number multiple of 6 (from 12 to 48), the latter is considered to be acceptable when the differences between two calculations are bounded by ± 0.01 % ($\pm 10^{-4}$) for the amplitude and ± 0.01 degree for the phase.

Figure 4.31 shows the differences between $\underline{Z}$ and $\underline{q}$ modifications calculated according to 30 and 36 edge divisions. The differences are again smaller for the volume velocity calculations, as explained during the iteration number discussion (see Subsection 4.3.3).

According to these results, the number of edge divisions should be of 30 (five per edge), but as a precaution and in order to avoid secondary source locations on axis x and y, the division number choice fell on 36 elements, ie 6 per edge.

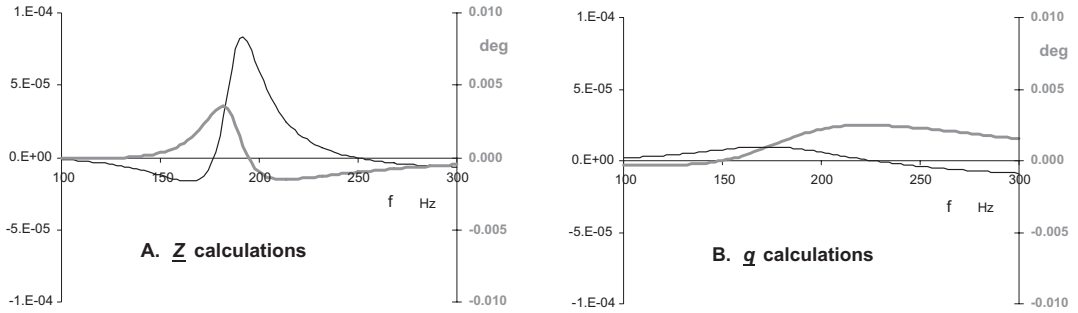

Figure 4.31 - *Differences between input impedance and volume velocity modifications calculated with 30 and 36 edge divisions (modulus in red and phase in blue)*

Finally, the measured $\underline{Z}$ and $\underline{q}$ modification curves of figures 4.29 and 4.30 are compared with the calculated ones resulting from GTD computation. The number of iterations is chosen according again to the prescriptions of Subsection 4.3.2. The results are given in figures 4.32 and 4.33.

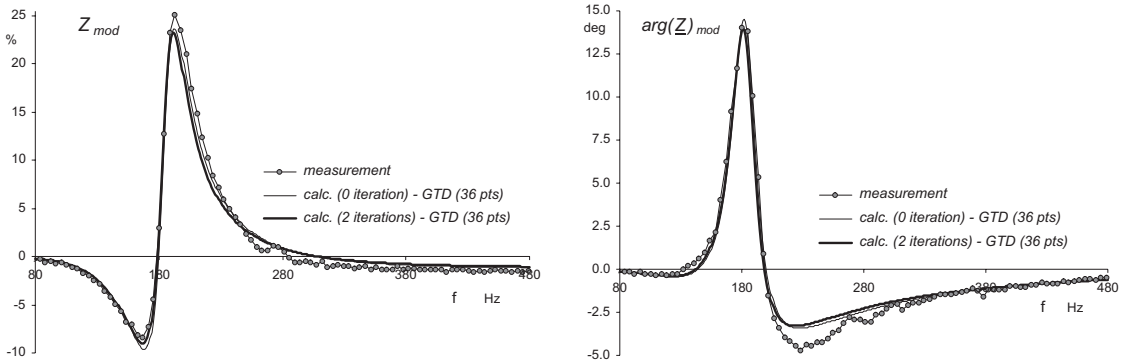

Figure 4.32 - *Measured input impedance modifications compared with calculations (GTD)*

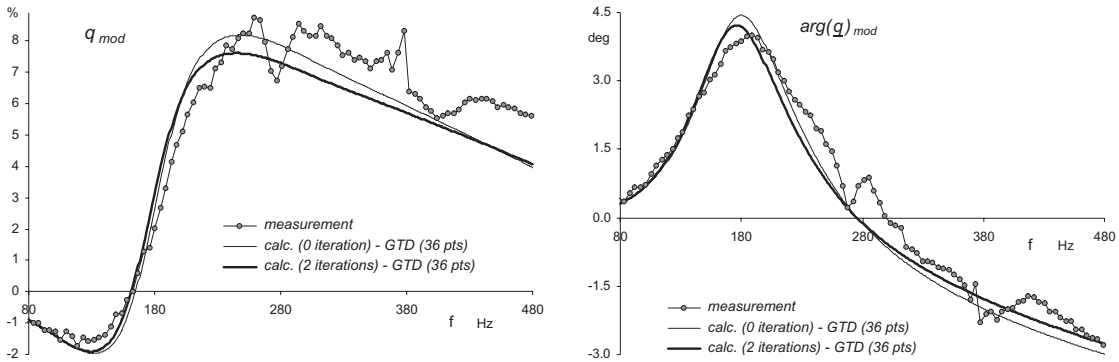

Figure 4.33 - *Measured volume velocity modifications compared with calculations (GTD)*

4.4.4 Comments

The comparisons between computations and measurements (fig. 4.32 and 4.33) appear to validate the use of GTD to calculate the limited baffle edge diffraction effects when all the observation points are located on the baffle, meaning that the observation angles θ_l are equal to zero. As previously mentioned, the curves shifting toward the high frequencies is also validated by the GTD computation.

As in Subsection 4.3.2, the post-processing errors are calculated first according to the equations of Appendix D. Without calculating all the 8192 cases, the computations were all the same carried out 128 times for each loudspeaker. The results are a series of curves surrounding the measured ones, without however being able to be ensure that the worst cases are found. As previously carried out and explained, it is more interesting to show the variations of calculation results according to measurement errors of $V_b \pm 0.05\ \mathrm{dm}^3$ and variations of $R_{e0} \pm 1\ \Omega$. These two parameters are chosen, among the others, because they act greatly upon the accuracy of the modification results (fig. 4.34 and 4.35). In view of these results and according to the same previously made comments, the calculations are again considered as being validated.

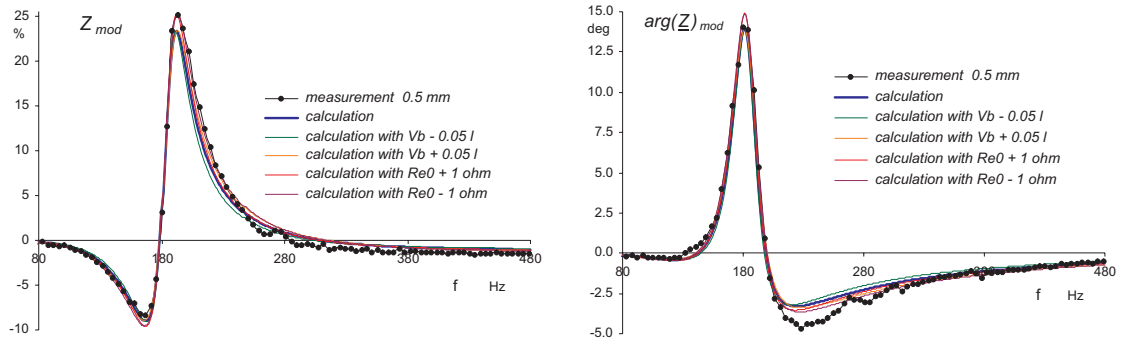

Figure 4.34 - *Measured input impedance modifications compared with six calculated curves according to V_b measurement errors and R_{e0} variations (2 iterations)*

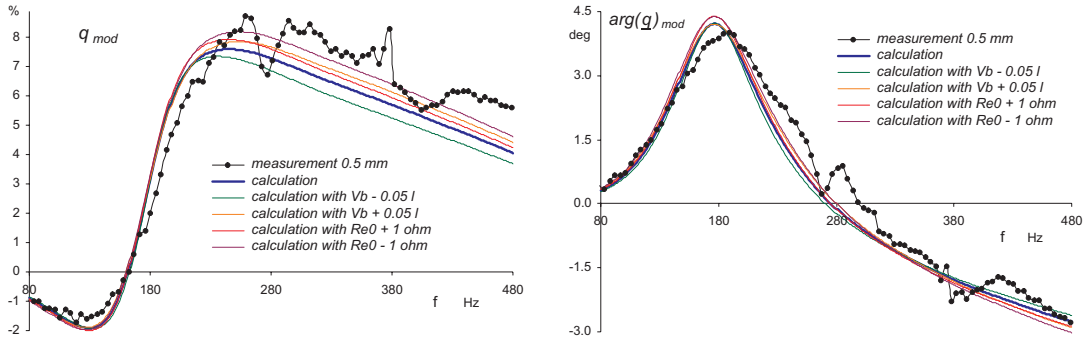

Figure 4.35 - *Measured volume velocity modifications compared with six calculated curves according to V_b measurement errors and R_{e0} variations (2 iterations)*

4.5 Two distant closed-box loudspeakers

4.5.1 Aim and measurement process

The configuration of two separated closed-box loudspeakers makes up the outcome of the thesis. It represents a "pseudo" realistic case, which can lead to the analysis of several loudspeakers mounted in arrays.

The measurement process is again the same as in Subsection 4.3.3, where the loudspeakers are driven by white noise. The equipment list is given in Appendix A. According to the same problems met during the previous experiment, the loudspeakers are put on one of the immovable stands belonging to the anechoic chamber, as shown in figure 4.36.

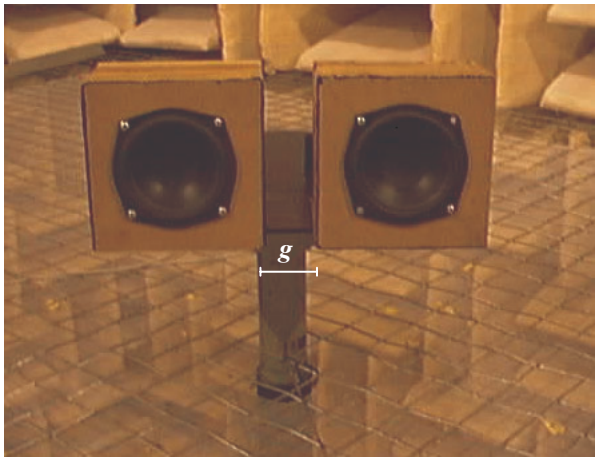

Figure 4.36 - *Picture of two closed-box loudspeakers mounted on an immovable stand and separated by a distance g*

The distance g separating the box edges is set to two values, ie 2 and 10 cm. The latter is chosen according to the calculation results of Section 3.6, in order to visualize the modifications decrease, while keeping measurable orders of magnitude.

4.5.2 Measured and calculated results

As previously, the TS parameters and the measured excitation ratios are again introduced in the computation sheets. In order to compare the different diffraction methods calculated in Section 3.6, the computations are carried out four times according to the four different combinations of GTD and UTD mentioned in Subsection 2.5.2.

Figures 4.37 and 4.38 show the input impedance modifications measured and calculated for an excitation ratio of 10 and according to the two distances g of 2 and 10 cm.

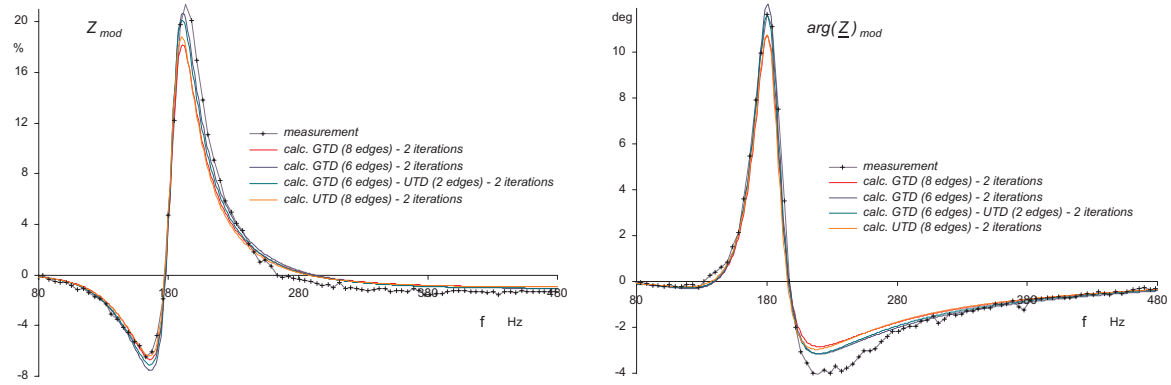

Figure 4.37 - *Input impedance modifications for g = 2 cm - comparisons between measurement results and GTD and UTD calculations*

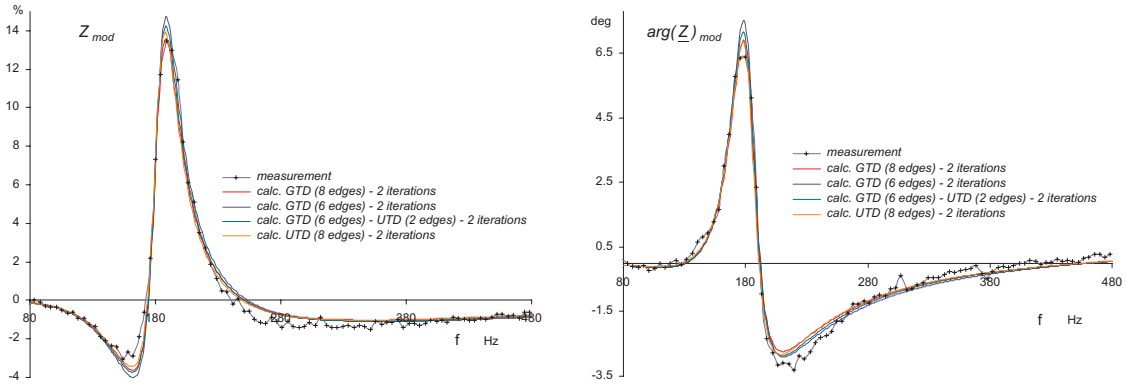

Figure 4.38 - *Input impedance modifications for g = 10 cm - comparisons between measurement results and GTD and UTD calculations*

These figures show good degrees of accuracy between the measurements and the four combinations of GTD and UTD calculations for both distances. The iteration number is again chosen according to the prescriptions of Subsection 4.3.2. The two calculations need the same number as previously in the case of adjacent boxes, ie 2.

Whilst the four calculation methods can be judged to be satisfactory, it is not obvious, however, to grade them in order of efficiency, because their differences are of the same order of magnitude as the error calculations carried out in the previous sections. Nevertheless, it is worth mentioning that the curves calculated on the eight edges with GTD(0°) and UTD are very close together (< 0.012 for the modulus and < 0.5 deg for the phase), and that the calculation results match the measurement results more closely for the distance of 10 cm than for the one of 2 cm.

Let us compute and post-process the volume velocity modifications in the same way. Thus, Figures 4.39 and 4.40 show comparisons between calculated and measured curves, for an excitation ratio of 10 and according to the two distances g of 2 and 10 cm.

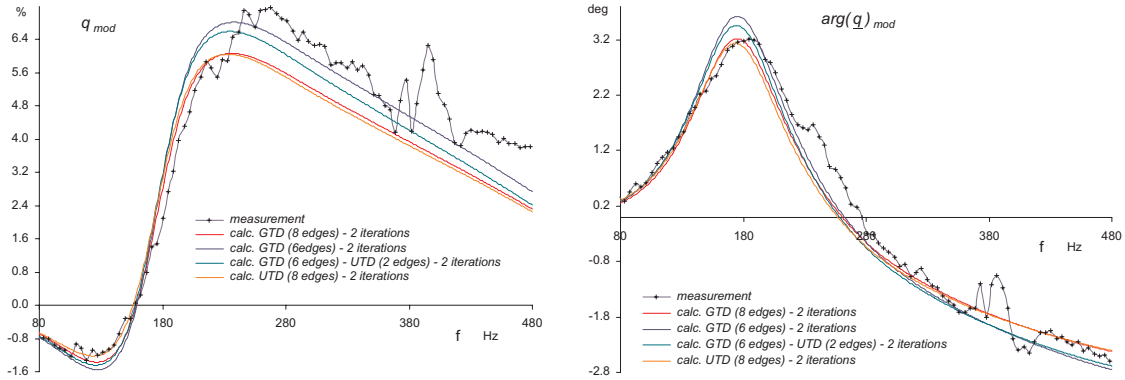

Figure 4.39 - *Volume velocity modifications for g = 2 cm - comparisons between measurement results and GTD and UTD calculations*

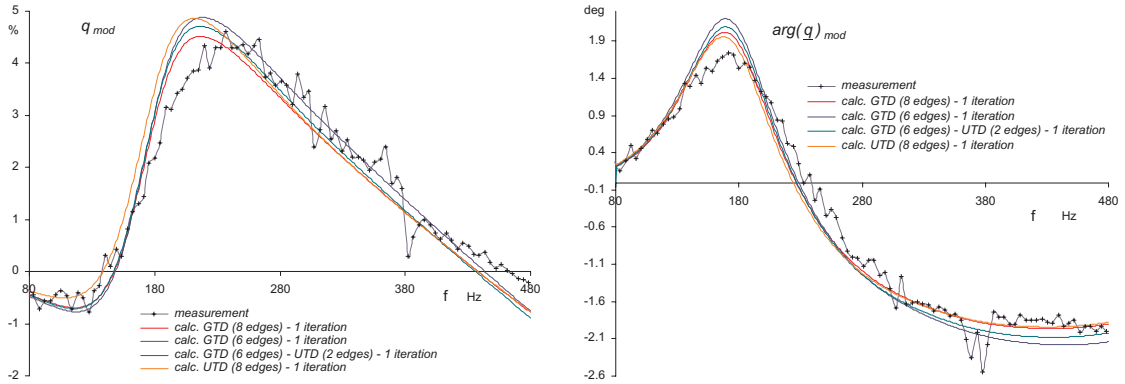

Figure 4.40 - *Volume velocity modifications for g = 10 cm - comparisons between measurement results and GTD and UTD calculations*

The comments on the above input impedance curves apply also to the volume velocity curves, apart from the number of iterations which, whilst also equal to 2 at 10 cm, drops to 1 at 2 cm (see Subsection 4.3.3).

Finally and in order to show the validation frequency domain, let us post-process and calculate these modifications at higher frequencies. Thus, according to a distance g of 10 cm, figures 4.41 and 4.42 enable measured curves to GTD and UTD calculated curves to be compared up to 1.6 kHz (piston domain higher frequency).

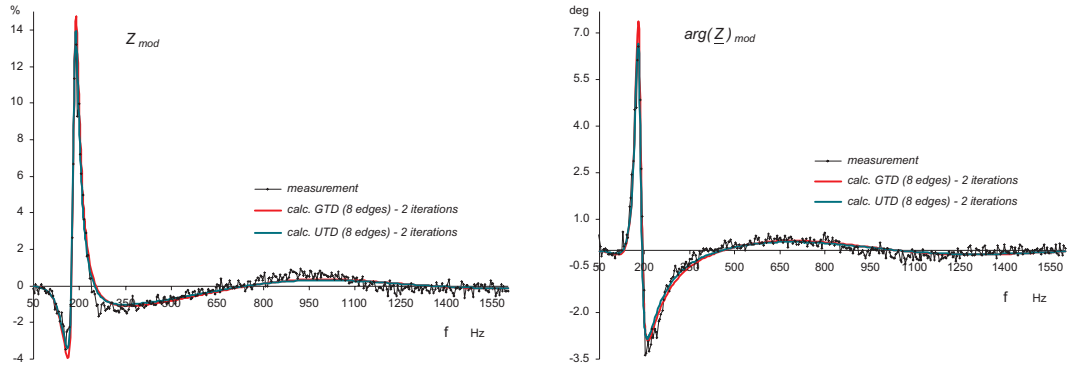

Figure 4.41 - *Input impedance modifications for g = 10 cm - comparisons of measurement results with GTD and UTD calculation curves up to 1.6 kHz*

Whilst it is not obvious to assess the comparison between $\underline{Z}$ calculated and measured curves, due to the small modification values above system resonance frequency, they appear nevertheless to follow the same tendency.

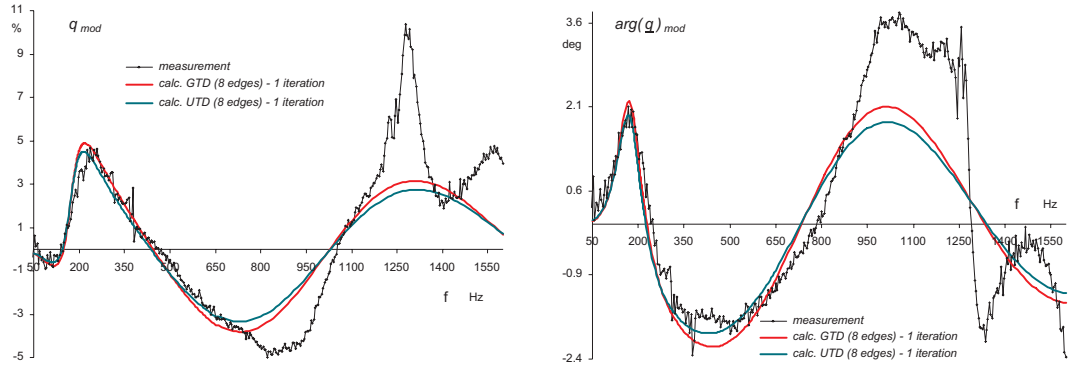

Figure 4.42 - *Volume velocity modifications for g = 10 cm - comparisons of measurement results with GTD and UTD calculation curves up to 1.6 kHz*

These last curves are very interesting because they bring to the fore the limits of the volume velocity measurement method, which should normally coincide with the frequency at which the box can no more be considered as an ideal acoustic compliance. In the present case, the curves show that the method cannot be used accurately above 900 Hz. It is worth noting that this frequency is lower than the frequency corresponding to the empty box first mode (1480 Hz).

4.6 Conclusion

This last part of the thesis has enabled the theories described in Chapter 2 and the calculations carried out in Chapter 3 to be validated, by means of a series of experiments carried out in an anechoic chamber.

This chapter started with the description of the measurement procedures chosen so as to ensure a sufficient degree of accuracy, corresponding more or less to that of the theoretical predictions. Thus, once the measurement set-ups were determined, a preliminary experiment was proposed in order to validate the interaction study in terms of volume velocity (in-box sound pressure) and input impedance modifications. This experiment enabled also a few measurement difficulties to be highlighted, such as those related to the rise of the voice-coil resistance due to increasing temperature, as well as those related to the non-linear and non-invariant behaviour of the TS parameters. The problems related to the non-linearity of the latter were circumvented by introducing into the calculation data the TS parameters measured individually for each loudspeaker at the excitation level corresponding to the one used during the experiment. As for the non-invariant behaviour of these parameters, it will be taken into account during the error calculations by using as tolerance margin the differences of the parameters measured before and after a warming-up period.

After having decided on the measurement method, found solutions to counter most of the possible difficulties and after having validated the choice of the measured quantities, the calculation validations were carried out through three experiments corresponding to the loudspeaker configurations studied in Chapter 3.

The first experiment allowed the interactions between two closed-box loudspeakers mounted in the same IEC baffle to be measured. At first, this experiment was carried out using pure tone excitations so as to measure input impedance and volume velocity modifications according to excitations ratio and difference of phase. Then, the experiment was renewed using white noise excitations in order to measure also the modifications according to the frequency. In both cases, the similitude between measurement and computation results, combined with error calculations, enabled the theoretical predictions to be validated.

In the second experiment, the IEC baffle was reduced to the dimensions of the front panels of two closed-box loudspeakers placed side-by-side. Unlike the previous configuration, the computations carried out in this one had to take into account the diffraction at the enclosure edges. According to the fact that all the observation points were located on the limited baffle (observation angles equal to zero), the diffracted field was calculated using the GTD. Showing a high degree of similitude, the comparisons between measurement and computation results appear to validate the theoretical predictions, and in particular the use of the GTD.

Making up the outcome of the thesis, the third configuration was identical to the previous one with the difference that the two closed-box loudspeakers were then separated. In this case, the theory required the use of the UTD to calculate the diffracted field corresponding to the observation points located close to the shadow boundaries. In order to save computation time, four different combinations of GTD and UTD were applied on the eight enclosure edges. Finally, the comparisons between the measurement results and the four computation results showed good degrees of accuracy, and that for different distances between the enclosures. The experiment has thus once again validated the theoretical predictions.

General conclusion

The original contributions of this thesis appear clearly in the approaches chosen to analyse the effects of an incident sound field on a loudspeaker. Thus, whereas these effects are generally studied as modifications of loudspeaker radiation impedance, this work analyses these modifications in behaviour in terms of input impedance and volume velocity, the latter allowing the radiated sound pressure to be calculated with and without taking into account the external field. The main conclusion lies in the fact that this approach has turned out to be a judicious choice, especially with regard to the good degree of accuracy observed in the comparison between computation and measurement results.

The orders of magnitude are such that the modifications can be calculated using numerical treatments. The latter turned out to be effective already after one or two iterations. In order to validate the calculation results, experimental techniques were chosen in order to enable these effects to be accurately measured. Thus, it was decided to measure the behaviour modifications directly at the loudspeaker electrical input terminals, in order to take into account the modifications occurring on the whole system. This proposed input impedance measurement technique proved to be very appropriate and accurate, due to the fact that the post-processed computations are based on two measured quantities of same nature (electrical voltage and current). However, as this method is only effective for frequencies located close to the system resonance, it was necessary to complete the experiment techniques by the measurement of the volume velocity. It was decided to obtain this quantity by measuring the sound pressure in the enclosure. Whilst this method offers the advantage of analysing the modifications in a larger frequency domain, the measurement results are considerably more disturbed due to the different nature of measured quantities (acoustical sound pressure and electrical voltage). Despite the presence of some interfering noise related to the various assemblies used during the experimentations, it is not overly presumptive to assert that the combination of these two measurement techniques enabled the theoretical predictions to be validated in all the three configurations studied in this thesis.

Whilst the input impedance and volume velocity modifications studied in this thesis can reach in some cases considerable orders of magnitude for one of the two loudspeakers, it is important to note that the modifications occurring on the resulting radiated sound pressure remain mostly negligible, especially in amplitude. These modifications are in fact of the same order of magnitude as those due to other disturbing effects such as the voice-coil warming up or the non-linearities. However, the phase modifications can be more problematical in applications such as active noise control for instance, where small changes can considerably reduce the system efficiency.

The technological spin-off effects may be of two sorts. The first one is closely linked to the primary aim of the thesis. This engineering approach consists in showing the importance of being aware of possible disturbing effects coming from an external sound field, in order to decide whether they must be compensated by the control or taken into account during the loudspeaker design phase. The second one ensues from the input impedance modification analysis. As previously mentioned, the latter offers the advantage of being easily measurable close to the system resonance. Thus, it should be interesting to use an electrodynamic loudspeaker as a force/pressure sensor with the aim of analysing acoustic loads, taking care of course to match the loudspeaker resonance with the frequency domain to be measured. To do that, the input impedance has to be measured first when the loudspeaker is mounted in a well-known reference assembly such as the one of a baffle, and then when the loudspeaker is loaded by the acoustic impedance to be measured.

It is obvious that the methods used in this thesis can be applied to various loudspeaker assemblies, such as for the combinations of several loudspeakers mounted in arrays, identical or different loudspeakers mounted in the same enclosure whilst also taking into account rear interactions (column or multidriver loudspeakers), loudspeaker mounted in vented or passive radiator box...

Finally, it would be sensible to confirm these methods by measuring other loudspeaker models, such as woofers or tweeters, so that the identified functions of Subsections 3.4.4 and 3.4.6 could also be put into general use. The results of volume velocity measurement could also be completed, for example, by measurement of the cone velocity (interferometry laser). It could also be interesting to extend the scope of this study to other loudspeaker technologies. The results could also be completed with time domain studies, in order to analyse the modifications in loudspeaker transient responses.

Appendix A

Test bench

A.1 General principle

The heart of the test bench is a PC-based data acquisition system. It comprises an input/output device with AD and DA converters TANGO 24 - Frontier, a digital input/output card DAKOTA placed in a slot of a MEM 400 PC. This equipment enables measurement signals to be easily generated and controlled (sinus wave, white noise,...), as well as data acquisition to be carried out (voltages, sound pressure,...).

The basic sampling frequency is 48 kHz with uniform 24-bit quantization. There are 16 inputs and 16 outputs.

The measurement process includes the two successive parts corresponding to the acquisition of quantities to be measured, and to the computation of the related values. The main softwares are *CoolEdit* and *Matlab*. The first one enables events to be digitally recorded (.wav files), while the second one is used for digital post-processing (*Mathematica* is also used in particular cases). The lengths of recorded samples are 10 or 30 seconds, according to the type of acquisition.

According to the required measurements, others devices were necessary, such as power amplifiers, measurement amplifiers, microphones, shunt resistance,... The following lists specify the equipment used for the various experiments.

A.2 Equipment lists

A.2.1 Experiment of Subsection 4.2.2

The equipment list below refers to figure A.1.

1	Generator Multifunction Synthesizer	HEWLETT PACKARD 8904A
2	Tone-Burst Generator	GENERAL RADIO 1396-B
3	Power Amplifier	AUDIOPERFORMANCE P211

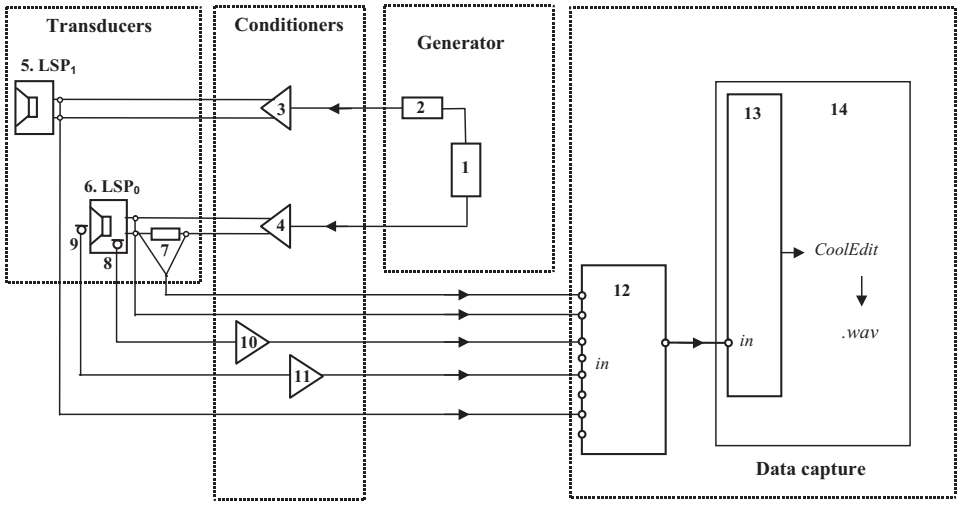

Figure A.1 - *Assembly diagram of the measurements using pure tones*

4	Power amplifier	QUAD 50E
5	4 loudspeakers PHL in a closed box	LEMA (LSP_1 in figure 4.3)
6	1 loudspeaker Tannoy 367X in a closed box	LEMA (LSP_0 in figure 4.3)
7	Precision shunt resistor 1 Ω	AOIP 501RE3
8	Microphone 1/2" 10 mV/Pa	BRUEL & KJAER 4134 + 2639
9	Microphone 1/4" 1.4 mV/Pa	BRUEL & KJAER 4136 + 2639
10-11	Measurement amplifiers	BRUEL & KJAER 2636
12	AD converters	TANGO 24 - FRONTIER Design Group
13	Digital input card	DAKOTA
14	Computer	MEM 400

The 1 Ω precision shunt resistor enables the loudspeaker input impedance to be measured.

A.2.2 Experiment of Subsection 4.3.2

The equipment list is the same as the previous one, excepted for the loudspeaker 5 (LSP_1) and its amplifier, which become:

3	Power Amplifier	QUAD 50E
5	1 Tannoy 367X loudspeaker in a closed box	LEMA (LSP_1 in figure 4.12)

A.2.3 Experiments of Subsection 4.3.3, Sections 4.4 and 4.5, and Appendix E

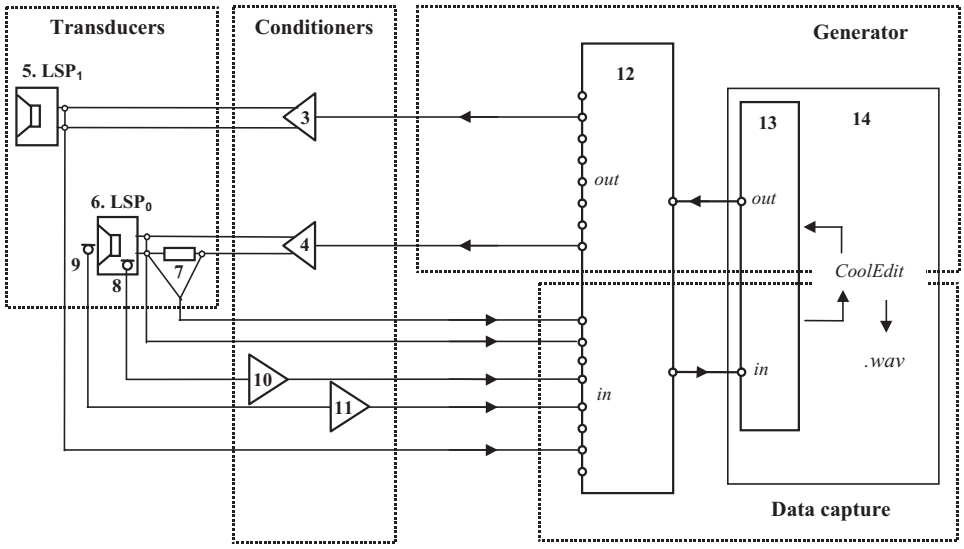

Figure A.2 - *Assembly diagram of the measurements using white noise*

The equipment list is the same as the one of Subsection A.2.1, where 1 and 2 are removed. The excitation signals are generated by 12, 13 and 14.

A.3 Matlab functions

The two main *Matlab* functions used during the post-processing computations are defined below [7].

- *Matlab* definition of *XCORR*: Cross-correlation function estimates

  $C = XCORR(A, B)$, where A and B are length M vectors (M>1), returns the length 2*M-1 cross-correlation sequence C. If A and B are of different length, the shortest one is zero-padded.

- *Matlab* definition of *TFE*: Transfer Function Estimate

  $T_{xy} = TFE(X, Y, NFFT, F_s, WINDOW)$ estimates the transfer function of the system with input X and output Y using Welch's averaged periodogram method. X and Y are divided into overlapping sections, each of which is detrended, then windowed by the WINDOW parameter, then zero-padded to length NFFT. The magnitude squared of the length NFFT DFTs of the sections of X are averaged to form P_{xx}, the Power Spectral Density of X. The products of the length NFFT DFTs of the sections of X and Y are averaged to form P_{xy}, the Cross Spectral Density of

X and Y. T_{xy} is the quotient of P_{xy} and P_{xx}; it has length NFFT/2+1 for NFFT even, (NFFT+1)/2 for NFFT odd, or NFFT if X or Y is complex. Specifying a scalar for WINDOW, a Hanning window of that length is used. F_s is the sampling frequency which does not effect the transfer function estimate but is used for scaling of plots.

$[Txy, F] = TFE(X, Y, NFFT, F_s, WINDOW, NOVERLAP)$ returns a vector of frequencies the same size as T_{xy} at which the transfer function is estimated, and overlaps the sections of X and Y by NOVERLAP samples.

Appendix B

TS parameters measurement

B.1 Method

The TS parameters are determined according to the delta compliance method, that is to say by measuring the loudspeaker input impedance $\underline{Z}$ versus frequency, first in a free assembly and secondly in an empty box assembly.

This method is based on the properties of $\underline{Z}$ which can be written:

$$\underline{Z} = R_e + \frac{(Bl)^2}{R_{ms}} \frac{(j\omega/\omega_s)\, Q_{ms}^{-1}}{(j\omega/\omega_s)^2 + (j\omega/\omega_s)\, Q_{ms}^{-1} + 1} \tag{B.1}$$

The quantities to be measured are:

1. the voltage $\underline{U}$ at the loudspeaker terminals
2. the loudspeaker input current $\underline{I}$ (a shunt resistor of 100 Ω is inserted instead of the 1 Ω in certain cases)

The necessity of the common ground (unbalanced inputs) leads to a phase reversal, ie $\underline{U_I} = -100\ \underline{I}$ (or - $\underline{I}$ for the resistor of 1 Ω).

The data acquisition refers to the method given in Appendix A for the measurements carried out using white noise.

B.2 Post-processing

In order to save computing time, the signals are undersampled at 6 kHz. The frequency range is limited from 50 to 1600 Hz.

The parameters are deduced from the two reduced input impedance frequency response curves (free air and closed-box assemblies), calculated using the *Matlab TFE* function.

The calculation is resumed below:

- .wav recording of the two voltages (at loudspeaker and shunt resistor terminals)
- Resampling at 6 kHz
- Computation of the input impedances using the *Matlab TFE* function
- Calculation of the input impedance in modulus Z and phase φ_Z
- Search of the impedance minimum
- Comparison between the latter and the ohm-meter measured R_e.
- Calculation of the reduced input impedance $z = Z/R_e$

The TS parameters may then be calculated from these reduced impedance curves, as follows:

- Search of Z_0 and z_0 (respectively Z and z maximum values)
- Choice of z_1 (chosen where the curve shows a good symmetry), normally $z_1 = \sqrt{z_0}$, but here z_1 is set to $1 + 2(z_0 - 1)/3$
- Search of an estimated frequency f_0 where the curve reaches its maximum value
- Search of the frequencies f_- and f_+ such that $z(f_-) = z(f_+) = z_1$
- Calculation of resonance frequencies $f_{s,c} = \sqrt{f_- f_+}$
- Calculation of mechanical quality factors $Q_{ms,mc} = \frac{f_{s,c}}{f_+ - f_-}\sqrt{\frac{z_0^2 - z_1^2}{z_1^2 - 1}}$
- Calculation of electrical quality factors $Q_{es,eco} = \frac{Q_{ms,mc}}{z_0 - 1}$
- Calculation of total quality factors $Q_{ts,tco} = \frac{Q_{ms,mc}}{z_0}$
- Calculation of the compliance ratio $\alpha = \frac{f_c Q_{eco}}{f_s Q_{es}} - 1$
- Calculation of $V_{as} = \alpha V_b$, V_b being measured previously
- Verification of the acoustic losses ratio $\frac{R_{as} + R_{ab}}{R_{as}} = \frac{f_c}{f_s}\frac{Q_{ms}}{Q_{mc}}$
- Verification of the masses ratio $\frac{m_{as} + 2m_{ar}}{m_{as} + m_{ar} + m_{ab}} = \frac{f_c Q_{es}}{f_s Q_{eco}}$
- Comparison between the resonance frequencies $f_{s,c}$ and the frequencies correponding to $\varphi_{Z_{s,c}} = 0$

B.3 Example of TS parameters determination

This section gives the TS parameters determination, for an excitation of 50 mV, of the two Tannoy loudspeakers 367X used during the experiments.

The net internal volume of the enclosure is determined as the empty box and driver lodging hole volumes minus magnet and cabinet volumes, ie $V_{b_{0,1}} \cong 0.7273 + 0.1414 - 0.2837 \cong 0.585 \pm 0.05\ \mathrm{dm}^3$.

The determination of the parameters follows the procedure of Section B.2.

LSP_0

$R_{e0} = 6.6\ \Omega$	$f_{s0} = 68.8$ Hz	$Q_{es0} = 0.69$	$Q_{ms0} = 2.62$	$Q_{ts0} = 0.55$
$V_{as0} = 3.59$ l	$f_{c0} = 181.7$ Hz	$Q_{eco0} = 1.87$	$Q_{mc0} = 6.67$	$Q_{tco0} = 1.46$

LSP_1

$R_{e1} = 6.8\ \Omega$	$f_{s1} = 73.8$ Hz	$Q_{es1} = 0.87$	$Q_{ms1} = 2.99$	$Q_{ts1} = 0.67$
$V_{as1} = 2.99$ l	$f_{c1} = 183.5$ Hz	$Q_{eco1} = 2.13$	$Q_{mc1} = 7.13$	$Q_{tco1} = 1.64$

Figures B.1 and B.2 show the reduced impedance curves in free and closed-box assemblies, and give the results of the *Matlab* determination of TS parameters:

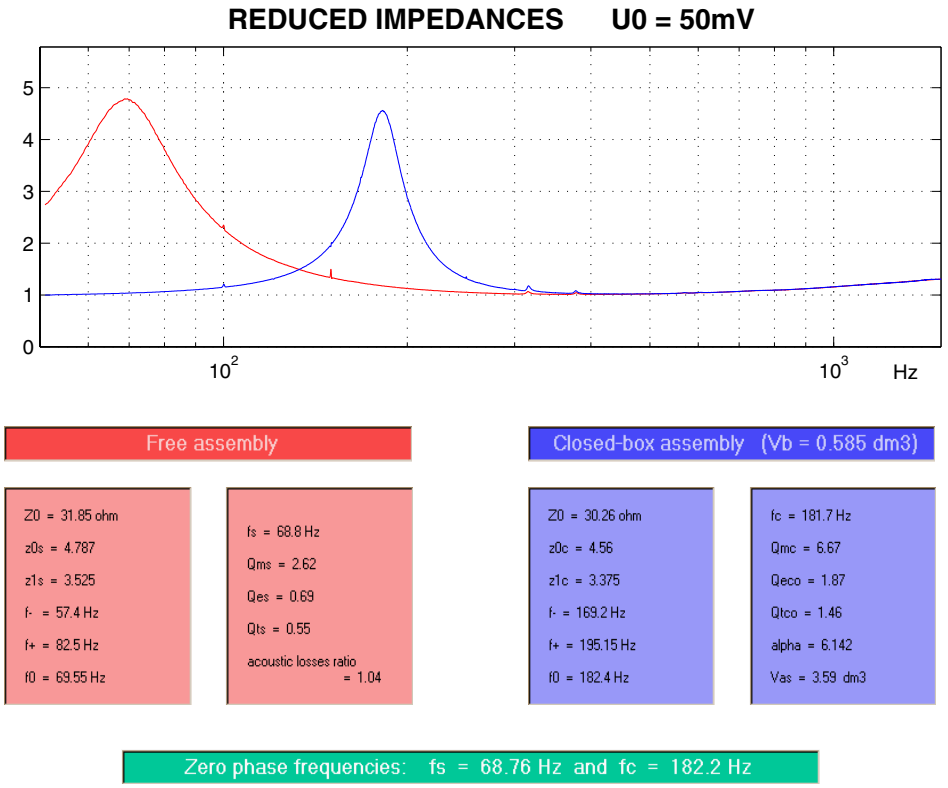

Figure B.1 - *LSP_0 TS parameters based on the measured input impedances in free and in closed-box assemblies*

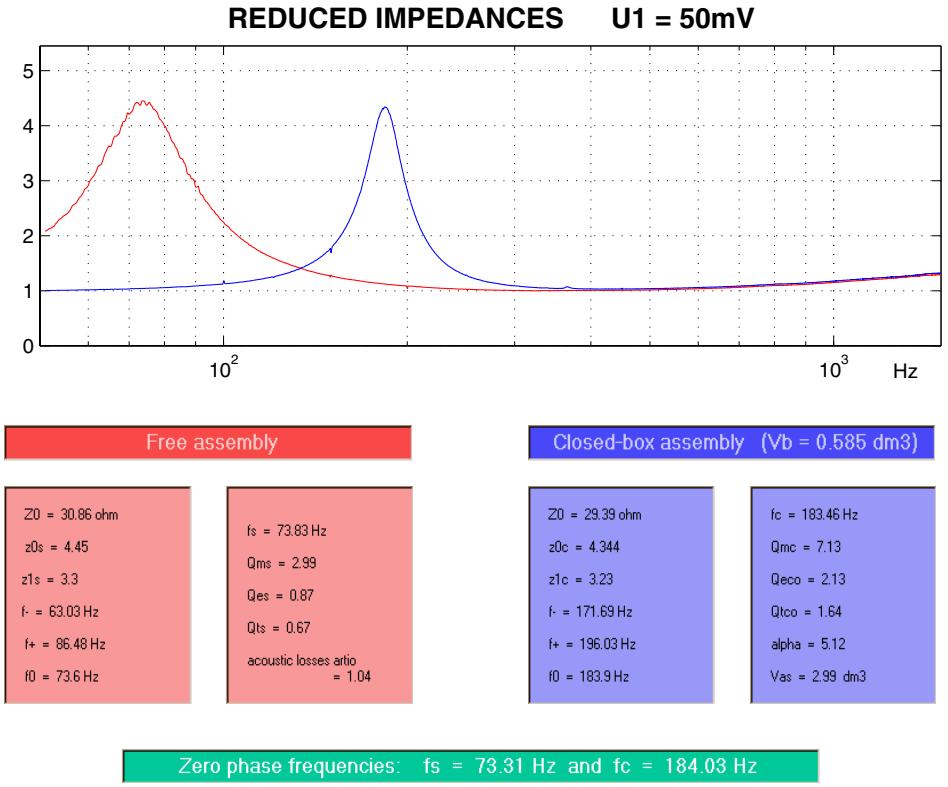

Figure B.2 - *LSP_1 TS parameters based on the measured input impedances in free and in closed-box assemblies*

The check on the acoustic losses ratio, assumed to be close to unity, gives:

for LSP_0: 0.98

for LSP_1: 1.01

The check on the acoustic masses ratio, assumed to be close to unity, gives:

for LSP_0: 1.04

for LSP_1: 1.04

In addition to this method, the calculation sheet gives an other estimation of f_s and f_c, ie when the $\varphi_{Z_{s,c}}$ is zero. The results give:

f_{s0} = 68.8 Hz f_{c0} = 182.2 Hz
f_{s1} = 73.3 Hz f_{c1} = 184 Hz

The comparison between both methods gives differences of $\pm$ 0.6 Hz at the most, which are quite acceptable within the framework of our study.

Appendix C

Source output resistance measurement

The R_g resistance value includes the resistance associated to:

- the output amplifier (*Quad 50 E* with an output transformer),
- the connecting wires (from amplifier to loudspeaker terminals in the anechoic chamber), and
- the connectors,

without forgetting the value of the shunt precision resistor (1 Ω).

Its measurement was made by replacing first the loudspeaker by precision resistors R_{meas} of 10 and 100 Ω and finally in open-circuit. The voltages across and at the terminals of R_{meas} are measured at the three frequencies 50, 200 and 500 Hz.

The following graphs give the output voltage versus the current for the two Quad amplifiers (their input voltages were 50 mV in all cases).

Based on equations written in figures C.1 and C.2, the R_g values are finally chosen for LSP_0 and LSP_1, as:

- R_{g_0} = 1.8 ± 0.1 Ω
- R_{g_1} = 0.8 ± 0.1 Ω (without shunt resistor)

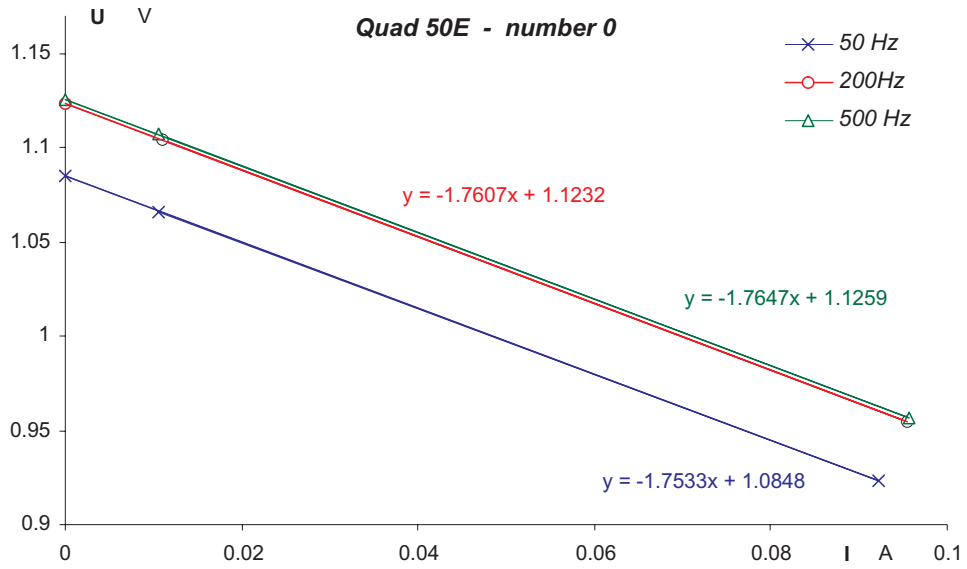

Figure C.1 - *$U_0(I_0)$ measured for three R_{meas} values (10, 100, ∞ Ω) and three frequencies (50, 200, 500 Hz)*

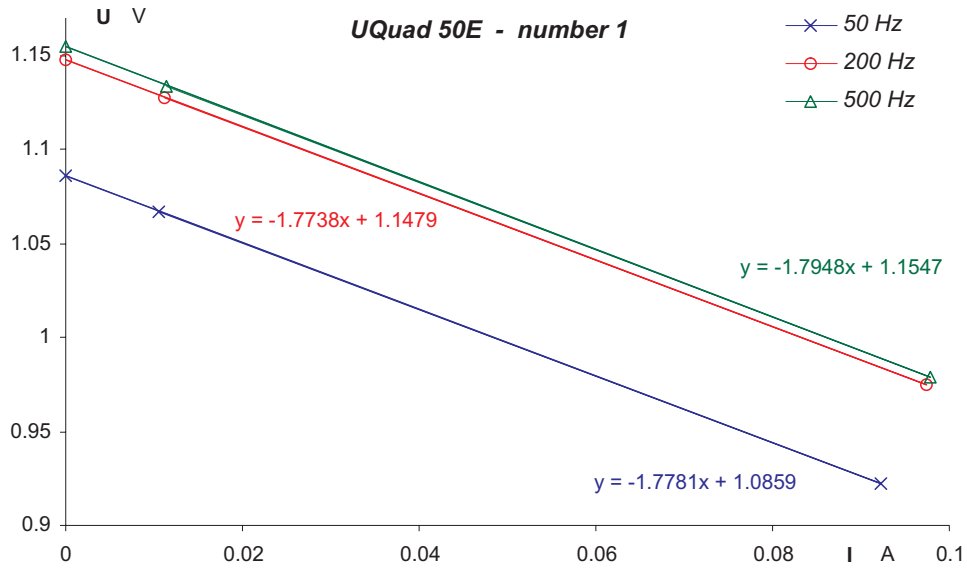

Figure C.2 - *$U_1(I_1)$ measured for three R_{meas} values (10, 100, ∞ Ω) and three frequencies (50, 200, 500 Hz)*

Appendix D

Errors calculation

The errors are calculated according to the propagation laws of maxima errors (positive and negative signs). Both final results are thus obtained by the most pessimistic combinations of all the fluctuating parameters. This calculation method [6, 10] may be written in its general form as:

$$\Delta y = \sum_{i=1}^{n} \frac{\delta y}{\delta x_i} \Delta x_i \qquad for \quad y = f(x_1, x_2, x_3, ..., x_n) \tag{D.1}$$

D.1 TS parameters

Measured and calculated according to the procedure described in Appendix B, the TS parameters can gently fluctuate depending on the uncertainties related to the frequency f_-, the frequency f_+, the reduced impedance z_0 and the net internal volume V_b, as followed:

$$\Delta f_{s,c} \;=\; \Delta f_+ \;\frac{f_-}{2\sqrt{f_- f_+}} \;+\; \Delta f_- \;\frac{f_+}{2\sqrt{f_- f_+}} \tag{D.2}$$

$$\Delta Q_{ms,mc} \;=\; \Delta f_+ \left\{ -\frac{\sqrt{f_- f_+}\;\sqrt{\frac{-\left[1-\frac{2}{3}(z_0-1)\right]^2+z_0^2}{-1+\left[1+\frac{2}{3}(z_0-1)\right]^2}}}{(f_+ - f_-)^2} + \frac{f_-\;\sqrt{\frac{-\left[1-\frac{2}{3}(z_0-1)\right]^2+z_0^2}{-1+\left[1-\frac{2}{3}(z_0-1)\right]^2}}}{2\sqrt{f_- f_+}\,(f_+ - f_-)} \right\} \;+$$

$$\Delta f_- \left\{ -\frac{\sqrt{f_- f_+}\ \sqrt{\frac{-\left[1-\frac{2}{3}(z_0-1)\right]^2+z_0^2}{-1+\left[1+\frac{2}{3}(z_0-1)\right]^2}}}{(f_+ - f_-)^2} + \frac{f_+\ \sqrt{\frac{-\left[1-\frac{2}{3}(z_0-1)\right]^2+z_0^2}{-1+\left[1-\frac{2}{3}(z_0-1)\right]^2}}}{2\ \sqrt{f_- f_+}\ (f_+ - f_-)} \right\} +$$

$$\Delta z_0\ \frac{\sqrt{f_- f_+}\ \frac{-\frac{4}{3}\left[1+\frac{2}{3}(z_0-1)\right]+2z_0}{-1+\left[1+\frac{2}{3}(z_0-1)\right]^2} - \frac{4\left[1+\frac{2}{3}(z_0-1)\right]\left[-\left(1+\frac{2}{3}(z_0-1)\right)^2+z_0^2\right]}{3\left[-1+\left(1+\frac{2}{3}(z_0-1)\right)^2\right]^2}}{2\ (f_+ - f_-)\ \sqrt{\frac{-\left[1+\frac{2}{3}(z_0-1)\right]^2+z_0^2}{-1+\left[1+\frac{2}{3}(z_0-1)\right]^2}}} \tag{D.3}$$

$$\Delta Q_{es,ec} \ = \ -\ \Delta f_+ \left\{ \frac{\sqrt{f_- f_+}\ \sqrt{\frac{-\left[1+\frac{2}{3}(z_0-1)\right]^2+z_0^2}{-1+\left[1+\frac{2}{3}(z_0-1)\right]^2}}}{(f_+ - f_-)^2\ (z_0-1)} + \frac{f_-\ \sqrt{\frac{-\left[1+\frac{2}{3}(z_0-1)\right]^2+z_0^2}{-1+\left[1+\frac{2}{3}(z_0-1)\right]^2}}}{2\ \sqrt{f_- f_+}\ (f_+ - f_-)\ (z_0-1)} \right\} +$$

$$\Delta f_- \left\{ \frac{\sqrt{f_- f_+}\ \sqrt{\frac{-\left[1+\frac{2}{3}(z_0-1)\right]^2+z_0^2}{-1+\left[1+\frac{2}{3}(z_0-1)\right]^2}}}{(f_+ - f_-)^2\ (z_0-1)} + \frac{f_+\ \sqrt{\frac{-\left[1+\frac{2}{3}(z_0-1)\right]^2+z_0^2}{-1}}}{2\ \sqrt{f_- f_+}\ (f_+ - f_-)\ (z_0-1)} \right\} -$$

$$\Delta z_0 \left\{ \frac{\sqrt{f_- f_+}\ \sqrt{\frac{-\left[1+\frac{2}{3}(z_0-1)\right]^2+z_0^2}{-1+\left[1+\frac{2}{3}(z_0-1)\right]^2}}}{(f_+ - f_-)\ (z_0-1)^2} - \frac{\sqrt{f_- f_+}\left[\frac{-\frac{4}{3}\left[1+\frac{2}{3}(z_0-1)\right]+2z_0}{-1+\left[1+\frac{2}{3}(z_0-1)\right]^2} - \frac{4\left[1+\frac{2}{3}(z_0-1)\right]\left[-\left(1+\frac{2}{3}(z_0-1)\right)^2+z_0^2\right]}{3\left[-1+\left(1+\frac{2}{3}(z_0-1)\right)^2\right]^2}\right]}{2\ (f_+ - f_-)\ (z_0-1)\ \sqrt{\frac{-\left[1+\frac{2}{3}(z_0-1)\right]^2+z_0^2}{-1+\left[1+\frac{2}{3}(z_0-1)\right]^2}}} \right\} \tag{D.4}$$

$$\Delta V_{as} \ = \ \Delta V_b \left(\frac{f_c\ Q_{ec}}{f_s\ Q_{es}} - 1\right) \ - \ \Delta Q_{es}\ \frac{f_c\ Q_{ec}}{f_s\ Q_{es}^2}\ V_b \ + \ \Delta Q_{ec}\ \frac{f_c}{f_s\ Q_{es}}\ V_b \ -$$
$$\Delta f_s\ \frac{f_c\ Q_{ec}}{f_s^2\ Q_{es}}\ V_b \ + \ \Delta f_c\ \frac{Q_{ec}}{f_s\ Q_{es}}\ V_b \tag{D.5}$$

Appendix E

Two face-to-face closed-box loudspeakers

E.1 Aim and process

The configuration of two closed-box loudspeakers mounted face-to-face also appears to be of interest in order to analyse the number of iterations necessary to calculate $\underline{Z}$ and $\underline{q}$ modifications for highly coupled loudspeakers.

The measurement process is again the same as in Subsection 4.3.3, where the loudspeakers are driven by white noise. The equipment list is given in Appendix A. The loudspeakers are put on a rail of 2 m (fig. E.1)

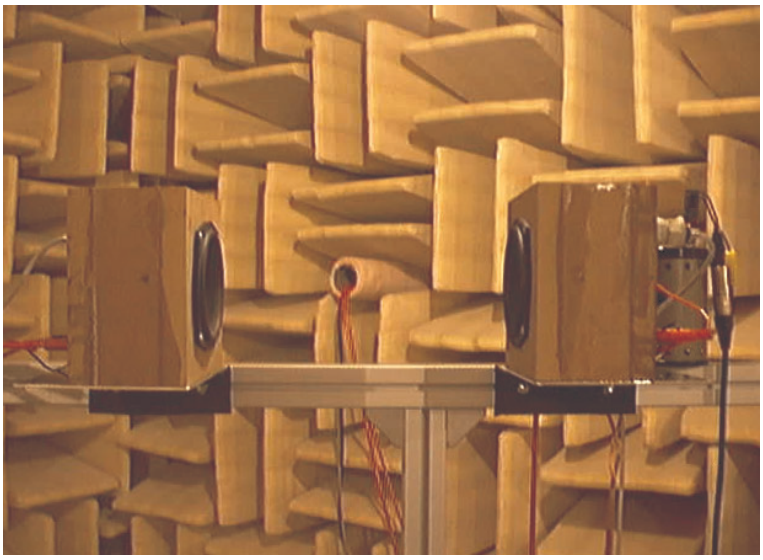

Figure E.1 - *Assembly picture of two face-to-face closed-box loudspeakers mounted on a rail*

The iteration number being directly related to the distance between loudspeakers, the measurements are carried out according to different g, ie 50, 20, 10 and 5 cm. Although no probable specific technological needs are met for small distances between the boxes, this case is nevertheless interesting due to the fact that it may bring into play a large amount of iterations. As previously, this number is considered to be acceptable when the differences between two consecutive iterations are bounded by $\pm$ 0.01 $\%$ for the modulus and $\pm$ 0.01 degree for the phase.

The calculations are carried out according to the GTD method. The comparisons between measured and calculated results let appear that the $LSP_{0,1}$ sound pressures calculated at the $LSP_{1,0}$ surface must be multiplied by a factor due to the presence of the $LSP_{1,0}$ box, which acts as an infinite baffle for each little $LSP_{0,1}$ radiating surface. We shall assume as a rough approximation that the wall is rigid, which is of course not correct given that the walls are in reality the membranes of the moving drivers. According to image source theory, this factor, called F_i in the following, decreases when g increases. Given that the diffraction effects are only calculated at emission for both closed-box loudspeakers, F_i also comprises the diffraction effects at the other box edges.

E.2 Results

According to the four distances g, the results coming from figures E.2, E.3, E.4, and E.5 are given in the table below, mentioning in each case the value found for F_i and the iteration number necessary to calculate $\underline{Z}$ and $\underline{q}$ according to the above prescriptions:

distance *g*	**50 cm**	**20 cm**	**10 cm**	**5 cm**
figure number	E.2	E.3	E.4	E.5
factor F_i	1.45	1.85	2.2	2.7
$\underline{Z}$ iteration number	1	2	5	16
$\underline{q}$ iteration number	0	2	3	9

In the first measurement case (g = 50 cm), the $\underline{q}$ modifications are spoilt by mistakes most likely coming from the small modification values and from the rail vibrations. Those disruptive factors have to be overcome to compare measurement results with calculations, that is why a polynomial approximation of order 40 has been computed.

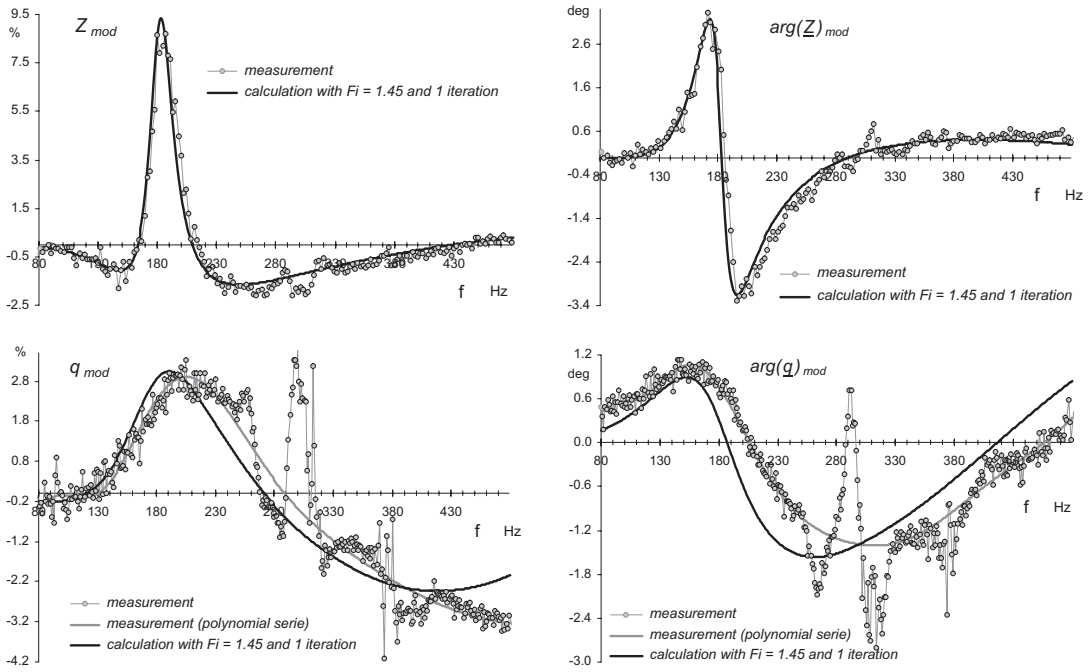

Figure E.2 - *Input impedance and volume velocity modifications for g = 50 cm - comparisons between measurements and calculations*

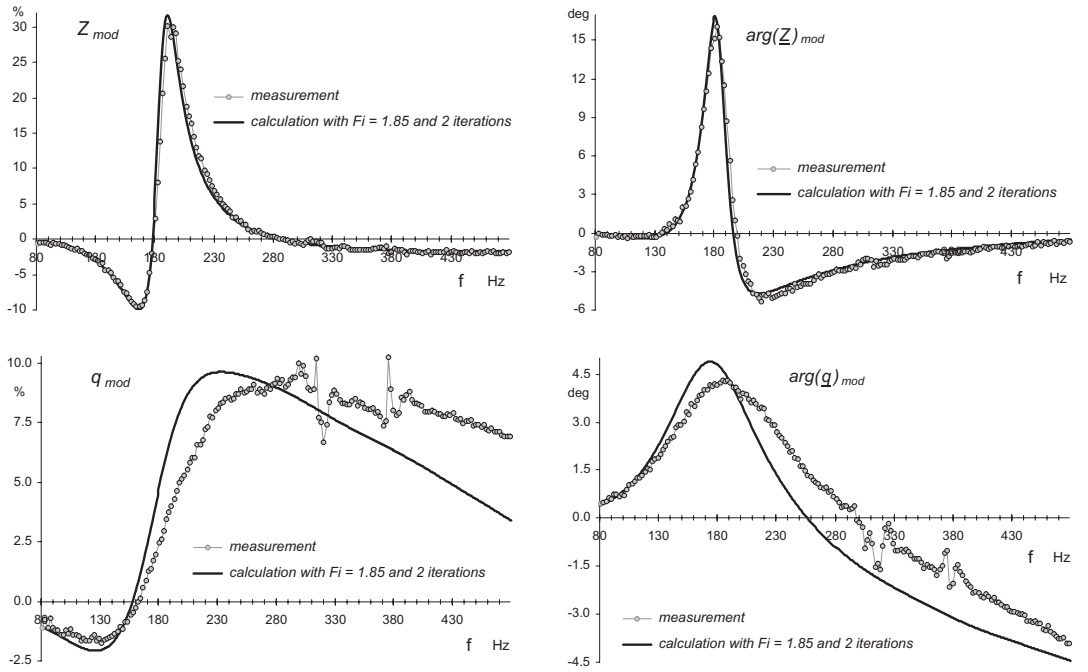

Figure E.3 - *Input impedance and volume velocity modifications for g = 20 cm - comparisons between measurements and calculations*

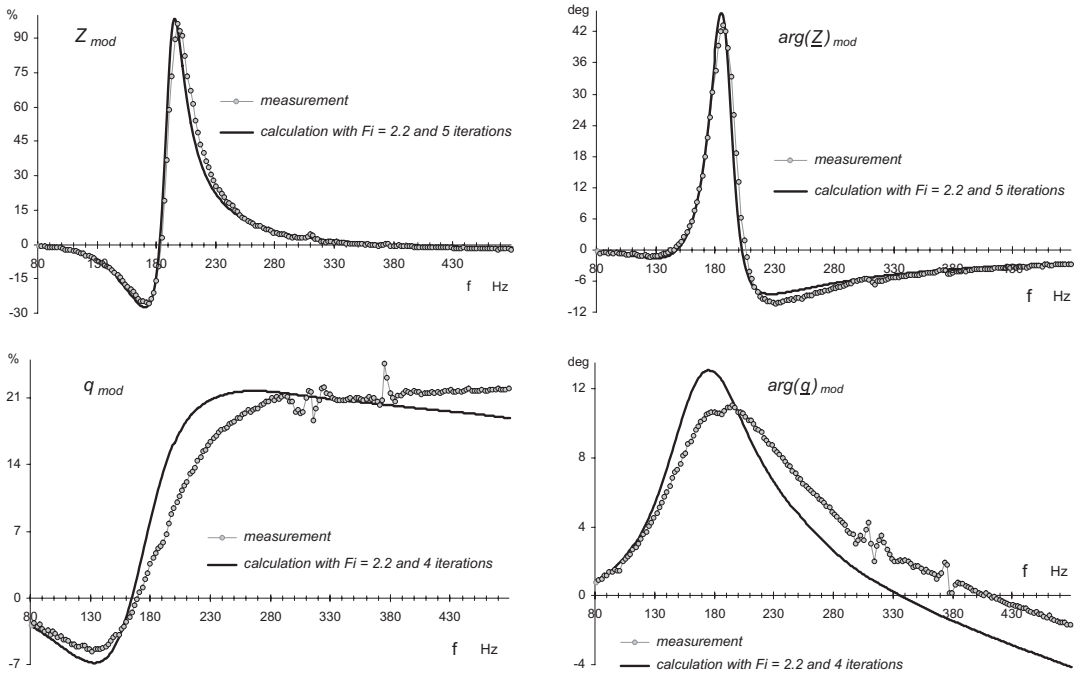

Figure E.4 - *Input impedance and volume velocity modifications for g = 10 cm - comparisons between measurements and calculations*

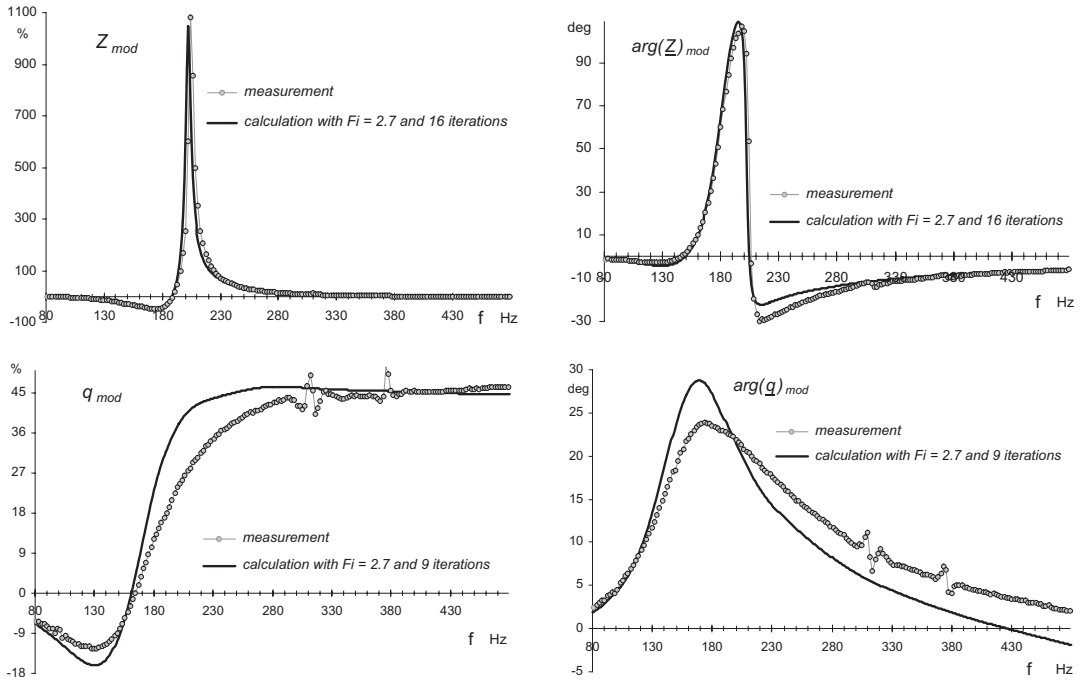

Figure E.5 - *Input impedance and volume velocity modifications for g = 5 cm - comparisons between measurements and calculations*

E.3 Comments

The fact that F_i reaches values exceeding 2 confirms that it does not come only from image source contributions. This factor decreases in a pseudo-logarithmic way, as shown in figure E.6.

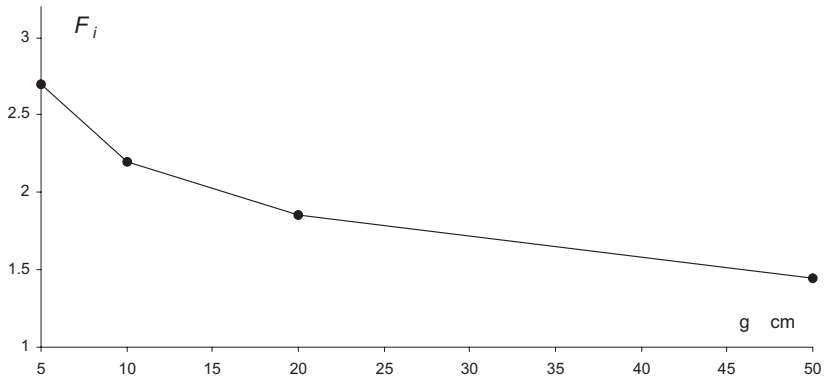

Figure E.6 - *Image source factor decrease with distance g*

As we can see, the number of iterations can require a large amount of calculations when the loudspeakers are located very close together. This is due to the huge orders of magnitude of $\underline{Z}$ (1500 $\%$ and 140 deg) and $\underline{q}$ modifications (60 $\%$ and 30 deg).

Whilst the calculations (corrected by F_i) of $\underline{Z}$ modifications correspond accurately to the measurements, the comparisons between measured and calculated $\underline{q}$ modifications lead us to assume that F_i must be a function varying according to the frequency. As these considerations go beyond the scope of this thesis, it has been decided not to go into this configuration analysis in greater depth.

Glossary of terms

a	m	*Radius of the projected surface*
$arg(\underline{q})_{mod}$	deg	*Volume velocity modifications in phase*
$arg(\underline{Z})_{mod}$	deg	*Input impedance modifications in phase*
c	m/s	*Speed of sound*
d	m	*Distance to the piston centre*
f	Hz	*Frequency*
f_c	Hz	*Resonance frequency of a closed-box loudspeaker*
f_s	Hz	*Resonance frequency of a loudspeaker in an infinite baffle*
g	m	*Distance between enclosures*
k	rad/m	*Wave number*
l	1	*Number of edge divisions*
m	1	*Second piston surface division number*
m_{ab}	$\mathrm{kg/m^4}$	*Acoustic mass associated to C_{ab}*
m_{ar}	$\mathrm{kg/m^4}$	*Acoustic radiation mass*
m_{as}	$\mathrm{kg/m^4}$	*Acoustic mass equivalent to m_s*
m_s	kg	*Mass of the moving system*
n	1	*First piston surface division number*
$\underline{p}$	Pa	*Sound pressure*
$\underline{p}_{01}$	Pa	*LSP_1 sound pressure at the immediate vicinity of LSP_0 membrane*
$\underline{p}_g$	Pa	*Pressure generator*
$\underline{p}_{in}$	Pa	*In-box sound pressure*
$\underline{p}_{nf}$	Pa	*Near-field sound pressure*
$\underline{q}$	$\mathrm{m^3/s}$	*Volume velocity*
q_{mod}	%	*Volume velocity modifications in modulus*
r	m	*Distance between pistons centres*
s_l	m	*Distance from diffracting edge element l to observation point*
$\underline{v}$	m/s	*Loudspeaker membrane velocity*
$\underline{v}_e$	m/s	*Membrane velocity due to an external force*
z	1	*Reduced input impedance*

Bl	Tm	*Electrodynamic coupling coefficient*
C_{ab}	m^3/Pa	*Acoustic compliance corresponding to the closed box*
C_{as}	m^3/Pa	*Acoustic compliance equivalent to* C_{ms}
C_{ms}	$\mathrm{m/N}$	*Mechanical compliance of loudspeaker suspensions*
C_s	F	*Capacitance corresponding to* m_s
C_r	F	*Capacitance corresponding to* m_{ar}
$\underline{I}$	A	*Current across the loudspeaker*
$\underline{E}$	V	*Induced voltage*
$\underline{F}$	N	*Excitation force*
$\underline{F}_{01}$	N	LSP_1 *force on* LSP_0 *membrane*
$\underline{F}_{ext}$	N	*External force on loudspeaker membrane*
$\underline{F}_g$	N	*Source force corresponding to* $\underline{U}_g$
$\underline{F}_i$	1	*"Image source" factor*
$\underline{F}_{re}$	N	*Medium reaction force*
L_e	H	*Inductance of the voice coil*
L_s	H	*Inductance equivalent to* C_{ms}
Q_{ec}	1	*Electrical quality factor of a closed-box loudspeaker*
Q_{mc}	1	*Mechanical quality factor of a closed-box loudspeaker*
Q_{tc}	1	*Total quality factor of a closed-box loudspeaker*
Q_e	1	*Electrical quality factor of a loudspeaker in an infinite baffle*
Q_{ms}	1	*Mechanical quality factor of a loudspeaker in an infinite baffle*
Q_t	1	*Total quality factor of a loudspeaker in an infinite baffle*
R	Ω	*Shunt Resistance*
R_{ab}	Ω_a	*Acoustic resistance associated to* C_{ab}
R_{ae}	Ω_a	*Acoustic resistance equivalent to* $R_g + R_e$
R_{al}	Ω_a	*Acoustic resistance of enclosure losses due to leakage*
R_{ar}	Ω_a	*Acoustic radiation resistance*
R_{as}	Ω_a	*Acoustic resistance equivalent to* R_{ms}
R_e	Ω	*DC resistance of loudspeaker voice coil*
R_g	Ω	*Output resistance of source including cables and connectors*
R_i	Ω	*Amplifier output resistance*
R_{meas}	Ω	*Measurement resistance*
R_{ms}	Ω_m	*Mechanical loss resistance*
R_s	Ω	*Electrical resistance equivalent to* R_{ms}
S_d	m^2	*Effective projected surface area of loudspeaker diaphragm*
$\underline{U}$	V	*Voltage at the loudspeaker terminals*
$\underline{U}_g$	V	*No-load voltage of a real voltage source*
$\underline{U}_i$	V	*Induce voltage inverse*
V_{as}	m^3	*Equivalent volume of air of a loudspeaker compliance*

V_b	m^3	*Net internal volume of the enclosure*
$\underline{X}_{ar}$	Ω_a	*Acoustic radiation reactance*
$\underline{Z}$	Ω	*Loudspeaker input impedance*
$\underline{Z}_{ab}$	Ω_a	*Acoustic impedance of the box*
$\underline{Z}_{ar}$	Ω_a	*Acoustic radiation impedance*
Z_c	$\mathrm{Pa\ s/m}$	*Characteristic acoustic impedance (ρc)*
$\underline{Z}_{mg}$	Ω_m	*Mechanical impedance corresponding to the mechanical and electrical parts of the loudspeaker*
Z_{mod}	$\%$	*Input impedance modifications in modulus*
$\underline{Z}_{mr}$	Ω_m	*Mechanical impedance corresponding to $\underline{Z}_{ar}$*

α	1	*Compliance ratio*
β	1	*Compliance factor*
ϕ	rad	*Excitations difference of phase*
φ	rad	*Angle to piston centre*
λ	m	*Wavelength*
λ_l	rad	*Reflection angle at the diffracting edge element l*
θ_l	rad	*Observation angle at the diffracting edge element l*
ρ	$\mathrm{kg/m}^3$	*Air mass density*
ω	$\mathrm{rad/s}$	*Angular frequency ($2\pi f$)*

Ω	rad	*Enclosure half wedge angle*

Acronyms and abbreviations

AD/DA	Analog Digital / Digital Analog
AES	Audio Engineering Society
DAGA	Deutsche Arbeitsgemeinshaft für Akustik
DC	Direct Current
EPFL	Ecole Polythechnique Fédérale de Lausanne Swiss federal Institute of Technology Lausanne
ETH	Eidgenössische Technische Hochschule Zürich Swiss federal Institute of Technology Zurich
GEA	Groupement Electroacoustique de la SFA Electro acoustics group of SFA
GTD	Geometric Theory of Diffraction
IEC	International Electrotechnical Commission
JAES	Journal of the Audio Engineering Society
JASA	Journal of the Acoustical Society of America
JSV	Journal of Sound and Vibration
LEMA	Laboratoire d'Electromagnétisme et d'Acoustique Laboratory of Electromagnetics and Acoustics
LCCCN	Library of Congress Catalog Card Number
LSP	Loudspeaker
NDT	Independent Nondestructive Testing
PPUR	Presses Polytechniques et Universitaires Romandes
RMS	Root Mean Square
SFA	Société Française d'Acoustique French Acoustical Society

SSA	Société Suisse d'Acoustique Swiss Acoustical Society
TFE	*Matlab* Transfer Function Estimate
TS	Thiele and Small
UTD	Uniform Theory of Diffraction
XCORR	*Matlab* Cross-correlation function estimates

References

[1] J. Backman. Computation of diffraction for loudspeaker enclosures. *JAES*, 37(5):353–362, May 1989.

[2] A. Branski. Acoustic modelling of surface sources. part 1, 2 and 3. *Archives of Acoustics*, 20(4):311–359, 1995.

[3] M.J. Hawksford and R.M. Bews. Application of the geometric theory of diffraction (gtd) to diffraction at the edges of loudspeaker baffles. *JAES*, 34(10):771–779, October 1986.

[4] D.L. Hutchins and R.G. Kouyoumjian. Calculation of the field of a baffled array by the geometrical theory of diffraction. *JASA*, 45(2):485–492, 1969.

[5] O. Jacobsen. Some aspects of the self and mutual radiation impedance concept with respect to loudspeakers. *JAES*, 24(2):82–92, March 1976.

[6] J.C. Le Roux. *Le haut-parleur électrodynamique: estimation des paramètres électroacoustiques aux basses fréquences et modélisation de la suspension*. PhD thesis, Académie de Nantes / Université du Maine, Avril 1994.

[7] The MathWorks, Inc., 24 Prime Park Way, Natick, MA 01760, USA. *MATLAB - Signal Processing Toolbox User's Guide*, December 1996. www.mathworks.com.

[8] P. Menounou, I.J. Busch-Vishniac, and D.T. Blackstock. Directive line source model: A new model for sound diffraction by half planes and wedges. *JASA*, 107(6):2973–2986, June 2000.

[9] H.P. Neff. Mutual impedance of circular pistons. *JAES*, 43(9):695–699, September 1995.

[10] P.-A. Paratte and P. Robert. *Systèmes de Mesure*. ISBN 2-88074-057-6. PPUR, CH-1015 Lausanne, Switzerland, 1986. Traité d'électricité de l'EPFL, volume XVII.

[11] R.L. Pritchard. Mutual acoustic impedance between radiators in an infinite rigid plane. *JASA*, 32(6):730–737, June 1960.

[12] M. Rossi. *Electroacoustique*. ISBN 2-88074-061-4. PPUR, CH-1015 Lausanne, Switzerland, 1986. Traité d'électricité de l'EPFL, volume XXI.

[13] E. Skudrzyk. *The Foundations of Acoustics*. ISBN 0-387-80988-0, LCCCN 76-161480. Springer-Verlag, Wien, Austria, 1971.

[14] R.H. Small. Closed-box loudspeaker system - part 1: Analysis. *JAES*, 20(10):798–808, December 1972.

[15] R.H. Small. Direct-radiator loudspeaker system analysis. *JAES*, 20(5):383–395, June 1972.

[16] R.H. Small. Closed-box loudspeaker system - part 2: Synthesis. *JAES*, 21(1):11–18, Jan./Feb. 1973.

[17] W.L. Stutyman and G.A. Thiele. *Antenna Theory and Design*. ISBN 0-471-04458-X. John Wiley and Sons, USA, 1981.

[18] H. Suzuki. Mutual radiation impedance of a double-disk source and its effects on the radiated power. *JAES*, 34(10):780–788, October 1986.

[19] U.P. Svensson, R.I. Fred, and J. Vanderkooy. An analytic secondary source model of edge diffraction impulse response. *JAES*, 106(5):2331–2344, November 1999.

[20] A.N. Thiele. Loudspeakers in vented boxes: part 1. *JAES*, 19(5):382–391, May 1971.

[21] A.N. Thiele. Loudspeakers in vented boxes: part 2. *JAES*, 19(6):471–483, June 1971.

[22] J. Vanderkooy. A simple theory of cabinet edge diffraction. *JAES*, 39(12):923–933, December 1991.

[23] J.R. Wright. Fundamentals of diffraction. *JAES*, 45(5):347–356, May 1997.

Complementary bibliography

(1980). *An Anthology of Articles on Loudspeakers from the pages of the Journal of the AES (1953-1977)*, volume 1-25 of *LCCCN 80-53465*, 60 East 42nd Street, New-York 10165. Publications Office, AES, Inc.

(1996). *MATLAB - The Language of Technical Computing Using Matlab Graphics*. The MathWorks, Inc., 24 Prime Park Way, Natick, MA 01760, USA. www.mathworks.com.

(1997). *MATLAB - Symbolic Math Toolbox User's Guide*. The MathWorks, Inc., 24 Prime Park Way, Natick, MA 01760, USA. www.mathworks.com.

(1999). *MATLAB - The Language of Technical Computing Using Matlab*. The MathWorks, Inc., 24 Prime Park Way, Natick, MA 01760, USA. www.mathworks.com.

Archer Hall, J. A. and Hutchins, D. A. (1980). A series approach for the determination of nearfield radiation patterns of axisymetric transducers under various conditions of baffle. *NDT International*, pages 151–158.

Bahder, T. B. (1995). *Mathematica for Scientists and Engineers*. ISBN 0-201-54090-8. Addison-Wesley Publishing Company, USA.

Benson, J. (1993). *Theory and Design of Loudspeaker Enclosures*. ISBN 0-9638929-0-8. Synergetic Audio Concepts, USA.

Beranek, L. L. (1954). *Acoustics*. LCCCN 53-12426. McGraw-Hill book company, USA, electrical and electronic engineering series edition.

Beranek, L. L. (1988). *Acoustical Measurements*. ISBN 0-88318-590-3, LCCCN 88-82582. American Institute of Physics, 975 Memorial Drive, Cambridge, MA 02138, USA. Revised Edition.

Bénaya, M. (1996). *La Construction des Appareils Audio*. ISBN 2-85535-247-9. ETSF: Editions Techniques et Scientifiques Française, 2-12, Rue de Bellevue, 75940 Paris Cedex 19.

Borwick, J. (1988). *Loudspeaker and Headphone Handbook*. ISBN 0-408-01387-7, LCCCN 87-25001. Butterworth and Co, England.

Bouwkamp, C. J. (1971). Numerical computation of the radiation impedance af a rigid annular ring vibrating in an infinite plane rigid baffle. *JSV*, 17(4):499–508.

Bruneau, A. M. (1979). Rayonnement d'un disque placé ou non dans un écran à la surface duquel la distribution de vitesse est connue. *Acustica*, 43(2):147–155.

Bruneau, A. M. (1981). Rayonnement d'un haut-parleur à diaphragme conique. *Acustica*, 48(2):86–96.

Bruneau, A. M. and Bruneau, M. (1980). Sur la réponse en fréquence des haut-parleurs. *Acta Acustica*, 44:308–322.

Bruneau, A. M. and Bruneau, M. (1986). Electrodynamic loudspeaker with baffle: motional impedance and radiation. *JAES*, 34(12):970–979.

Bruneau, M. (1983). Introduction aux théories de l'acoustique. Université du Maine, Route de Laval, 72041 Le Mans, France.

Bruneau, M. (1998). *Manuel d'Acoustique Fondamentale*. ISBN 2-86601-712-9, ISSN 1264-4692. HERMES Editions, Paris.

Colloms, M. (1997). *High Performance Loudspeakers*. Number 5th edition in ISBN 0471-97091-3 (PPC), ISBN 0471-97089-1 (Pr). John Wiley & Sons, Baffins Lane, Chichester, West Sussex, PO19 1UD, England.

Crane, P. H. G. (1967). Method for the calculation of the acoustic radiation impedance of unbaffled and partially baffled piston sources. *JSV*, 5(2):257–277.

Crane, P. H. G. (1970). The acoustic self-radiation impedance of a rigid oscillating disc near a similar stationary disc. *JSV*, 11(1):115–120.

D'Appolito, J. (1999). *Le haut-Parleur: Manipulations et Mesures Electroacoustiques - des techniques analogiques aux méthodes d'analyse numérique sur PC*. ISBN 286661114-4. Publitronic / Elektor, 21/23 rue des Ardennes, 75920 Paris cedex 19, France.

Davis, D. and Davis, C. (1987). *Sound System Engineering*. ISBN 0-672-21857-7. Howard W. Sams & Co. - A Division of Macmillan, Inc., 4300 West 62nd Street, Indianapolis, IN 46268, 2nd edition.

Degeorges, J. F. and Tichy, J. (1987). Energy radiation and propagation in the nearfield of a vibrating plate. In *NOISE-CON 87*, pages 189–194. The Pennsylvania State University.

Del Pedro, M. and Pahud, P. (1992). *Mécanique Vibratoire - Systèmes discrets linéaires*. ISBN 2-88074-243-9. PPUR, CH-1015 Lausanne, Switzerland.

Eargle, J. M. (1997). *Loudspeaker Handbook*. ISBN 0-412-09721-4. Chapman & Hall, 115 Fifth Avenue, New York, NY 10003.

Frankort, F. J. M. (1975 No.2). *Vibration and sound radiation of loudspeaker cones*. Philips research laboratories, PhD Thesis, Delft University of Technology, B.V. Uitgeversmaatschappij Centrex, cederlaan 4, P.O. Box 76, Eindhoven, Netherlands.

Harms, H.-F., Nordseewerke, T., and Gonsschorek, K.-H. (1998). Near field emc analysis by a combination of utd and mom. *International Wroclaw symposium on electromagnetic compatibility*, EMC98.

Herzog, P. (2000). Perturbations de l'impédance de rayonnement d'une source compacte. In *Proceedings of the 5th French Congress on Acoustics*, ISBN 2-88074-470-9, pages 664–667, Lausanne, Switzerland. PPUR.

Hiraga, J. (1998). *Les haut-Parleurs*. ISBN 2-10-004114-2. Dunod, Paris, France.

Ingard, K. U. and Morse, P. M. (1968). *Theoretical Acoustics*. ISBN 07-043330-5, LCCCN 67-15428. McGraw-Hill Book Company, USA.

Jordan, D. W. and Smith, P. (1995). *Mathematical Techniques - An Introduction for the Engineering, Physical, and Mathematical Sciences*. ISBN 0-19-856268-3 (Hbk). Oxford University Press, Walton Street, Oxford OX2 6DP, England.

Junger, M. C. and Perulli, M. (1978). *Elements d'Acoustique Physique*. Maloine S.A., 27, rue de l'Ecole-de-Médecine, 75006 Paris, France.

Keele, Jr., D. B. (1974). Low-frequency loudspeaker assessment by nearfield sound-pressure measurement. *JAES*, 22(3):154–162.

Klapman, S. J. (1940). Interaction impedance of a system of circular pistons. *JASA*, 11:289–295.

Kluth, M.-P. (1999). *FAQ LATEX Française - Pour débutants et confirmés*. ISBN 2-7117-8641-2. Vuibert Informatique, Paris.

Kunt, M., Bellanger, M., de Coulon, F., Gueguen, C., Hasler, M., Moreau, N., and Vetterli, M. *Traitement de l'Information - Volume1 - Techniques Modernes de Traitement Numérique des Signaux*. ISBN 2-88074-207-2. PPUR, CH-1015 Lausanne, Switzerland.

Lamport, L. (1999). *LATEX - A Document Preparation system - User's Guide and Reference Manual*. ISBN 0-201-52983-1. Addison-Wesley, library of congress cataloging-in-publication data edition.

Lee, J. and Seo, I. (1996). Radiation impedance computations of a square piston in a rigid infinite baffle. *JSV*, 198(3):299–312.

Loyez, P. (1998). *Techniques des Haut-parleurs & des Enceintes Acoustiques*. ISBN 2-10-004124-4. Dunod, Paris.

Maeder, E. R. (1996). *The Mathematica Programmer 2*. ISBN 0-12-464992-0. Academic press, A Division of Harcourt Brace & Company, 525 B Street, Suite 1900, San Diego, California 92101-4495.

Marchand, E. W. and Wolf, E. (1962). Boundary diffraction wave in the domain of the rayleigh-kirchhoff diffraction theory. *Journal of the Optical Society of America*, 52(7):761–767.

Meissner, M. (1983). Mechano-acoustic feedback in the case of an interaction between a sound source and a resonance system. *Archives of Acoustics*, 8(3):235–248.

Merriweather, A. S. (1969). Acoustic radiation impedance of a rigid annular ring vibrating in an infinite rigid baffle. *JSV*, 10(3):369–379.

Olson, H. F. (1969). Direct radiator loudspeaker enclosure. *JAES*, 17(1):22–29.

Pierce, A. D. (1991). *Acoustics - An Introduction to its Physical Principles and Applications*. ISBN 0-88318-612-8, LCCCN 89-80362. Acoustical Society of America, 500 Sunnyside Boulevard, Woodbury, New-York 11797, USA.

Porter, J. and Geddes, E. (1989). Loudspeaker cabinet edge diffraction. *JAES*, 37(11):908–918.

Rasmussen, S. and Rasmussen, K. B. (1994). On loudspeaker cabinet diffraction. *JAES*, 42(3):147–150.

Rossi, M. (1988). *Acoustics and Electroacoustics*. ISBN 0-89006-255-2, LCCCN 88-2176. Artech House, 685 Canton Street Norwood, MA 02062, USA.

Rudgers, A. J. (1987). Radiation impedances of interacting acoustic sources expressed in terms of the individual source green's functions. 82(2):709–710.

Rumsey, F. and McCormick, T. (1994). *Son et Enregistrement - Théorie et Pratique*. ISBN 2-212-05501-3. Eyrolles, 61, Bld Saint-Germain - 75240 Paris Cedex 05.

Shaw, T. and Tigg, J. (1994). *Applied Mathematica - Getting started, getting it done*. ISBN 0-201-54217-X. Addison-Wesley Publishing Company, USA.

Stepanishen, P. R. (1970). An approach to computing time-dependent interaction forces and mutual radiation impedance between pistons in a rigid planar baffle. *JASA*, 49.

Stephenson, G. and Radmore, P. M. (1990). *Advanced Mathematical Methods for Engineering and Science Students*. ISBN 0-521-36312-8. Cambridge University Press, The Pitt Building, Trumpington Street, Cambridge CB2 1RP, England.

Thompson, W. J. (1976). Radiation from a spherical acoustic source near a scattering sphere. *JASA*, 60(4):781–787.

Wang, H. C. and Shaw, R. P. (1985). Acoustic radiation from a baffled piston. *Microsoftware for Engineers*, 1(2):91–96.

Weems, D. B. (1990). *Designing, Building and Testing Your Own Speaker System - With Projects*. ISBN 0-8306-3374-X. TAB Books, Division of McGraw-Hill, Inc., Blue Ridge Summit, PA 17294-0850, 3rd edition.

Wright, J. R. and Bank, G. (1990). Radiation impedance calculation for a rectangular piston. *JAES*, 38(5):350–354.

List of Figures

Author's conference proceedings

- V.Adam, "Communication parlée et handicap auditif." Poster Session In *Journées Auditions*, Anzère, Switzerland, Janvier 1996.
- V. Adam, V. Chritin, M. Rossi, E. van Lancker. "Infrasonic monitoring of snow-avalanche activity. What do we know and where do we go from here?" In *International Symposium on Snow and Avalanches*, Chamonix, France, May 1997 and In *Annals of Glaciology*, 26:324-328.
- V. Adam, M. Rossi. "Near field of a loudspeaker array." In *DAGA 98, Fortschritte der Akustik*, pages 406-407, ETH-Zurich, Switzerland, Mars 1998.
- V. Martin, V. Adam, M. Rossi. "Predictive calculations for active noise control by anticipation and consequencies of the violation of causality; numerical and experimental results." In *Active 99*, pages 801-812, Fort Lauderdale, Florida, USA, December 1999.
- V. Adam. "Amplitude and phase synthesis of loudspeaker systems." In *AES 108th Convention*, preprint number 5161, Paris, France, February 2000.
- V. Adam. "Comportement d'un haut-parleur soumis à un champ extérieur (cas de haut-parleurs électrodynamiques - Aspects théoriques et expérimentaux)." In *Proceedings of the 5th French Congress on Acoustics*, ISBN 2-88074-470-9, pages 660-663, Lausanne, Switzerland, September 2000. PPUR.
- V. Adam. "Interactions of (two) closed-box loudspeaker systems." In *CD(2) of the 17th International Congress on Acoustics*, ISBN 88-88387-01-3, number 4B.10.04, Rome, Italy, September 2001.
- M. Rossi, V. Adam, O. Meylan. "A generalized model of sound emission transducers in active noise control and array." In *CD (3) of the 17th International Congress on Acoustics*, ISBN 88-88387-01-3, number 3D.08.02, Rome, Italy, September 2001.

Curriculum Vitae

The author was born in Sion, Switzerland, in 1969. She received a Master degree in microtechnical Engineering from the Swiss Federal Institute of Technology in Lausanne (EPFL), Switzerland, in 1995.

In 1995 she joined the Electromagnetics and Acoustics Laboratory (LEMA) of the EPFL to work as a research assistant. She was involved in different European and industrial projects, in which she collaborated on electrodynamic loudspeaker analyses and syntheses. Her fields of research have included near field sound pressure, phase response, interaction between sources, and loudspeakers mounted in arrays.

In 1999, she began a Ph.D. thesis in the same laboratory. In this context, she studied the effects of an incident sound field on the behaviour of electrodynamic loudspeakers, with the aim of providing computation and measurement methods allowing to predict whether these effects have to be taken into account.

Since 1999, she is a committee member of the Electro Acoustics Group (GEA) of the French Acoustical Society (SFA). She is also member of the Audio Engineering Society (AES) and the Swiss Acoustical Society (SSA).